AN ABSTRACT OF THE THESIS OF

Yau-Tang Tsai for the degree of Doctor of Philosophy in Civil Engineering presented on October 29, 1986.

Title: Ocean Wave-Soil-Caisson Interaction

Redacted for Privacy

Abstract approved: _____
William G. McDougal

Caissons on permeable seabeds have been designed and constructed for a variety of needs in coastal and offshore engineering. An evaluation of the adequacy of the foundation beneath the structure is required for an economic and safe design. To address this requirement, a two-dimensional analytical model of the foundation response is developed. The caisson is assumed to be placed on a rubblemound bedding layer overlying a soil of finite depth. The soil is considered to be homogeneous, isotropic, and linearly poroelastic. The soil responses, including displacements, stresses and porewater pressure, are modeled by Biot consolidation theory. This theory couples the soil skeleton motion and fluid flow. A boundary layer approximation technique is employed which enables the soil motion and pore pressure in the Biot theory to be solved separately. Linearity allows the wave-soil-caisson system to be decomposed into scattering and radiation problems. In the scattering problem, the caisson is assumed to be fixed and the soil response depends on the wave pressure on the mudline alone. In the radiation problem, the soil

and wave forces on the caisson determined in the scattering problem impose caisson motion which in turn forces the soil response. Both problems are solved for the total stress employing classical elasticity. In the vicinity of the mudline, the boundary layer approximation yields one-dimensional Terzaghi consolidation theory to adjust the soil response due to fluid flow. In solving both scattering and radiation problems, a mixed-type boundary condition arises at the mudline. This mathematical complication is simplified by applying a solution technique developed for a contact problem of a rectangular stamp on a thin elastic layer. This thin layer limitation is to ensure negligible shear stress and vertical normal stress along the exposed surface of the seabed.

The analytical solution is verified by comparison with a numerical solution developed for an elastic soil of finite depth. Results are in good agreement. In addition, large-scale experiments were conducted at the O. H. Hinsdale Wave Research Facility at Oregon State University. The wave flume is 342 ft long, 12 ft wide, and 15 ft deep. A 10-ft-high, 8-ft-long and 4-ft-wide caisson was placed on a bedding layer and 1 to 3 ft of underlying soil. The caisson was exposed to 0.68 to 4.40 ft waves with periods of 1.77 to 8.84 sec. Wave pressures were measured on the face of the caisson. Pore pressures were monitored in the bedding layer and soil under the caisson. Displacements of the caisson were also monitored. Comparison indicates that the theory may underestimate the horizontal and vertical displacements, but the predicted pore pressure is in good agreement with the data.

Ocean Wave-Soil-Caisson Interaction

by

Yau-Tang Tsai

A THESIS

submitted to

Oregon State University

in partial fulfillment of
the requirements for the
degree of

Doctor of Philosophy

Completed October 29, 1986

Commencement June 1987

APPROVED:

Redacted for Privacy

Professor of Civil Engineering in charge of major

Redacted for Privacy

Head of Department of Civil Engineering

Redacted for Privacy

Dean of Graduate School

Date thesis is presented October 29, 1986

Typed by Jackie Tandy for Yau-Tang Tsai

ACKNOWLEDGMENT

Sincere thanks is expressed to Dr. William G. McDougal for his guidance, support and personal friendship. Deep appreciation is extended to Dr. Charles K. Sollitt, Dr. Ronald B. Guenther, and Dr. Ted S. Vinson for their invaluable suggestions. Gratitude is expressed to Jackie Tandy, for her patience in typing this text. Acknowledgement is made to Marianne McDougal, who carefully read the manuscript and offered valuable comments. Thanks is also extended to my family for their patience and love.

This research was supported by the Oregon State University Sea Grant College Program, National Oceanic and Administration Office of Sea Grant, Dept. of Commerce, under Grant No. NA81AA-D-00086 (Project No. R/CE-13).

TABLE OF CONTENTS

TABLE OF CONTENTS (continued)

TABLE OF CONTENTS (continued)

LIST OF FIGURES

LIST OF FIGURES (continued)

LIST OF FIGURES (continued)

LIST OF FIGURES (continued)

LIST OF FIGURES (continued)

LIST OF TABLES

OCEAN WAVE-SOIL-CAISSON INTERACTION

1. INTRODUCTION

1.1 Motivation and Objective

Caissons are often constructed as box-like units with a closed bottom and partitions to provide strength. This type of caisson is usually filled with sand or gravel to increase the weight which provides stability. Caisson-type structures are commonly employed as breakwaters, bulkheads, and seawalls. Caissons have been used quite extensively in the Great Lakes, Europe, and Asia. In Holland caissons were employed to create a storm surge barrier at the entrances to Oosterschelde and Easternschelde. Many ports have caisson-type quay walls, for instance, Taichung, Taiwan and Shibath, Kuwait. In Japan, caissons have been widely used for seawalls to protect reclaimed land from the sea. Additionally, caisson-like gravity structures have been used in the North Sea and Prudhoe Bay for oil exploration and production platforms.

To reduce differential settlement and eccentric loading, a gravel or crushed-stone bedding layer is commonly placed below the caisson. This bed provides drainage and a foundation which distributes the structure and wave loads to the underlying soil. However, there is still a risk of failure at the caisson toe and in the underlying foundation. These failures often result from wave-induced scouring, high porewater pressure and large stresses developed in the foundation soil. These processes may lead to rapid and deep erosion at the toe as well as liquefaction of the foundation material. An

example is the failure of a 400-m caisson breakwater in Algiers which tilted seaward due to erosion [Agerschou et al. (1983)]. Because of this type of problem, an understanding of the failure mechanisms for the foundation and an evaluation of the foundation stability are necessary.

Present design practice has relied heavily on model tests and static analysis. However, physical models are costly and time-consuming and the accuracy of the test results are highly dependent upon the facilities and techniques. The static analysis only considers the static load applied to an impermeable seabed. Hence no porewater pressure and displacements are considered. It is known that a caisson founded on a poroelastic soil will respond dynamically when subjected to wave forces. When soil is subjected to wave-induced cyclic pressure and caisson-induced cyclic motion, porewater pressure, stresses, and displacements are created. The decrease of effective stresses due to porewater pressure has a great influence on the shearing strength and bearing capacity of the soil. However, few design guidelines on the dynamic load approach are available.

Durand and Monkmeyer (1982), Liu (1985), and Dias and Monkmeyer (1986) have developed analytical solutions to estimate the wave-induced dynamic porewater pressure underneath a fixed caisson or a fixed plate founded on a porous rigid seabed. However, Stematiu and Stera (1985) pointed out that the structure-soil interaction is extremely significant in the foundation design of a caisson. This interaction results in high local stresses in the soil skeleton. Attempts to model the combined effect of porewater pressure and dis-

placements were made by Lindenberg et al. (1982) and Stematiu and Stera (1985) using finite element methods. Finite element models have the disadvantage that they do not provide the physical insight into the problem which is often revealed in an analytical solution. The first steps toward an analytical solution were made by Mynett and Mei (1982) for a caisson sitting directly on the seabed, assuming the soil to be a poroelastic half-space. These assumptions limit the range of application of the model in many practical applications. Therefore, the objective of this project is to develop an analytical model to estimate foundation stresses, porewater pressures, and structure motions for wave-loaded caissons. The caisson is founded on a rubblemound bedding layer overlying a soil of finite depth.

1.2 Literature Review

1.2.1 Wave-Seabed Interaction

The degree of the interaction of surface water waves and the seabed depends upon wave and soil properties. The interaction may result in the modification of the wave field, such as wave damping and a local change in wave kinematics. Significant wave damping may occur if the seabed is soft, rough, or porous. This damping is accentuated if the waves propagate a long distance in shallow water. The propagation of the waves may also cause significant bed deformation, liquefaction or the triggering of large-scale mass movement of soil. These may induce large loads on structures such as cables, buried pipelines, piles, and footings. These soil responses tend to reduce the strength of the soil, which also contributes to the potential for foundation failure.

A variety of assumptions and techniques have been employed to evaluate the wave-soil interaction process. McDougal et al. (1981) have categorized the common assumptions in modeling wave-seabed interaction as: 1) impermeable soil, rigid skeleton; 2) porous soil, rigid skeleton, compressible or incompressible fluid; 3) impermeable soil, deformable skeleton; and 4) porous soil, deformable skeleton, and compressible fluid. These categories are given in order of increasing sophistication. Also the problem changes from a one-phase system to a two-or three-phase system. These assumptions also reflect the nature of the bottom response. Wave-induced pore pressure in a permeable, stiff, dense sand may be represented by the porous soil and rigid skeleton. However, for a sand or silt with a lower relative density, the assumption of a porous soil and deformable skeleton is more representative of the bottom response.

The assumption of an impermeable, rigid and smooth seabed associated with inviscid fluid has been widely made for most wave theories. If the real fluid effects are taken into account, the viscous damping due to the boundary layer near the bottom is significant for shallow water waves [Jonsson (1966), Dalrymple et al. (1984), and Liu (1986)]. A number of solutions have been developed which include bottom friction which causes wave energy dissipation [Ozhan and Shi-igai (1977), Kamphuis (1978), Nielsen (1983), and Liu and Tsay (1985)].

If the soil is assumed to be porous and rigid, Darcy's law has often been used to describe the flow within the soil skeleton. The porewater pressure is then governed by the Laplace equation. Based

on this assumption, Putnam (1949) derived an equation for wave-induced pressures in a sand layer of finite depth. Sleath's (1970) experiments strongly supported this assumption for both fine and coarse sand. Tsui and Helfrich (1983) compared measured pressure in the laboratory with second-order wave theory predictions. Both are in good agreement for short waves, but the measured pressures decay with depth more rapidly than predicted.

Beyond the assumption of a rigid soil skeleton, various solutions have been developed which model the seabed as an impermeable, linearly elastic continuum. These solutions can include inertia effects, layers with different elastic moduli, and traveling waves [Mallard and Dalrymple (1977), Dawson (1978) and Kraft and Helfrich (1983)]. There is excellent agreement between predictions from an elastic theory of seafloor response and field measurements of the water column pressure and bottom horizontal and vertical accelerations [Dawson et al. (1981)].

To examine both pore pressure and stress, Demars and Vanover (1985) developed a decoupled rigid bed model which uses elastic theory for porewater pressure. The theory and experimental measurements were in reasonable agreement. A more consistent approach is to consider the coupled response of the elastic deformation of the soil skeleton and the pore fluid interaction. This approach was developed by Yamamoto (1977) and Yamamoto et al. (1978). They employed Biot consolidation theory [Biot (1941)] to study the response of a poro-

elastic soil of finite or infinite depth to water waves and succeeded in verifying the theoretically predicted pore pressure by laboratory experiments.

Biot theory has been successfully used to model a variety of wave-seabed interaction problems. Madsen (1978) assumed the soil to be an anisotropic medium and explicitly solved the porewater pressure and effective stresses for an infinite homogeneous bed. McDougal et al. (1981) developed an analytical model to quantify the response of a horizontal, three-layered, soil-geotextile-soil system to propagating waves and concluded that the permeability and degree of saturation of the soil are significant to the Biot solution. Yamamoto has continued to apply Biot consolidation theory in the marine environment and has developed solutions for an inhomogeneous seabed approximated by many layers of homogeneous soils, each of which has different properties (1981) and for an inhomogeneous seabed with nonlinear elastic moduli and nonlinear Coulomb damping (1982). These theoretical solutions were also verified by physical models [Yamamoto et al. (1983a), Yamamoto and Schuckman (1984)]. Mei and Foda (1981a) studied the wave-induced stress in a poroelastic medium based on Biot theory and developed a boundary layer approximation which simplifies the mathematical treatment.

Biot theory has also been applied to predict seabed responses to random waves. Rahman and Layas (1986) have developed an analytical model to predict the wave-induced pressure on the seafloor, stresses, and porewater pressure in the soils by formulating the solution in a stochastic framework. Seafloor responses to random waves were based

on Madsen's (1978) solutions to the Biot equations. From the responses, the local seafloor instability was then developed in probabilistic terms. Similarly, Jaber et al. (1986) also developed a probabilistic analysis based on Yamamoto's (1983b) solutions to the Biot equations for seabed response, but the interaction of waves with the pervious and deformable bed is included.

A further extension of Biot theory has been given by McDougal and Liu (1986). The Biot equations were cross-differentiated, integrated over depth, and time-averaged to yield a one-dimensional consolidation equation with a mean accumulation source term which is associated with the surface water waves. From this equation, two analytical models for deep soil and shallow soil were developed, respectively, following the methodology of earthquake engineers to predict the pore pressure accumulation in marine soils.

1.2.2 Wave-Soil-Structure Interaction

The stability of a structure founded on the seabed requires a consideration of the porewater pressure in the underlying soil, the deformation of the seabed, and the stresses in the subsoil. To examine these processes various assumptions similar to the wave-soil interaction problem have been invoked.

The assumption of an impermeable and rigid seabed is usually made for wave-structure interaction problems, such as wave reflection, diffraction, and wave forces [Ippen (1966), Dean and Dalrymple (1984)]. In essence, these problems include no wave-seabed or structure-seabed interaction.

Analytical solutions with the assumption of permeable and rigid seabed have been developed to estimate the wave-induced seepage pressure under a caisson. Durand and Monkmeyer (1982) applied Dual integral equations to the mixed boundary value problem governed by the two-dimensional potential flow theory. Dias and Monkmeyer (1986) used the same technique to develop the solution for the problem of wave-induced seepage on a plate resting on the seabed. In contrast to the Dual integral equations, the Riemann-Hilbert method was employed by Liu (1985) to solve the mixed boundary value problem. Both analytical methods assume a porous rigid soil and a fixed caisson. Their solutions are all in reasonable agreement with laboratory measurements and applicable to any soil depth.

Broughton (1975) developed a finite element method by treating the soil as a linearly elastic material. The movements of the soil and the deck of an oil production platform and the contact stresses due to the interaction of the platform with a stratified seabed were determined. The results show that the rotation of the structure base provides a significant contribution to the horizontal movement of the structure at the deck level and that peak values of vertical contact stress occur near the outer edge of the structure. However, a linear elastic solution may overestimate the possible failure load of the soil foundation. Therefore, Munro et al. (1985) attempted to include the nonlinear behavior of the seabed in a finite element simulation of a soil-structure interaction system. This model allowed elasto-plastic soil properties, foundation stratigraphy, and structure embedment to be incorporated. The results show that the vertical

spring constant from the finite element solution is close to that obtained from the elastic half-space equation. However, both the horizontal and rocking stiffness from the finite element solution are considerably lower than those obtained from the elastic half-space equation.

Rahman et al. (1977) developed a finite element method to evaluate the pore pressure under the Ekofisk tank by assuming the soil is poroelastic. They used a one-dimensional storage equation by replacing the volumetric strain term with a pore pressure generation function and introducing the coefficient of volume compressibility. This yields one equation for one unknown, pore pressure. They evaluated the pore pressure generation function empirically. Laboratory tests were conducted to determine the number of cycles of loading that are required to develop a pore pressure ratio of 100% under undrained conditions. The analysis provides a time history of pore pressure response of the soil underlying the Ekofisk tank during a storm and suggests that the critical support conditions are most likely to develop around the outer edges of the tank. Similarly, Zen (1984) developed a finite element method model to predict the pore pressure in the underlying soil that supports a caisson breakwater resting on a rubblemound foundation. He also used the storage equation to evaluate the residual pore pressure, but employed the Endochronic technique to estimate the pore pressure generation. The results show

that wave height, wave period, subsoil permeability, and thickness of rubblemound are the major factors affecting the pore pressure.

A more realistic representation of the soil properties is given by Biot consolidation theory. Several numerical and analytical wave-soil-structure interaction models have been developed using Biot theory.

To verify the predicted deformations and pore pressure developed in the subsoil due to waves for the storm surge barrier in the Netherland, large model tests were conducted. deQuerlerij et al. (1979) used the Biot equation as a guideline to determine the model scale. These tests revealed unexpected large hydraulic gradients which led to a redesign of the original foundation bed. Lindenberg et al. (1982) established a finite element simulation of Biot equations to predict the foundation displacement and pore pressures. The results were compared with a large-scale model test. General agreement was found between the calculations and the measurements.

Stematiu and Stera (1985) have also developed a finite element simulation based on Biot equations to predict the pore pressure and stresses in the subsoil under a caisson breakwater. They concluded that the structure-soil interaction should be a major consideration in the foundation stability.

Mynett and Mei (1982) have developed an analytical model based on Biot equations to predict the pore pressure and stresses in a half-space subsoil under a rectangular caisson. The boundary layer approximation was applied to correct the solutions of the outer region problem, which was solved by means of complex variables.

1.3 Biot Consolidation Theory

The saturated soil is considered to be a poroelastic continuum which is a two-phase or three-phase system consisting of porewater, air, and the elastic soil skeleton. Terzaghi (1943) proposed a one-dimensional consolidation theory assuming that the grains constituting the soil are more or less bound together by molecular forces and constitute a porous material with elastic properties. The consolidation theory describes the deformation of a porous elastic material, the pores of which are filled with fluid. Thus the deformation may cause fluid flow and excess porewater pressure. Biot (1941) developed a three-dimensional consolidation theory which de scribes the interaction of pore fluid and soil skeleton. This theory may be employed to determine the distribution of stresses, water content, and settlement as a function of time in a soil under given loads. This has been termed the "quasi-static" Biot consolidation theory because soil inertia terms were neglected. Inertia was included in later Biot papers (1956a, 1956b).

A detailed derivation of the Biot equations was given by Verruijt (1969). The Biot equations consist of three stress equilibrium equations for the x, y, and z directions and a fourth equation which is the continuity equation for the pore fluid. This fourth equation has been called the storage equation. Biot theory has the following basic assumptions [Foda (1980)]: 1) isotropy of the material, 2) reversibility of stress-strain relation under final equilibrium condition, 3) linearity of stress-strain relation, 4) small

strains, 5) compressibility of the pore fluid, and 6) applicability of Darcy's law to the fluid flow through the porous skeleton. In spite of these assumptions, Biot theory has been shown to be a relevant model for small responses in dense sands and silts. Accordingly, Biot theory is employed in this study.

1.4 The Boundary Layer Approximation

The Biot equation couples the motions of fluid and solid phases. This coupling increases the mathematical difficulty. Only in a few cases can the Biot equations be solved analytically. In other cases the only recourse is to resort to a numerical method [Christian and Boehmer (1970), Hwang et al. (1971), and Booker (1973)]. If only simple, harmonic responses are to be modeled, the mathematics is simplified considerably. Such an assumption is invoked in this study. Unfortunately, this precludes the examination of pore pressure accumulation and net soil deformations.

Mei and Foda (1981a) developed a boundary layer approximation which decouples the pore pressure and soil motion. The boundary layer develops near the mudline. Near the mudline drainage is relatively unimpeded and there is significant relative motion between the fluid and the solid. Farther from the mudline there is little drainage so the fluid and solid tend to move in phase. This is termed the outer region problem, which can be reduced to solving a classical elastostatic problem. However, the boundary conditions on the mudline are not satisfied. Hence, corrections are made according to the boundary layer solution so that the boundary condition on the mudline are satisfied. This approximate solution is in good agreement with

the exact solution developed by Yamamoto (1977) for a wave-soil interaction problem.

Mathematically, in the boundary layer approximation, a physical quantity f is given by

$$f = f^{o} + f^{b} \tag{1.4.1}$$

where f^{o} belongs to the outer region solution and f^{b} is the boundary correction which is significant only within the boundary layer. Physically, the boundary layer approximation implies that the distribution of the applied forces over the fluid and the solid skeleton has to be adjusted according to their relative stiffnesses. Applications of the boundary layer approximation have been given by Mei and Foda (1981b, 1982) and by Mynett and Mei (1982, 1983).

1.5 The Contact Problem of a Rectangular Block on a Thin Elastic Layer

The bottom-founded caisson is similar to a rigid stamp attached to an elastic layer: the so-called contact problem in elasticity. A mixed boundary condition occurs along the mudline where stress conditions are imposed on the exposed portion and displacement conditions are imposed under the caisson [Kreyszig 1983]. It is difficult to analytically solve mixed boundary-value problems. A number of numerical solutions have been developed [Francavilla and Zienkiewicz (1975), and Tseng and Olson (1981)]. At present, only approximate analytical solutions can be obtained for contact problems corresponding to either very thick or very thin elastic layers [Alblas and Kuipers (1969, 1970b)]. Even so, the contact problems for small but

finite depth elastic layers are quite difficult. Alblas and Kuipers (1969) applied the technique of Wiener-Hopf to solve the displacements at the upper boundary of a thin elastic layer loaded by a rectangular block for heave and pitch. Their solutions will be employed to quantify the displacement boundary conditions along the exposed mudline immediately adjacent to the caisson. Results for the surge condition will be approximated from the known solution for heave. The details are addressed in Appendix B.

1.6 Scope

A rigid caisson is founded on a rubblemound foundation overlying a poroelastic seabed of finite depth. Caisson motions are induced by wave and soil forces. The caisson motion is transmitted to the subgrade through a permeable yet stiff rubble base. Thus, both displacements and pore pressure are transmitted to the subgrade. Stress singularities are developed at the toe and heel of the rubble foundation. The dynamic response of the soil due to these applied displacements and stresses is analytically modeled.

The governing equations for the analytical model are based on Biot consolidation theory. The boundary layer approximation developed by Mei and Foda (1981a) is employed to decouple the pore pressure and the displacements of the solid skeleton in the Biot theory. The mathematical difficulty of solving a mixed-type boundary-value problem is addressed by employing an approximation technique developed for contact problems on thin elastic layers [Alblas and Kuipers (1969), (1970a)]. The problem is then separated into scattering and radiation problems. The limitation of the thin soil

layer assumption in the analytical solution is discussed and compared with the finite element results for an infinitely long strip placed on a finite thickness elastic layer. The behavior of the solution is then examined for a variety of wave and soil conditions. Large-scale experiments were conducted to verify the analytical solution.

2. BOUNDARY-VALUE PROBLEM

2.1 General Assumptions

The wave-soil-caisson interaction problem is depicted in Fig. 2.1.1, in which h is the still water depth; d is the thickness of the soil skeleton; b is the thickness of the rubble bedding layer; 2c' is the width of the caisson; and 2c is the width of the mound foundation on the mudline through which the dynamic response of the caisson completely transfers to the soil skeleton. 2c is defined by 2V:1H slope rule [Bowles (1982)], and is termed the effective width of the caisson base.

The following assumptions are made in the analytical model:

1. Caisson and rubble bedding layer
   a) The rectangular caisson is infinitely long in the direction normal to the plane of the figure and the waves are normally incident. This allows a reduction to a two-dimensional problem.
   b) The caisson is impermeable and rigid.
   c) There is no slip between the caisson and the thin rubblemound foundation. Thus, the rigid body displacements of the caisson will be completely transferred to the softer seabed below. Accordingly, the shaded portion in Fig. 2.1.1 forms an entire rigid body.
   d) The mound foundation is hydraulically permeable but mechanically stiff compared with the underlying soil.

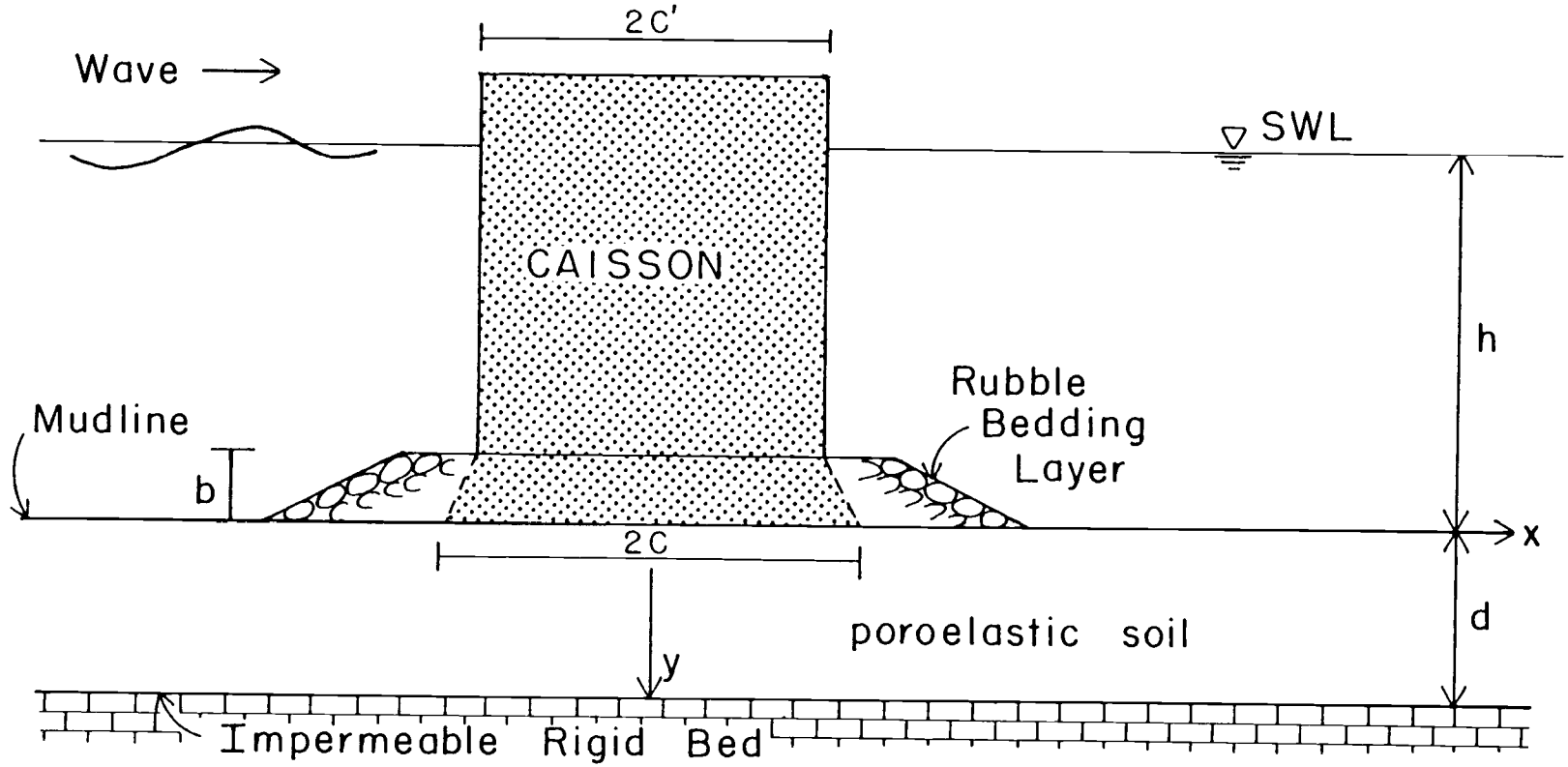

Figure 2.1.1. Definition sketch for the coordinate system and wave-soil-caisson system.

2. Soil

   a) The soil stratum is confined by a horizontal mudline above and a horizontal impermeable, rigid bed below.

   b) The soil is considered to be homogeneous, isotropic, linearly elastic, permeable, and saturated with water.

3. Water column

   a) Small amplitude wave theory is assumed to be applicable.

   b) The water depth is constant.

   c) The domain being modeled is small with respect to the horizontal length scale of soil-induced wave decay. Therefore, the soil and wave responses are decoupled.

2.2 Governing Equations

Mei and Foda (1982) provided a derivation of the Biot equations based on conservation of momentum and conservation of mass of the solid and fluid. In the equations of conservation of momentum, gravity terms are neglected which are small compared with the stress and pressure terms for the dynamic wave loading cases.

Solid

$$\bar{\rho}_s (1-\bar{n}) \frac{\partial \dot{v}_i}{\partial t} = \frac{\partial \tau'_{ij}}{\partial x_j} - (1-\bar{n}) \frac{\partial p}{\partial x_i} + \frac{\bar{n}^2}{\mu} \bar{\rho}_w g(\dot{u}_i - \dot{v}_i) \qquad (2.2.1a)$$

Fluid

$$\bar{\rho}_w \bar{n} \frac{\partial \dot{u}_i}{\partial t} = -\bar{n} \frac{\partial p}{\partial x_i} - \frac{\bar{n}^2}{\mu} \bar{\rho}_w g(\dot{u}_i - \dot{v}_i) \qquad (2.2.1b)$$

in which $\bar{\rho}_s$ and $\bar{\rho}_w$ are the solid and fluid densities, respectively; $\dot{v}$ and $\dot{u}$ are the solid and fluid velocity vectors, respectively; p is the pore water pressure; $\bar{n}$ is the porosity; μ is the coefficient of permeability; τ'_{ij} is the effective stress tensor; t is time; and g is the gravitational acceleration. The parameters with an overbar denote the sum of the values at static equilibrium and the values due to the dynamic perturbation. For instance, $\bar{n} = n_o + n$, in which n_o is the static porosity, and n is the dynamic perturbation.

The equations of conservation of mass for the solid and fluid phases are given by

Solid

$$\frac{\partial}{\partial t} [(1-\bar{n}) \bar{\rho}_s] + \frac{\partial}{\partial x_i} [\bar{\rho}_s (1-\bar{n}) \dot{v}_i] = 0 \qquad (2.2.2a)$$

Fluid

$$\frac{\partial}{\partial t} (\bar{n}\bar{\rho}_w) + \frac{\partial}{\partial x_i} (\bar{\rho}_w \bar{n} \dot{u}_i) = 0 \qquad (2.2.2b)$$

The governing equations for both the outer region and boundary layer correction were derived by Mei and Foda (1981a). Their derivation is presented for completeness.

2.2.1 Outer Region Approximation

The governing equation for this region will be derived where $(\ )^o$ denotes a parameter in the outer region. For sandy sea beds, the inertia terms in (2.2.1) are negligibly small compared with the stress or pressure terms [Mynett and Mei (1982)]. This observation was also made by Dalrymple and Liu (1982) for sands and other stiff materials in which the shear modulus and permeability are high. For these materials the shear wave velocity in the soil is much greater than the celerity of the free surface water waves and the quasi-static assumption is valid. Neglecting the inertia terms and summing the two equations of conservation of momentum yields

$$\frac{\partial(\tau'^{o}_{ij} - p^o\delta_{ij})}{\partial x_j} = 0 \tag{2.2.3}$$

in which δ_{ij} is the kronecker delta. This equation suggests the introduction of the total stress tensor

$$\tau^o_{ij} = \tau'^{o}_{ij} - p^o\delta_{ij} \tag{2.2.4}$$

Hence, (2.2.3) may be written

$$\frac{\partial \tau^o_{ij}}{\partial x_j} = 0 \tag{2.2.5}$$

This is a quasi-static equation of motion excluding body forces.

Applying Hooke's law for total stress

$$\tau_{ij} = \frac{2G\nu}{1-2\nu}\,\delta_{ij}\,\frac{\partial v_\ell}{\partial x_\ell} + G\left(\frac{\partial v_i}{\partial x_j} + \frac{\partial v_j}{\partial x_i}\right) \tag{2.2.6}$$

to (2.2.5) yields

$$\frac{2G\nu}{1-2\nu}\,\delta_{ij}\,\frac{\partial^2 v^o_\ell}{\partial x_\ell \partial x_j} + G\,\frac{\partial}{\partial x_j}\left(\frac{\partial v^o_i}{\partial x_j} + \frac{\partial v^o_j}{\partial x_i}\right) = 0 \tag{2.2.7}$$

In (2.2.6) G and ν are the shear modulus and Poisson's ratio of the soil, respectively; (v_i, v_j, and v_ℓ are the displacement vectors corresponding to the total stress tensor.

In a two-dimensional problem, the following two equations can easily be obtained from (2.2.7).

$$\nabla^2 u^o + \frac{1}{1-2\nu} \frac{\partial}{\partial x}\left(\frac{\partial u^o}{\partial x} + \frac{\partial v^o}{\partial y}\right) = 0 \qquad (2.2.8a)$$

$$\nabla^2 v^o + \frac{1}{1-2\nu} \frac{\partial}{\partial y}\left(\frac{\partial u^o}{\partial x} + \frac{\partial v^o}{\partial y}\right) = 0 \qquad (2.2.8b)$$

in which x and y are the horizontal and vertical axes of the Cartesian coordinates system; $u^o$and v^o are the displacements corresponding to the total stress in the x and y direction, respectively; and $\nabla^2(\cdot)$ is the LaPlacian operator. Equations (2.2.8a) and (2.2.8b) are the governing equations from which the displacements of the soil skeleton will be determined.

The porewater pressure is still unknown; thus, one more equation is required. This equation will be derived from the equations for conservation of mass and momentum.

Linearizing the equations of conservation of mass, (2.2.2a) and (2.2.2b), by neglecting the second order terms and then adding them yields

$$\frac{\partial \dot{v}_i^o}{\partial x_i} + n_o \frac{\partial}{\partial x_i}(\dot{u}_i^o - \dot{v}_i^o) = -\frac{n_o}{\bar{\rho}_w} \frac{\partial \bar{\rho}_w}{\partial t} \qquad (2.2.9)$$

If there is air in the porewater, the compressibility of the pore fluid (water plus a small amount of air) is significantly different from the compressibility of pure water. The combined air-water compressibility β' is defined by the relation

$$\beta' \, dp^o = \frac{d\bar{\rho}_w}{\bar{\rho}_w} \tag{2.2.10}$$

where β' is related to the compressibility of pure water β and the degree of saturation of soils s_r by

$$\beta' = \beta + \frac{1-s_r}{p_a} \tag{2.2.11}$$

in which p_a is the absolute porewater pressure which may be approximated by the absolute static pressure for wave-induced pressure fluctuations in soils [Yamamoto (1977)].

It follows that (2.2.9) may be written

$$\frac{\partial \dot{v}_i^o}{\partial x_i} + n_o \frac{\partial}{\partial x_i} (\dot{u}_i^o - \dot{v}_i^o) = -\beta' n_o \frac{\partial p^o}{\partial t} \tag{2.2.12}$$

This is the storage equation which physically states that the rate of change of fluid pressure is due to the dilation of pore fluid and the volume strain of the soil skeleton.

The quasi-static assumption for the sandy sea bed implies that the relative velocity between pore fluid and the solid skeleton is small [Mynett and Mei (1982)], i.e. $\dot{u}_i^o \simeq \dot{v}_i^o$; thus, (2.2.12) takes the form

$$\frac{\partial \dot{v}_i^o}{\partial x_i} = -\beta' n_o \frac{\partial p^o}{\partial t} \tag{2.2.13}$$

Eliminating the pressure term by using the derivative of (2.2.4) with respect to time

$$\frac{\partial p^o}{\partial t} \delta_{ij} = \frac{\partial \tau'^o_{ij}}{\partial t} - \frac{\partial \tau^o_{ij}}{\partial t} \tag{2.2.14}$$

gives

$$\frac{\partial \tau_{ij}^{o}}{\partial t} = \frac{\partial \tau_{ij}'^{o}}{\partial t} + \frac{1}{\beta' n_o} \frac{\partial \dot{v}_i^{o}}{\partial x_i} \delta_{ij} \qquad (2.2.15)$$

Also taking a time derivative of Hooke's law for the effective stress $\tau_{ij}'^{o}$, and applying (2.2.6), yields

$$\frac{\partial \tau_{ij}'^{o}}{\partial t} = \frac{2G\nu}{1-2\nu} \delta_{ij} \frac{\partial \dot{v}_\ell^{o}}{\partial x_\ell} + G \left(\frac{\partial \dot{v}_i^{o}}{\partial x_j} + \frac{\partial \dot{v}_j^{o}}{\partial x_i}\right) \qquad (2.2.16)$$

Substitution into (2.2.15) yields

$$\frac{\partial \tau_{ij}^{o}}{\partial t} = G \left(\frac{\partial \dot{v}_i^{o}}{\partial x_j} + \frac{\partial \dot{v}_j^{o}}{\partial x_i}\right) + \left(\frac{2G\nu}{1-2\nu} + \frac{1}{\beta' n_o}\right) \frac{\partial \dot{v}_\ell^{o}}{\partial x_\ell} \delta_{ij} \qquad (2.2.17)$$

For plane strain, tensor contraction of (2.2.17) using (2.2.13) introduces the relation of total stress components and the porewater pressure [Mynett and Mei (1982)]

$$p^{o} = - \frac{\tau_{xx}^{o} + \tau_{yy}^{o}}{2(1+m_o)} \qquad (2.2.18a)$$

in which

$$m_o = \frac{\beta' n_o G}{1-2\nu} \qquad (2.2.18b)$$

and is a parameter indicating the relative stiffness between the solid matrix and the pore fluid. For a saturated soil, m_o is in the order of $0\ (10^{-2})$; thus, the pore pressure is approximately the negative of the average of two total normal stress components.

The governing equations, (2.2.8a) and (2.2.8b), will be solved for specified boundary conditions; the shear stress and normal stresses may be obtained from

$$\tau_{xy}^{o} = G \left(\frac{\partial u^{o}}{\partial y} + \frac{\partial v^{o}}{\partial x}\right) \qquad (2.2.19a)$$

$$\tau_{xx}^{o} = 2G \left(\frac{\partial u^{o}}{\partial x} + \frac{\nu}{1-2\nu} \left(\frac{\partial u^{o}}{\partial x} + \frac{\partial v^{o}}{\partial y}\right)\right) \qquad (2.2.19b)$$

$$\tau^{o}_{yy} = 2G \left(\frac{\partial v^{o}}{\partial y} + \frac{\nu}{1-2\nu} \left(\frac{\partial u^{o}}{\partial x} + \frac{\partial v^{o}}{\partial y}\right)\right) \qquad (2.2.19c)$$

The pore pressure is given by (2.2.18a), and the effective stresses are given by (2.2.4).

It is convenient to define dimensionless variables which will be denoted by upper case letters. Lengths and displacements are scaled by the effective caisson half-width, c; and stresses and pressures are scaled by the mudline pressure amplitude due to the free surface propagating waves, p_o. The dimensionless governing equations are given as

$$\nabla^2 U^{o} + \frac{1}{1-2\nu} \frac{\partial}{\partial X} \left(\frac{\partial U^{o}}{\partial X} + \frac{\partial V^{o}}{\partial Y}\right) = 0 \qquad (2.2.20a)$$

$$\nabla^2 V^{o} + \frac{1}{1-2\nu} \frac{\partial}{\partial Y} \left(\frac{\partial U^{o}}{\partial X} + \frac{\partial V^{o}}{\partial Y}\right) = 0 \qquad (2.2.20b)$$

2.2.2 The Boundary Layer Correction

The governing equation for the boundary layer correction will be derived from the momentum equations and the storage equation. Scaling techniques will be applied according to the characteristics of the boundary layer. Again, $(\ )^{b}$ denotes a parameter in the boundary layer.

Taking the leading terms of (2.2.1a) and (2.2.1b) yields

$$\rho_{so} (1-n_o) \frac{\partial \dot{v}_i^{b}}{\partial t} = \frac{\partial \tau'^{b}_{ij}}{\partial x_j} - (1-n_o) \frac{\partial P^{b}}{\partial x_i} + \frac{n_o^2}{k'} (\dot{u}_i^{b} - \dot{v}_i^{b}) \qquad (2.2.21a)$$

$$\rho_{wo} n_o \frac{\partial \dot{u}_i^{b}}{\partial t} = -n_o \frac{\partial P^{b}}{\partial x_i} - \frac{n_o^2}{k'} (\dot{u}_i^{b} - \dot{v}_i^{b}) \qquad (2.2.21b)$$

in which

$$k' = \frac{\mu}{\rho_{wo} g} \tag{2.2.21c}$$

and is the intrinsic permeability. Summing and applying (2.2.16) leads to

$$G\left(\frac{\partial^2 \overset{\bullet}{v}_i^b}{\partial x_j^2} + \frac{1}{1-2\nu} \frac{\partial}{\partial x_i} \frac{\partial \overset{\bullet}{v}_\ell^b}{\partial x_\ell}\right) - \frac{\partial}{\partial x_i} \frac{\partial P^b}{\partial t} = \rho_{so}(1-n_o) \frac{\partial^2 \overset{\bullet}{v}_i^b}{\partial t^2} + \rho_{wo} n_o \frac{\partial^2 \overset{\bullet}{u}_i^b}{\partial t^2} \tag{2.2.22a}$$

in vector form

$$G\left(\nabla^2 \dot{\vec{v}}^b + \frac{1}{1-2\nu} \nabla (\nabla \cdot \dot{\vec{v}}^b)\right) - \nabla P_t^b = \rho_{so}(1-n_o) \dot{\vec{v}}_{tt}^b + \rho_{wo} n_o \dot{\vec{u}}_{tt}^b \tag{2.2.22b}$$

Taking a derivative of (2.2.20b) with respect to x_i and applying (2.2.12) to eliminate the term of relative velocity of fluid and solid yields

$$k' \frac{\partial^2 p^b}{\partial x_i^2} = \frac{\partial \overset{\bullet}{v}_i^b}{\partial x_i} + \beta' n_o \frac{\partial p^b}{\partial t} - \rho_{wo} k' \frac{\partial^2 \overset{\bullet}{u}_i^b}{\partial x_i \partial t} \tag{2.2.23a}$$

in vector form

$$k' \nabla^2 p^b = \nabla \cdot \dot{\vec{v}}^b + \beta' n_o p_t^b - \rho_{wo} k' (\nabla \cdot \dot{\vec{u}}^b)_t \tag{2.2.23b}$$

In the boundary layer it is expected that $\frac{\partial}{\partial y} >> \frac{\partial}{\partial x}$. If the boundary thickness is denoted by δ, then

$$\frac{\partial/\partial x}{\partial/\partial y} \sim \left(\frac{\delta}{c}\right) << 1 \tag{2.2.24}$$

where c is the effective half-width of the caisson base and used as a

length scale. Hence, the combined momentum equation (2.2.22b) is dominated by the term

$$G \frac{\partial^2 \dot{\vec{v}}^b}{\partial y^2} \sim O\left(\frac{G}{\delta^2}\right) \dot{\vec{v}}^b \tag{2.2.25}$$

The inertia terms are negligible since

$$\frac{\rho_{so}(1-n_o)\ddot{\vec{v}}^b_{tt}}{G \frac{\partial^2 \dot{\vec{v}}^b}{\partial y^2}} \sim \frac{\rho_{so}\sigma^2\delta^2}{G} = \frac{\sigma^2\delta^2}{c_s^2} = \frac{\delta^2}{\ell^2} << 1 \tag{2.2.26}$$

in which σ is the angular wave frequency; c_s is the shear wave velocity and defined as $\sqrt{\frac{G}{\rho_{so}}}$; and ℓ is the shear wave length.

Likewise, the inertia term in (2.2.23b) is also neglected. Equations (2.2.22b) and (2.2.23b) consequently become

$$G\left(\nabla^2 \dot{\vec{v}}^b + \frac{1}{1-2\nu}\nabla\left(\nabla \cdot \dot{\vec{v}}^b\right)\right) - \nabla p_t^b = 0 \tag{2.2.27}$$

$$k'\nabla^2 p^b = \nabla \cdot \dot{\vec{v}}^b + \beta' n_o p_t^b \tag{2.2.28}$$

To examine the order of the vertical and horizontal velocities of the solid skeleton, the curl of (2.2.27) is taken and it can be shown that

$$\nabla^2(\nabla \times \dot{\vec{v}}^b) = 0 \tag{2.2.29}$$

and since the dominant term in the LaPlacian is clearly $\frac{\partial^2}{\partial y^2}$, thus

$$\frac{\partial^2}{\partial y^2}(\nabla \times \dot{\vec{v}}^b) \simeq 0 \tag{2.2.30}$$

to the leading order. The curl $(\nabla \times \dot{\vec{v}}^b)$ vanishes identically outside the boundary, $|y| >> \delta$; therefore, it must be zero throughout, i.e.

$$\nabla \times \dot{\vec{v}}^b = 0 \tag{2.2.31}$$

Thus, the boundary layer correction of the solid velocity is irrotational and results in

$$\frac{\partial \dot{v}^b}{\partial x} = \frac{\partial \dot{u}^b}{\partial y} \tag{2.2.32}$$

which implies

$$\frac{\dot{u}^b}{\dot{v}^b} \sim 0 \left(\frac{\delta}{c}\right) << 1 \tag{2.2.33}$$

the horizontal velocity is much less than the vertical. Consequently, to the leading order the two components of (2.2.27) are given by

$$G\left(\frac{\partial^2 \dot{u}^b}{\partial y^2} + \frac{1}{1-2\nu} \frac{\partial^2 \dot{v}^b}{\partial x \partial y}\right) - \frac{\partial^2 p^b}{\partial x \partial t} = 0 \tag{2.2.34a}$$

$$G\left(\frac{\partial^2 \dot{v}^b}{\partial y^2} + \frac{1}{1-2\nu} \frac{\partial^2 \dot{v}^b}{\partial y^2}\right) - \frac{\partial^2 p^b}{\partial y \partial t} = 0 \tag{2.2.34b}$$

Integrating (2.2.34b) in y gives

$$G \frac{2(1-\nu)}{1-2\nu} \frac{\partial \dot{v}^b}{\partial y} = \frac{\partial p^b}{\partial t} \tag{2.2.35}$$

Because both v^b and p^b vanish outside the boundary layer, the integration constant that is a function of time also vanishes.

Similarly, taking the dominant terms of (2.2.28) yields

$$k' \frac{\partial^2 p^b}{\partial y^2} = \frac{\partial \dot{v}^b}{\partial y} + \beta' n_o \frac{\partial p^b}{\partial t} \tag{2.2.36}$$

Substituting $\frac{\partial \dot{v}^b}{\partial y}$ from (2.2.35), (2.2.36) takes the form

$$\frac{\partial p^b}{\partial t} = c_v \frac{\partial^2 p^b}{\partial y^2} \tag{2.2.37}$$

This is the one-dimensional Terzaghi consolidation equation in which c_v is the coefficient of consolidation.

$$c_v = k' \left(\beta' n_o + \frac{1}{G} \frac{1-2\nu}{2(1-\nu)}\right)^{-1} \tag{2.2.38}$$

It is useful to introduce dimensionless variables, which are denoted by upper case letters, to scale the problem. x is scaled by the effective caisson half-width c and y by the boundary layer thickness δ.

$$X = x/c \tag{2.2.39a}$$

$$Y^b = y/\delta \tag{2.2.39b}$$

and the time by the wave frequency

$$T^b = t\sigma \tag{2.2.39c}$$

(2.2.37) then takes the form

$$\frac{\partial p^b}{\partial T^b} = \frac{c_v}{\sigma\delta^2} \frac{\partial^2 p^b}{\partial (Y^b)^2} \tag{2.2.40}$$

The scale of the boundary layer thickness follows to be

$$\delta = \sqrt{\frac{k'}{\sigma}} \left(\beta' n_o + \frac{1}{G} \frac{1-2\nu}{2(1-\nu)}\right)^{-1/2} \tag{2.2.41}$$

The dynamic mudline pressure amplitude of the incident progressive wave p_o is used to scale both pore pressure and stresses

$$(P^b, T^b_{ij}) = (p^b, \tau^b_{ij})/p_o \tag{2.2.42}$$

Substituting the above dimensionless variables into (2.2.35) yields

$$G \frac{2(1-\nu)}{1-2\nu} \frac{\partial \dot{v}^b}{\delta \partial Y^b} = p_o \sigma \frac{\partial P^b}{\partial T^b} \tag{2.2.43}$$

This suggests a dimensionless solid vertical velocity

$$\dot{V}^b = \dot{v}^b / \frac{p_o \sigma \delta}{G} = \dot{v}^b / \frac{p_o \sigma c}{G} \left(\frac{\delta}{c}\right) \tag{2.2.44}$$

and from (2.2.33) the dimensionless solid horizontal velocity appears to be

$$\dot{U}^b = \dot{u}^b / \frac{p_o \sigma c}{G} \left(\frac{\delta}{c}\right)^2 \tag{2.2.45}$$

In a dimensionless form the consolidation equation (2.2.40) reads

$$\frac{\partial P^b}{\partial T^b} = \frac{\partial^2 P^b}{\partial (Y^b)^2} \tag{2.2.46}$$

This is the governing equation of porewater pressure in the boundary layer.

The dimensionless solid vertical velocity correction is readily obtained from (2.2.43)

$$\frac{\partial \dot{V}^b}{\partial Y^b} = \frac{1-2\nu}{2(1-\nu)} \frac{\partial P^b}{\partial T^b} \tag{2.2.47a}$$

and the horizontal from (2.2.34a) and (2.2.45)

$$\frac{\partial^2 \dot{U}^b}{\partial (Y^b)^2} = \frac{1-2\nu}{2(1-\nu)} \frac{\partial P^b}{\partial X \partial T^b} \tag{2.2.47b}$$

Hence, the dimensionless solid velocities, $\dot{U}^b$ and $\dot{V}^b$, can be expressed in terms of dimensionless pore pressure P^b.

Also from Hooke's law and (2.2.47), taking the dominant terms, the dimensionless effective normal stresses are obtained.

$$T'^b_{xx} = \frac{\nu}{1-\nu} P^b \tag{2.2.48a}$$

$$T'^b_{yy} = P^b \tag{2.2.48b}$$

and the irrotationality of (2.2.31) implies that the shear stress is zero, i.e.

$$T^b_{xy} = 0 \quad (2.2.48c)$$

If the outer region variables are introduced

$$\delta Y^b = cY \quad (2.2.49)$$

and

$$\varepsilon = \frac{\delta}{c} \quad (2.2.50)$$

then the solid velocities are given as

$$\dot{V}^b(Y) = \varepsilon \frac{1-2\nu}{2(1-\nu)} \int \frac{\partial P^b}{\partial T^b} dY^b \quad (2.2.51a)$$

$$\dot{U}^b(Y) = \varepsilon^2 \frac{1-2\nu}{2(1-\nu)} \int [\int \frac{\partial^2 P^b}{\partial X \partial T^b} dY^b] dY^b \quad (2.2.51b)$$

after variables are changed. Thus, the displacement components for boundary layer correction are at most of order ε and can be ignored.

The boundary layer correction is summarized as

$$\begin{Bmatrix} P^b \\ T'^b_{xx} \\ T'^b_{yy} \\ T^b_{xy} \end{Bmatrix} = \begin{Bmatrix} 1 \\ \frac{\nu}{1-\nu} \\ 1 \\ 0 \end{Bmatrix} P^b \quad (2.2.52)$$

Only P^b remains unknown and is obtained by solving (2.2.46) with specified boundary conditions.

2.3 Boundary Conditions

The boundary conditions for the wave-soil-caisson problem are:

1. Along the exposed portion of the mudline, the wave pressure and the total normal stress are continuous and the shear stress is negligible [McDougal et al. (1981)].
2. Under the structure, the displacements are continuous at the caisson-soil interface.
3. At the bottom of the soil along an underlying rigid bed, no- slip conditions are imposed.

For convenience, all length scales will be nondimensionalized by c (the effective half-width of the caisson), and the pore pressure and stresses are nondimensionalized by p_o (the incident wave mudline pressure amplitude). Dimensionless variables are denoted with upper case letters. Mathematically, these conditions for the exposed portion of the mudline are expressed as

$$T_{xy}(X,0) = 0 \qquad ; 1 < |X| < \infty \qquad (2.3.1a)$$

$$T_{yy}(X,0) = -P_w(X)e^{-i\sigma t} \qquad ; 1 < |X| < \infty \qquad (2.3.1b)$$

in which $P_w(X)$ is the pressure distribution function along the mudline. Underneath the caisson, the displacement boundary conditions read

$$U(X,0)\big|_{caisson} = U(X,0)\big|_{soil} \qquad ; |X| < 1 \qquad (2.3.2a)$$

$$V(X,0)\big|_{caisson} = V(X,0)\big|_{soil} \qquad ; |X| < 1 \qquad (2.3.2b)$$

Along the underlying rigid bed, the no-slip conditions are

$$U(X,D) = 0 \qquad ;0<|X|<\infty \qquad (2.3.3a)$$

$$V(X,D) = 0 \qquad ;0<|X|<\infty \qquad (2.3.3b)$$

These boundary conditions are summarized in Fig. 2.3.1.

The soil displacement and the caisson motion are coupled. The wave forces along the exposed portion of the mudline induce soil stresses and displacements underneath the caisson. The wave forces on the caisson induce caisson motions which result in stresses and displacements in the soil away from the caisson. Linearity allows these two effects to be decoupled into scattering and radiation problems. In the scattering problem, the caisson is assumed to be fixed and the soil response is completely driven by the wave pressure on the mudline. The forces on the caisson determined in the scattering problem are applied on the caisson in the radiation problem. These forces result in caisson motion on an otherwise static seabed. The sum of these two components, the scattering problem and the radiation problem, yields the total response. This technique is illustrated in Fig. 2.3.2.

2.3.1 The Outer Region Problem

2.3.1.1 The Scattering Problem. For the scattering problem the caisson is fixed and the mudline boundary conditions are

$$T^{o}_{xy}(X,0) = 0 \qquad ;0<|X|<\infty \qquad (2.3.4a)$$

$$T^{o}_{yy}(X,0) = -P_{w}(X)e^{-i\sigma t} \qquad ;1<|X|<\infty \qquad (2.3.4b)$$

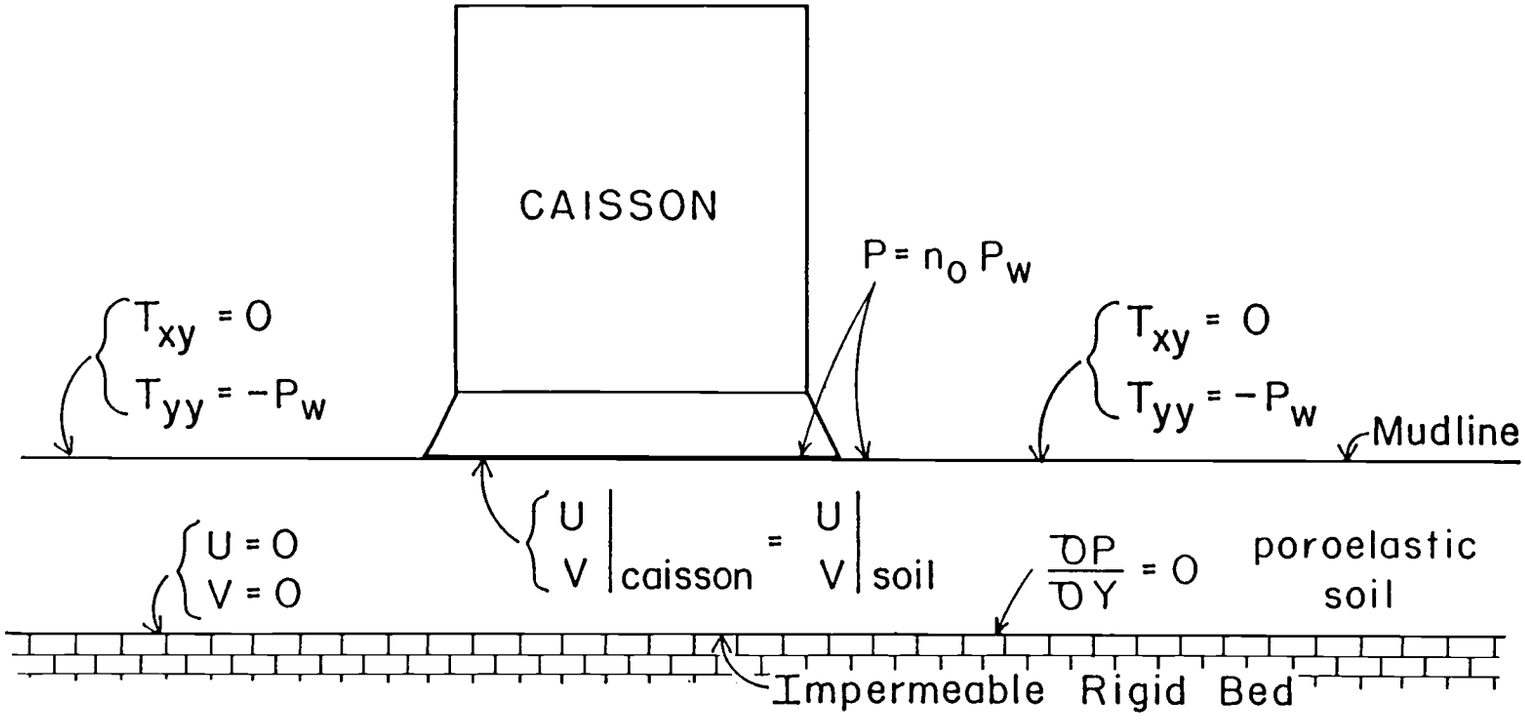

Figure 2.3.1. Boundary conditions for the wave-soil-caisson problem.

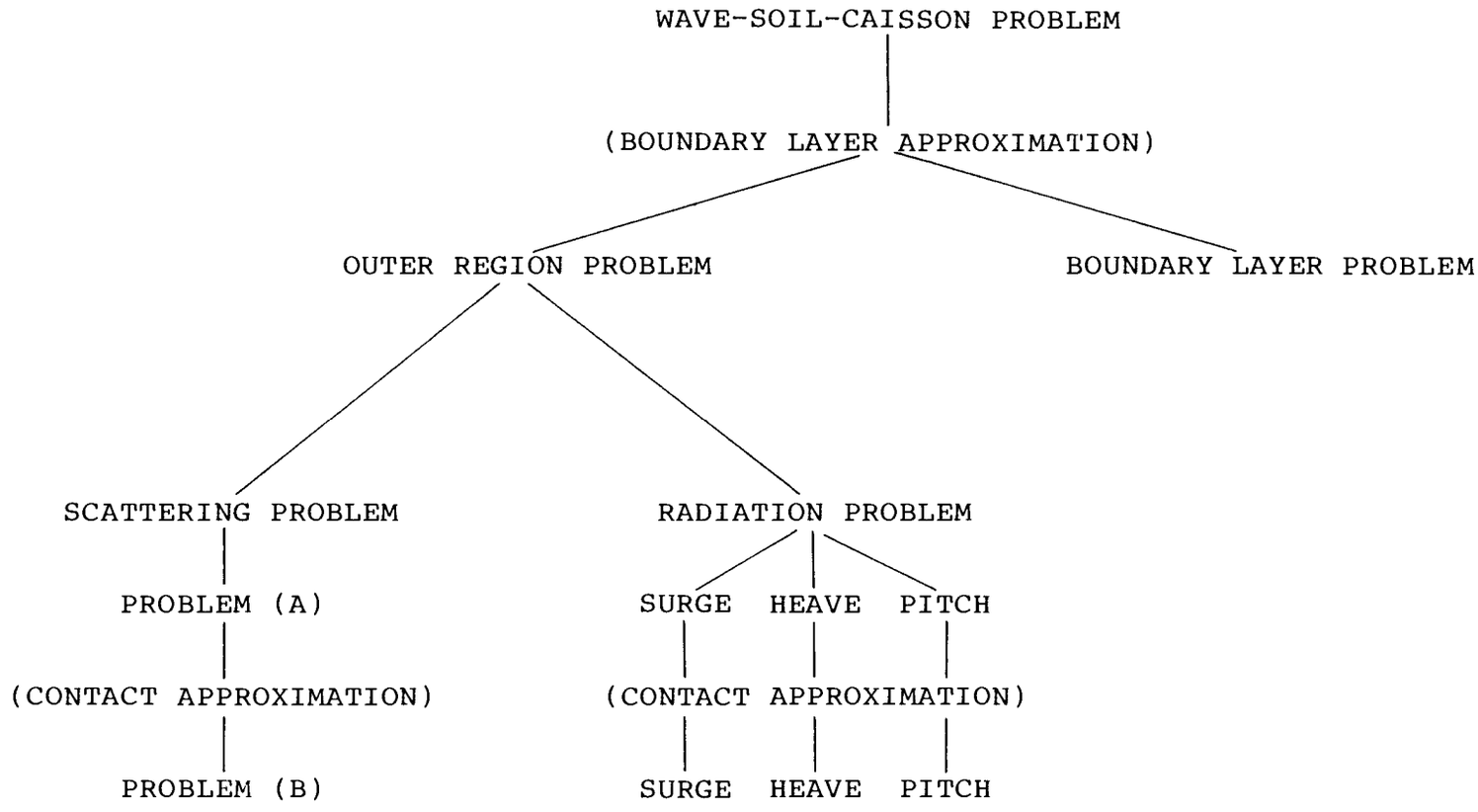

Figure 2.3.2. Decomposition of the wave-soil-caisson problem.

$$U^o(X,0) = 0 \qquad ;|X|<1 \qquad (2.3.4c)$$

$$V^o(X,0) = 0 \qquad ;|X|<1 \qquad (2.3.4d)$$

and, along the underlying rigid bed, no-displacement conditions given by (2.3.3a) and (2.3.3b) are imposed. The conditions along the mudline yield a mixed boundary-value problem. This is addressed by seeking a sequence of two solutions: one which satisfies the stress boundary conditions [problem (a)] and then one which satisfies the displacement boundary conditions [problem (b)].

The mudline boundary conditions for problem (a) are

$$^{a}T^{o}_{xy}\ (X,0) = 0 \qquad ;0<|X|<\infty \qquad (2.3.5a)$$

$$^{a}T^{o}_{yy}\ (X,0) = \begin{cases} -P_w(X)e^{-i\sigma t} & ;1<|X|<\infty \\ 0 & ;|X|<1 \end{cases} \qquad (2.3.5b)$$

The solution for the mudline stress boundary conditions (and no-displacements at the lower rigid bed) yields a solution for the displacements along the mudline: $^{a}U^{o}(X,0)$ and $^{a}V^{o}(X,0)$. These displacements are modified to provide the boundary conditions for problem (b). The first modification is that under the structure the displacements are set equal zero. The second modification is based on the solution to the contact problem on a thin layer developed by Alblas and Kuipers (1969). This solution provides appropriate displacements adjacent to the structure. This solution has been extended to the surge displacement and made applicable for all $|X|>1$. Details are presented in Appendix B. The resulting boundary conditions for problem (b) are

$$b_{U^o}(X,0) = \begin{cases} a_{U^o}(X,0)\ \mathrm{th}\left(2\sqrt{\frac{(1-\nu)(-1-X)}{\pi D}}\right) & ;-\infty<X\leq -1 \\ 0 & ;|X|\leq 1 \\ a_{U^o}(X,0)\ \mathrm{th}\left(2\sqrt{\frac{(1-\nu)(X-1)}{\pi D}}\right) & ;1\leq X<\infty \end{cases} \qquad (2.3.6a)$$

$$b_{V^o}(X,0) = \begin{cases} a_{V^o}(X,0)\ \mathrm{th}\left(2\sqrt{\frac{A(-1-X)}{\pi D}}\right) & ;-\infty<X<-1 \\ 0 & ;|X|\leq 1 \\ a_{V^o}(X,0)\ \mathrm{th}\left(2\sqrt{\frac{A(X-1)}{\pi D}}\right) & ;1\leq X<\infty \end{cases} \qquad (2.3.6b)$$

The functions cosh(x), sinh(x), and tanh(x) are abbreviated as ch(x), sh(x), and th(x), respectively. The solutions for these mudline displacement boundary conditions (and no-slip bottom conditions) satisfy the original mixed boundary-value problem with (2.3.4) on the mudline.

These boundary conditions for the scattering problem are illustrated in Fig. 2.3.3.

2.3.1.2 The Radiation Problem The radiation problem is a moving caisson on an otherwise static soil. The response of the soil must satisfy the caisson displacement conditions on the mudline. The caisson responds to both wave and soil loadings from the scattering problem and the resistance to deformation in the radiation problem. The scattering loads are known but the motion is still unknown. A dynamic boundary condition must also be prescribed to solve for the unknown caisson motion. This condition yields the amplitude of the caisson motion.

Underneath the caisson the motions are specified while on the exposed portion of the mudline zero stress conditions apply. Mathematically, these conditions are as follows.

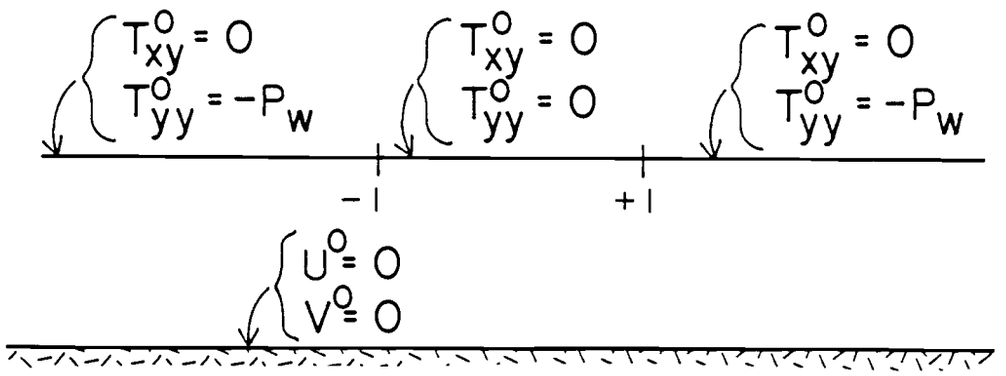

problem (a)

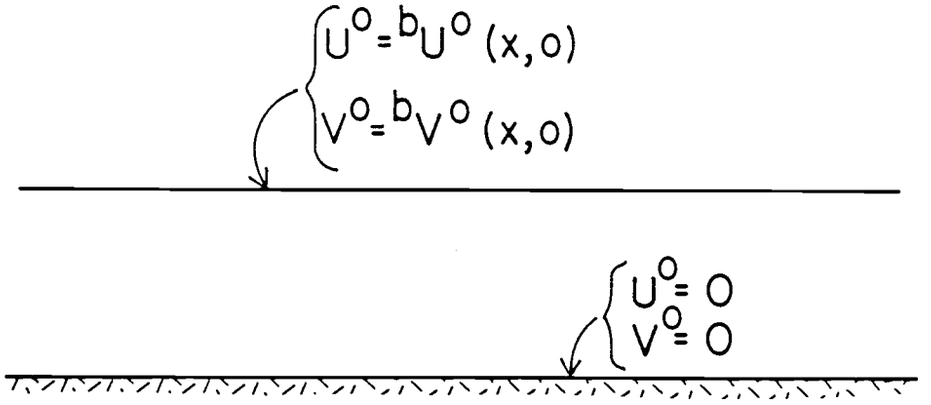

problem (b)

Figure 2.3.3. Boundary conditions for the outer scattering problem.

$$T^{o}_{xy}(X,0) = 0 \qquad ;1<|X|<\infty \qquad (2.3.7a)$$

$$T^{o}_{yy}(X,0) = 0 \qquad ;1<|X|<\infty \qquad (2.3.7b)$$

$$U^{o}(X,0)\big|_{caisson} = U^{o}\big|_{soil} \qquad ;|X|<1 \qquad (2.3.7c)$$

$$V^{o}(X,0)\big|_{caisson} = V^{o}\big|_{soil} \qquad ;|X|<1 \qquad (2.3.7d)$$

These boundary conditions are of the mixed-type, and are depicted in Fig. 2.3.4.

The caisson motion and the accompanying soil deformation are coupled. However, linearity allows the soil response to be decomposed into three problems corresponding to each of the three degrees of freedom of caisson motion. The caisson is assumed to be rigid and the effects of the structural damping in the caisson are assumed to be negligible compared with the soil.

According to (2.3.7), the respective boundary conditions at the mudline for the problems of surge, heave and pitch are the following.

(1). Surge

Assume the normal stress T^{o}_{yy} at the caisson-soil interface is negligibly small. Thus the boundary conditions for the problem of surge are

$$T^{o}_{yy}(X,0) = 0 \qquad ;0<|X|<\infty \qquad (2.3.8a)$$

$$T^{o}_{xy}(X,0) = 0 \qquad ;1<|X|<\infty \qquad (2.3.8b)$$

$$U^{o}(X,0) = U^{o}_{c} \qquad ;|X|<1 \qquad (2.3.8c)$$

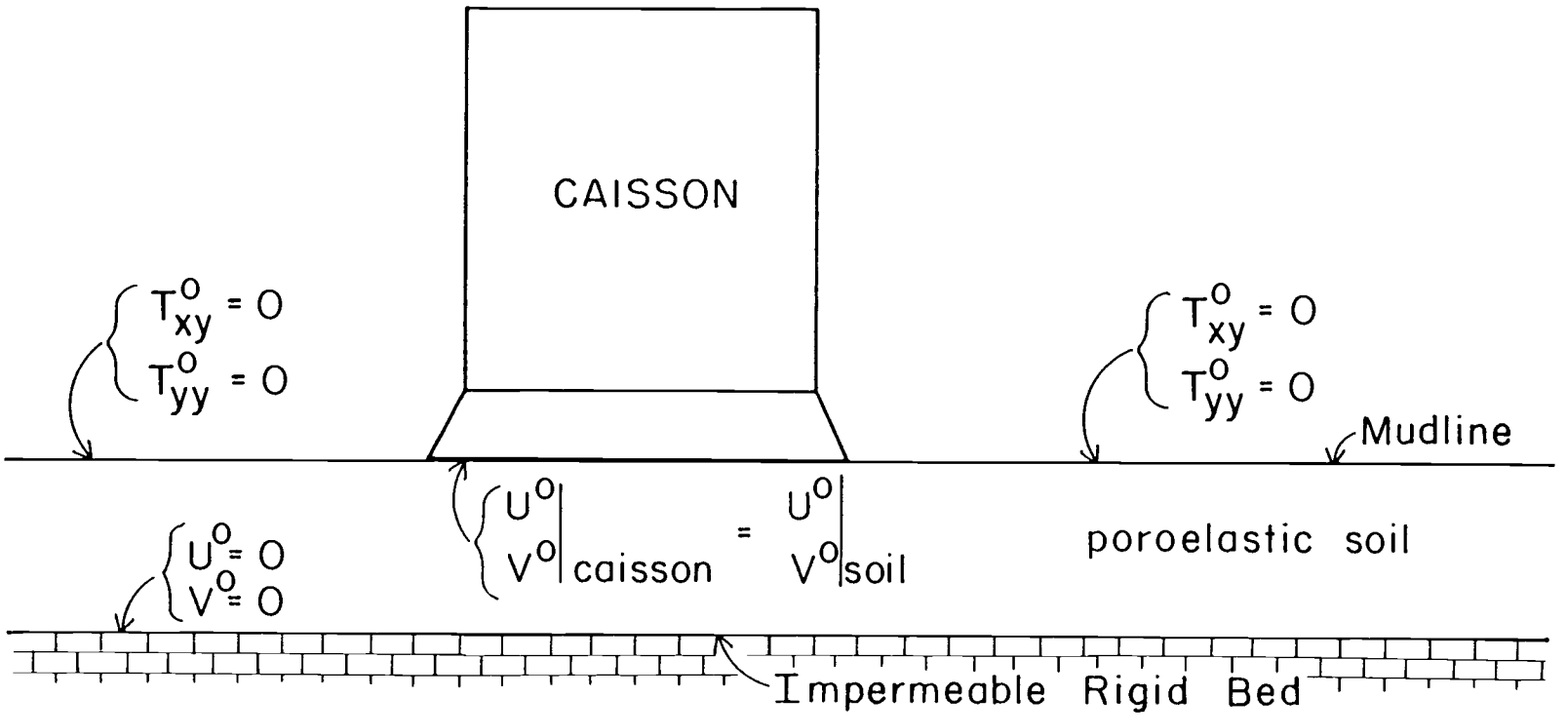

Figure 2.3.4. Boundary conditions for the outer radiation problem.

(2). Heave

Assuming the shear stress T^o_{xy} at the caisson-soil interface is negligibly small results in the following boundary conditions.

$$T^o_{xy}(X,0) = 0 \qquad ;0<|X|<\infty \qquad (2.3.9a)$$

$$T^o_{yy}(X,0) = 0 \qquad ;1<|X|<\infty \qquad (2.3.9b)$$

$$V^o(X,0) = V^o_c \qquad ;|X|<1 \qquad (2.3.9c)$$

(3). Pitch

Assuming the shear stress T^o_{xy} at the caisson-soil interface is negligibly small results in the following boundary conditions.

$$T^o_{xy}(X,0) = 0 \qquad ;0<|X|<\infty \qquad (2.3.10a)$$

$$T^o_{yy}(X,0) = 0 \qquad ;1<|X|<\infty \qquad (2.3.10b)$$

$$V^o = -\alpha_c X \qquad ;|X|<1 \qquad (2.3.10c)$$

These conditions are still of the mixed-type. Displacement conditions over the entire upper boundary may be written by introducing ${}^1U^o_f$, ${}^2V^o_f$, and ${}^3V^o_f$, which account for the unknown displacements along the exposed portion of the mudline.

(1) surge

$$T^o_{yy}(X,0) = 0 \qquad ;0<|X|<\infty \qquad (2.3.11a)$$

$$U^o(X,0) = U_c + {}^1U^o_f \qquad ;0<|X|<\infty \qquad (2.3.11b)$$

(2) heave

$$T^o_{xy}(X,0) = 0 \qquad ;0<|X|<\infty \qquad (2.3.12a)$$

$$V^o(X,0) = V_c + {}^2V_f^o \qquad ;0<|X|<\infty \qquad (2.3.12b)$$

(3) pitch

$$T_{xy}^o(X,0) = 0 \qquad ;0<|X|<\infty \qquad (2.3.13a)$$

$$V^o(X,0) = -\alpha_c X + {}^3V_f^o \qquad ;0<|X|<\infty \qquad (2.3.13b)$$

These are no longer mixed-type boundary conditions, and the boundary-value problem can be easily solved. In (2.3.11b), (2.3.12b), and (2.3.13b), the displacements ${}^1U_f^o$, ${}^2V_f^o$, and ${}^3V_f^o$ can be evaluated by employing the thin soil layer contact problem solution technique presented in Appendix B. The assumption of thin layer [i.e. (d <<2c)] is to ensure negligible stresses along the exposed surface. This assumption will be examined numerically in Chapter 4. To satisfy the original boundary conditions, the solutions for the above assumed boundary conditions are expected to produce relatively small stresses along the exposed seabed surface. From Appendix B

$${}^1U_f^o = U_c \begin{cases} 1 - \text{th}\left(2\sqrt{\dfrac{(1-\nu)(-1-X)}{\pi D}}\right) & ;-\infty<X\leq -1 \\ 1 - \text{th}\left(2\sqrt{\dfrac{(1-\nu)(X-1)}{\pi D}}\right) & ;1\leq X<\infty \end{cases} \qquad (2.3.14a)$$

$${}^2V_f^o = V_c \begin{cases} 1-\text{th}\left(2\sqrt{\dfrac{A\,(-1-X)}{\pi D}}\right) & ;-\infty<X\leq -1 \\ 1-\text{th}\left(2\sqrt{\dfrac{A\,(X-1)}{\pi D}}\right) & ;1\leq X<\infty \end{cases} \qquad (2.3.14b)$$

$${}^3V_f^o = X_c \begin{cases} 1-\text{th}\left\{2\sqrt{\dfrac{A\,(-1-X)}{\pi D}}\left(1 + i\,\hat{\underline{S}}'(0)\right)\right\} & ;-\infty<X\leq -1 \\ 1-\text{th}\left\{2\sqrt{\dfrac{A\,(X-1)}{\pi D}}\left(1 + i\,\hat{\underline{S}}'(0)\right)\right\} & ;1\leq X<\infty \end{cases} \qquad (2.3.14c)$$

In (2.3.8c), (2.3.9c) and (2.3.10c), U_c, V_c, and α_c are the displacements of the caisson in surge, heave and pitch, respectively. A positive α_c is in the counterclockwise direction. These displacements are unknown, but may be determined from the dynamic boundary conditions on the soil-caisson interface. These conditions are determined from the equations of the motion of the caisson.

$$\begin{pmatrix} m & 0 & 0 \\ 0 & m & 0 \\ 0 & 0 & I_m \end{pmatrix} \begin{Bmatrix} \ddot{u}_c \\ \ddot{v}_c \\ \ddot{\alpha}_c \end{Bmatrix} = \begin{Bmatrix} f_{w1} \\ f_{w2} \\ f_{w3} \end{Bmatrix} + \begin{Bmatrix} f_{s1} \\ f_{s2} \\ f_{s3} \end{Bmatrix} + \begin{Bmatrix} f_{r1} \\ f_{r2} \\ f_{r3} \end{Bmatrix} \qquad (2.3.15)$$

where m is the mass of the caisson, I_m is the inertia moment of mass of the caisson, $\ddot{u}_c$, $\ddot{v}_c$, and $\ddot{\alpha}_c$ are the accelerations of the surge, heave, and pitch of the caisson, respectively; f_{wj} are the wave forces on the caisson; f_{sj} are the exciting soil loads on the caisson determined in the scattering problem; and f_{rj} are the restoring forces on the caisson when the caisson is moving. The exciting and restoring forces are obtained by integrating the stresses along the caisson-seabed interface.

2.3.2 The Boundary Layer Corrections

Along the mudline, the summation of the pressure from the boundary correction and outer region solution is equal to the wave-induced porewater pressure. Along the rigid bed underlying the soil, the normal derivative of the pore pressure must be zero, i.e.

at Y=0 $$P^o + P^b = n_o P_w(X) \qquad 0 \leq |X| < \infty \qquad (2.3.18)$$

at Y=D $$\frac{\partial(P^o + P^b)}{\partial Y} = 0 \qquad 0 \leq |X| < \infty \qquad (2.3.19)$$

3. SOLUTIONS TO THE ANALYTICAL MODEL

3.1 General Solution to the Dynamic Response of the Soil Skeleton

For convenience, the non-dimensionalized elastic equations (2.2.20a) and (2.2.20b) are rewritten

$$\nabla^2 U^o + \frac{1}{1-2\nu}\frac{\partial}{\partial X}\left(\frac{\partial U^o}{\partial X} + \frac{\partial V^o}{\partial Y}\right) = 0 \qquad (3.1.1a)$$

$$\nabla^2 V^o + \frac{1}{1-2\nu}\frac{\partial}{\partial Y}\left(\frac{\partial U^o}{\partial X} + \frac{\partial V^o}{\partial Y}\right) = 0 \qquad (3.1.1b)$$

Since the poroelastic layer occupies the space $-\infty < X < \infty$, $0 < Y < D$, a Fourier transform may be applied with respect to X to equation (3.1.1). Consequently, the transformed equations are

$$-s^2 \hat{U}^o + \frac{\partial^2 \hat{U}^o}{\partial Y^2} + \frac{1}{1-2\nu}\left(-s^2 \hat{U}^o + is\frac{\partial \hat{V}^o}{\partial Y}\right) = 0 \qquad (3.1.2a)$$

$$-s^2 \hat{V}^o + \frac{\partial^2 \hat{V}^o}{\partial Y^2} + \frac{1}{1-2\nu}\left(is\frac{\partial \hat{U}^o}{\partial Y} + \frac{\partial^2 \hat{V}^o}{\partial Y^2}\right) = 0 \qquad (3.1.2b)$$

where the Fourier transform is denoted as

$$\hat{U}^o = \hat{U}^o(s,Y) = \frac{1}{\sqrt{2\pi}}\int_{-\infty}^{\infty} U^o(X,Y)e^{-isX}dX \qquad (3.1.3a)$$

$$\hat{V}^o = \hat{V}^o(s,Y) = \frac{1}{\sqrt{2\pi}}\int_{-\infty}^{\infty} V^o(X,Y)e^{-isX}dX \qquad (3.1.3b)$$

and the transform of a derivative is given by

$$\frac{1}{\sqrt{2\pi}}\int_{-\infty}^{\infty}\frac{\partial U^o}{\partial X}e^{-isX}dX = is\,\hat{U}^o \qquad (3.1.3c)$$

Since s can be treated as a parameter in the above equations, $\hat{U}^o$ and $\hat{V}^o$ are functions of Y only. Thus, (3.1.2) is a second-order ordinary simultaneous differential equation.

$$\frac{d^2\hat{U}^o}{dY^2} - \frac{2(1-\nu)s}{1-2\nu}\hat{U}^o + \frac{is}{1-2\nu}\frac{d\hat{V}^o}{dY} = 0 \qquad (3.1.4a)$$

$$\frac{is}{1-2\nu}\frac{d\hat{U}^o}{dY} + \frac{2(1-\nu)}{1-2\nu}\frac{d^2\hat{V}^o}{dY^2} - s^2\hat{V}^o = 0 \qquad (3.1.4b)$$

Written in matrix form, (3.1.4) yields

$$\begin{bmatrix} \mathbf{D}^2 - \frac{2(1-\nu)s^2}{1-2\nu} & \frac{is}{1-2\nu}\mathbf{D} \\ \frac{is}{1-2\nu}\mathbf{D} & \frac{2(1-\nu)}{1-2\nu}\mathbf{D}^2 - s^2 \end{bmatrix} \begin{Bmatrix} \hat{U}^o \\ \hat{V}^o \end{Bmatrix} = 0 \qquad (3.1.5)$$

in which **D** is the differential operator. This is a system of two simultaneous, linear and homogeneous ordinary differential equations of second order. Employing Cramer's rule [Wylie and Barret (1982)], if (3.1.5.) has a nontrivial solution, then its characteristic equation is

$$\begin{vmatrix} \lambda^2 - \frac{2(1-\nu)s^2}{1-2\nu} & \frac{is}{1-2\nu}\lambda \\ \frac{is}{1-2\nu}\lambda & \frac{2(1-\nu)}{1-2\nu}\lambda^2 - s^2 \end{vmatrix} = 0 \qquad (3.1.6)$$

When expanded, (3.1.6) is a fourth degree equation in λ:

$$\lambda^4 - 2s^2\lambda^2 + s^4 = 0 \qquad (3.1.7)$$

Solving for λ yields two sets of double roots.

$$\lambda = \pm s \; ; \pm s \tag{3.1.8}$$

Since (3.1.7) is of order four, the number of independent constants in the general solution of the system must also be four. Also, because of the finite thickness of the elastic layer, the solutions are given by hyperbolic functions as opposed to exponential solutions.

$$\hat{U}^o(s,Y) = a_1 ch(sY) + a_2 sh(sY) + a_3 Ych(sY) + a_4 Ysh(sY) \tag{3.1.9a}$$

$$\hat{V}^o(s,Y) = b_1 ch(sY) + b_2 sh(sY) + b_3 Ych(sY) + b_4 Ysh(sY) \tag{3.1.9b}$$

There are eight unknown coefficients and only four boundary conditions. Four of the constants are not independent. Substituting (3.1.9) into (3.1.4) and requiring the coefficients of ch(sY), sh(sY), Ych(sY) and Ysh(sY) to satisfy the equations yield

$$b_1 = i\left[(3-4\nu)\frac{a_3}{s} - a_2\right] \tag{3.1.10a}$$

$$b_2 = i\left[(3-4\nu)\frac{a_4}{s} - a_2\right] \tag{3.1.10b}$$

$$b_3 = -ia_4 \tag{3.1.10c}$$

$$b_4 = -ia_3 \tag{3.1.10d}$$

Accordingly, the general solution takes the form

$$\hat{U}^o(s,Y) = a_1 ch(sY) + a_2 sh(sY) + a_3 Ych(sY) + a_4 Ysh(sY) \tag{3.1.11a}$$

$$\hat{V}^o(s,Y) = -i\{a_1 sh(sY) + a_2 ch(sY) + a_3[Ysh(sY) - \frac{3-4\nu}{s} ch(sY)]$$

$$+ a_4[Ych(sY) - \frac{3-4\nu}{s} sh(sY)]\} \qquad (3.1.11b)$$

The coefficients a_1, a_2, a_3, and a_4 will be quantified by applying the proper boundary conditions.

Taking inverse transformations, (3.1.11a) and (3.1.11b) read

$$U^o(X,Y) = \frac{1}{\sqrt{2\pi}} \int_{-\infty}^{\infty} \hat{U}^o(s,Y) e^{isX} ds \qquad (3.1.12a)$$

$$V^o(X,Y) = \frac{1}{\sqrt{2\pi}} \int_{-\infty}^{\infty} \hat{V}^o(s,Y) e^{isX} ds \qquad (3.1.12b)$$

For evaluating stresses, the following derivatives are required,

$$\frac{\partial U^o}{\partial X} = \frac{1}{\sqrt{2\pi}} \int_{-\infty}^{\infty} is\, \hat{U}^o(s,Y) e^{isX} ds \qquad (3.1.13a)$$

$$\frac{\partial U^o}{\partial Y} = \frac{1}{\sqrt{2\pi}} \int_{-\infty}^{\infty} \frac{\partial \hat{U}^o(s,Y)}{\partial Y} e^{isX} ds \qquad (3.1.13b)$$

$$\frac{\partial V^o}{\partial X} = \frac{1}{\sqrt{2\pi}} \int_{-\infty}^{\infty} is\, \hat{V}^o(s,Y) e^{isX} ds \qquad (3.1.13c)$$

$$\frac{\partial V^o}{\partial Y} = \frac{1}{\sqrt{2\pi}} \int_{-\infty}^{\infty} \frac{\partial \hat{V}^o(s,Y)}{\partial Y} e^{isX} ds \qquad (3.1.13d)$$

The inverse Fourier transform cannot be evaluated explicitly, but can be evaluated with a fast Fourier transform technique.

A superscript a,b,1,2, or 3 will be used to denote the quantities referring to problem (a), problem (b), surge, heave, and pitch, respectively, when the boundary conditions are applied.

3.2 Solutions for the Scattering Problem

3.2.1 Problem (a)

The general solution for this problem has been given by (3.1.11). The homogeneous boundary conditions (2.3.3a), (2.3.3b) and (2.3.5a) enable the determination of ${}^{a}a_2$, ${}^{a}a_3$, ${}^{a}a_4$ in terms of ${}^{a}a_1$. Then ${}^{a}a_1$ is determined by the total normal stress boundary condition at the mudline,(2.3.5b). It follows that

$$ {}^{a}a_1 = \frac{[(1-2\nu)(3-4\nu)sh^2(sD) - s^2D^2]\ \hat{f}_w(s)}{s[(1-2\nu)^2 + (3-4\nu)ch^2(sD) + s^2D^2]} \tag{3.2.1a} $$

$$ {}^{a}a_2 = \frac{(1-2\nu)[sD - (3-4\nu)ch(sD)sh(sD)]\ \hat{f}_w(S)}{s[(1-2\nu)^2 + (3-4\nu)ch^2(sD) + s^2D^2]} \tag{3.2.1b} $$

$$ {}^{a}a_3 = \frac{[sD - (3-4\nu)ch(sD)sh(sD)]\ \hat{f}_w(s)}{(1-2\nu)^2 + (3-4\nu)\ ch^2(sD) + s^2D^2} \tag{3.2.1c} $$

$$ {}^{a}a_4 = \frac{[(3-4\nu)ch^2(sD) - (1-2\nu)]\ \hat{f}_w(s)}{(1-2\nu)^2 + (3-4\nu)ch^2(sD) + s^2D^2} \tag{3.2.1d} $$

where

$$ \hat{f}_w(s) = \frac{i}{2G}\ \hat{P}_w(s)e^{-i\sigma t} \tag{3.2.2} $$

3.2.2 Problem (b)

Taking the Fourier transforms of the boundary conditions (2.3.3a), (2.3.3b), (2.3.6a) and (2.3.6b), the unknown coefficients in (3.1.11) are obtained without difficulty.

$$ {}^{b}a_1 = {}^{b}\hat{U}^{o}\ (s,0) \tag{3.2.3a} $$

$$b_{a_2} = \frac{-b\hat{U}^o(s,0)\left[D - \frac{3-4\nu}{s}\,ch(sD)sh(sD)\right]\frac{3-4\nu}{s} + iD^2 b\hat{V}^o(s,D)}{D^2 - \left(\frac{3-4\nu}{s}\right)^2 sh^2(sD)} \tag{3.2.3b}$$

$$b_{a_3} = \frac{-b\hat{U}^o(s,0)\left[D - \frac{3-4\nu}{s}\,ch(sD)sh(sD)\right] + i\,\frac{3-4\nu}{s}\,b\hat{V}^o(s,0)sh^2(sD)}{D^2 - \left(\frac{3-4\nu}{s}\right)^2 sh^2(sD)} \tag{3.2.3c}$$

$$b_{a_4} = \frac{-\frac{3-4\nu}{s}\,b\hat{U}^o(s,0)sh^2(sD) - ib\hat{V}^o(s,0)\left[D + \frac{3-4\nu}{s}\,ch(sD)sh(sD)\right]}{D^2 - \left(\frac{3-4\nu}{s}\right)^2 sh^2(sD)} \tag{3.2.3d}$$

3.2.3 Soil Loads from the Scattering Problem

From (2.2.19a) and (2.2.19c), the Fourier transforms of the shear and vertical normal stresses on the caisson bottom due to the scattering problem are given by

$$b\hat{T}^o_{xy}\Big|_{Y=0} = G\left(\frac{\partial b\hat{U}^o}{\partial Y} + is\,b\hat{V}^o\right) \tag{3.2.4a}$$

$$b\hat{T}^o_{yy}\Big|_{Y=0} = 2G\left[\frac{\partial b\hat{V}^o}{\partial Y} + \frac{\nu}{1-2\nu}\left(is\,b\hat{U}^o + \frac{\partial b\hat{V}^o}{\partial Y}\right)\right] \tag{3.2.4b}$$

Integrating the stresses along the caisson base yields the horizontal, vertical and moment loads, respectively.

$$f_{s1} = c \int_{-1}^{1} \left[\frac{1}{\sqrt{2\pi}} \int_{-\infty}^{\infty} b\hat{T}^{o}_{xy}\Big|_{Y=0} e^{isX} ds\right] dX e^{-i\sigma t} = F_{s1} e^{-i\sigma t} \qquad (3.2.5a)$$

$$f_{s2} = c \int_{-1}^{1} \left[\frac{1}{\sqrt{2\pi}} \int_{-\infty}^{\infty} b\hat{T}^{o}_{yy}\Big|_{Y=0} e^{isX} ds\right] dX e^{-i\sigma t} = F_{s2} e^{-i\sigma t} \qquad (3.2.5b)$$

$$f_{s3} = -c^2 \int_{-1}^{1} X\left[\frac{1}{\sqrt{2\pi}} \int_{-\infty}^{\infty} b\hat{T}^{o}_{yy}\Big|_{Y=0} e^{isX} ds\right) dX e^{-i\sigma t} = F_{s3} e^{-i\sigma t} \qquad (3.2.5c)$$

3.3 Solutions for the Radiation Problem

3.3.1 Wave and Restoring Forces

Expressing the wave forces in terms of their complex amplitudes, F_{wj}, and simple periodic in time yields

$$f_{wj} = F_{wj} e^{-i\sigma t} \qquad (3.3.1)$$

The restoring forces are obtained by integrating stresses along the caisson base and can be expressed by the forces for unit motion.

$$f_{r1} = c \int_{-1}^{1} {}^{1}T^{o}_{xy}\Big|_{Y=0} dX = F_{r1} U_o e^{-i\sigma t} \qquad (3.3.2a)$$

$$f_{r2} = c \int_{-1}^{1} {}^{2}T^{o}_{yy}\Big|_{Y=0} dX = F_{r2} V_o e^{-i\sigma t} \qquad (3.3.2b)$$

$$f_{r3} = -c^2 \int_{-1}^{1} X\, {}^{3}T^{o}_{yy}\Big|_{Y=0} dX = F_{r3} \alpha_o e^{-i\sigma t} \qquad (3.3.2c)$$

in which F_{r1}, F_{r2}, and F_{r3} are the restoring forces for the unit surge, heave and pitch motion of the caisson, respectively. The displacements are also assumed to be simple periodic

$$\begin{Bmatrix} U_c \\ V_c \\ \alpha_c \end{Bmatrix} = \begin{Bmatrix} U_o \\ V_o \\ \alpha_o \end{Bmatrix} e^{-i\sigma t} \tag{3.3.3}$$

where U_o, V_o, and α_o are the coupled amplitudes of the caisson motion.

3.3.2 Surge Motion of the Caisson

The displacement at the upper boundary, (2.3.11b), can be re-written as

$$ {}^1U^o(X,0) = U_c \begin{cases} 1 - \text{th}\left[2\sqrt{\frac{(1-\nu)(-1-X)}{\pi D}}\right] & ;-\infty<X\leq -1 \\ 1 & ;|X|\leq 1 \\ 1 - \text{th}\left[2\sqrt{\frac{(1-\nu)(X-1)}{\pi D}}\right] & ;1\leq X<\infty \end{cases} \tag{3.3.4}$$

if (2.3.14a) is introduced. For convenience, $f_1(X)$ is introduced to represent the bracketed expressions on the right-hand side of (3.3.4). Thus, (3.3.4) can be replaced by

$$ {}^1U^o(X,0) = U_c\, f_1(X) \tag{3.3.5}$$

From the Fourier transformations of boundary conditions, (2.3.3a), (2.3.3b), (2.3.11a) and (3.3.5), the unknown coefficients are obtained

$$ {}^1a_1 = U_c\, \hat{f}_1(s) \tag{3.3.6a}$$

$$ {}^1a_2 = -\frac{[s^2D^2 + 2(1-\nu)(3-4\nu)\,\text{ch}^2(sD)]\,{}^1a_1}{2(1-\nu)[sD + (3-4\nu)\text{ch}(sD)\text{sh}(sD)]} \tag{3.3.6b}$$

$$ {}^1a_3 = -\frac{s[2(1-\nu) + (3-4\nu)\,\text{sh}^2(sD)]\,{}^1a_1}{2(1-\nu)[sD + (3-4\nu)\text{ch}(sD)\text{sh}(sD)]} \tag{3.3.6c}$$

$$ {}^{1}a_4 = \frac{s\ {}^{1}a_1}{2(1-\nu)} \tag{3.3.6d} $$

The caisson motion U_c, which is still unknown, will be solved by applying the dynamic boundary condition, (2.3.15),

$$ m\ \ddot{u}_c = f_{w1} + f_{s1} + f_{r1} \tag{3.3.7} $$

Integrating the shear stress along the caisson-soil interface yields the restoring force for unit surge motion of the caisson.

$$ F_{r1} = 2cG \int_{-1}^{1} \{\frac{1}{\sqrt{2\pi}} \int_{-\infty}^{\infty} [s\ {}^{1}a_2' - (1-2\nu)\ {}^{1}a_3'\ ]\ \hat{f}_1(s)\ e^{isX} ds\} dX \tag{3.3.8} $$

in which

$$ {}^{1}a_2' = {}^{1}a_2/{}^{1}a_1 \tag{3.3.9a} $$

$$ {}^{1}a_3' = {}^{1}a_3/{}^{1}a_1 \tag{3.3.9b} $$

Substitution of (3.3.1), (3.3.2a), (3.3.3), (3.3.8), and (3.2.5a) into (3.3.7), yields

$$ U_o = -(F_{s1} + F_{w1})/(F_{r1} + m\sigma^2) \tag{3.3.10} $$

where F_{r1} and F_{s1} can be evaluated numerically.

3.3.3 Heave Motion of the Caisson

If (2.3.14b) is introduced, the displacement at the upper boundary, (2.3.12b), is given by

$$
{}^{2}V^{o}(X,0) = V_c \begin{cases} 1 - \text{th}\left[2\sqrt{\frac{A(-1-X)}{\pi D}}\right] & ;-\infty<X\leq -1 \\ 1 & ;|X|\leq 1 \\ 1 - \text{th}\left[2\sqrt{\frac{A(X-1)}{\pi D}}\right] & ;1\leq X<\infty \end{cases} \qquad (3.3.11)
$$

With the bracketed expressions denoted by $f_2(X)$, (3.3.11) reads

$$
{}^{2}V^{o}(X,0) = V_c\, f_2(X) \qquad (3.3.12)
$$

This, combined with (2.3.3a), (2.3.3b) and (2.3.12a), provides the unknown coefficients

$$
{}^{2}a_1 = \frac{-i[(1-2\nu)(3-4\nu)\text{sh}^2(sD) - s^2D^2]\, V_c \hat{f}_2(s)}{2(1-\nu)\,[sD - (3-4\nu)\text{ch}(sD)\text{sh}(sD)]} \qquad (3.3.13a)
$$

$$
{}^{2}a_2 = \frac{-i(1-2\nu)\, V_c\, \hat{f}_2(s)}{2(1-\nu)} \qquad (3.3.13b)
$$

$$
{}^{2}a_3 = \frac{-is\, V_c\, \hat{f}_2(s)}{2(1-\nu)} \qquad (3.3.13c)
$$

$$
{}^{2}a_4 = \frac{is[(1-2\nu) - (3-4\nu)\text{ch}^2(sD)]\, V_c\, \hat{f}_2(s)}{2(1-\nu)\,[sD - (3-4\nu)\text{ch}(sD)\text{sh}(sD)]} \qquad (3.3.13d)
$$

Similar to the surge motion, the displacement amplitude of heave is solved by employing the equation of motion, (2.3.15),

$$
V_o = -(F_{s2} + F_{w2})/(F_{r2} + m\sigma^2) \qquad (3.3.14)
$$

in which the restoring force for unit heave motion of the caisson is given by

$$
F_{r2} = 2cG \int_{-1}^{1} \left\{ \frac{1}{\sqrt{2\pi}} \int_{-\infty}^{\infty} [2(1-\nu)\, {}^{2}a_4' - s\, {}^{2}a_1']\hat{f}_2(s) e^{isX} ds \right\} dX \qquad (3.3.15)
$$

and

$$ {}^{2}a_1' = {}^{2}a_1/[V_c\ \hat{f}_2(s)] \tag{3.3.16a} $$

$$ {}^{2}a_4' = {}^{2}a_4/[V_c\ \hat{f}_2(s)] \tag{3.3.16b} $$

3.3.4 Pitch Motion of the Caisson

By introducing (2.3.14c), the displacement at the upper boundary, (2.3.13b), is rewritten as

$$ {}^{3}V^{o}(x,0) = \alpha_c \begin{cases} 1 - \text{th}\left\{2\sqrt{\frac{A(-1-X)}{\pi D}}\,[1 + i\hat{S}_-'(0)]\right\} & ;-\infty<X\leq -1 \\ -X & ;|X|\leq 1 \\ 1 - \text{th}\left\{2\sqrt{\frac{A(X-1)}{\pi D}}\,[1 + i\hat{S}_-'(0)]\right\} & ;1\leq X<\infty \end{cases} \tag{3.3.17} $$

${}^{3}V^{o}$ is related to $f_3(X)$ by

$$ {}^{3}V^{o}(X,0) = \alpha_c\ f_3(X) \tag{3.3.18} $$

Employing (2.3.3a), (2.3.3b) and (2.3.13a) to solve for these coefficients,

$$ {}^{3}a_1 = \frac{-i[(1-2\nu)(3-4\nu)\text{sh}^2(sD) - s^2D^2]\alpha_c\hat{f}_3(s)}{2(1-\nu)[sD - (3-4\nu)\text{ch}(sD)\text{sh}(sD)]} \tag{3.3.19a} $$

$$ {}^{3}a_2 = \frac{-i(1-2\nu)\ \alpha_c\ \hat{f}_3(s)}{2(1-\nu)} \tag{3.3.19b} $$

$$ {}^{3}a_3 = \frac{-is\ \alpha_c\ \hat{f}_3(s)}{2(1-\nu)} \tag{3.3.19c} $$

$$ {}^{3}a_4 = \frac{is[(1-2\nu) - (3-4\nu)ch^2(sD)]\ \alpha_c \hat{f}_3(s)}{2(1-\nu)[sD - (3-4\nu)ch(sD)sh(sD)]} \qquad (3.3.19d) $$

Employing the dynamic boundary condition, (2.3.15), the amplitude of the angular displacement α_o is determined

$$ \alpha_o = -(F_{s3} + F_{w3})/(F_{r3} + I_m \sigma^2) \qquad (3.3.20) $$

in which

$$ F_{r3} = -2c^2 G \int_{-1}^{1} X\{\frac{1}{\sqrt{2\pi}} \int_{-\infty}^{\infty} [2(1-\nu)\ {}^{3}a_4' - s\ {}^{3}a_1']\hat{f}_3(s)e^{isX}ds\}dX \qquad (3.3.21) $$

and

$$ {}^{3}a'_1 = {}^{2}a'_1 \qquad (3.3.22a) $$

$$ {}^{3}a'_4 = {}^{2}a'_4 \qquad (3.3.22b) $$

3.4 Solutions to the Boundary Layer Correction

Solving the consolidation equation (2.2.46), for simple harmonic waves, it is assumed that

$$ P^b = A(X)\ B\ (Y^b)\ e^{-iT^b} \qquad (3.4.1) $$

Substituting (3.4.1) into (2.2.46) and solving for $B(Y^b)$, yields

$$ B(Y^b) = a_1'\ ch(\frac{1-i}{\sqrt{2}}\ Y^b) + a_2'\ sh(\frac{1-i}{\sqrt{2}}\ Y^b) \qquad (3.4.2) $$

Thus

$$ P^b = a_1(X)\ ch(\frac{1-i}{\sqrt{2}}\ Y^b) + a_2(X)\ sh(\frac{1-i}{\sqrt{2}}\ Y^b) \qquad (3.4.3) $$

Applying the boundary conditions (2.3.16) and (2.3.17), $a_1(X)$ and $a_2(X)$ are readily obtained.

$$a_1(X) = n_o\, p_w(X) - P\Big|_{Y^b=0} \tag{3.4.4a}$$

$$a_2(X) = \left[P^o\Big|_{Y^b=0} - n_o\, P_w(X)\right] \operatorname{th}\left(\frac{1-i}{\sqrt{2}}\, D^b\right)$$

$$- \frac{1+i}{\sqrt{2}}\, \frac{\partial P^o}{\partial Y^b}\Big|_{Y^b=D^b} \frac{1}{\operatorname{ch}\left(\frac{1-i}{\sqrt{2}}\, D^b\right)} \tag{3.4.4b}$$

Hence

$$p^b = \left\{\left[P^o\Big|_{Y^b=0} - n_o\, p_w(X)\right]\left[\operatorname{th}\left(\frac{1-i}{\sqrt{2}}\, D^b\right) \operatorname{sh}\left(\frac{1-i}{\sqrt{2}}\, Y^b\right)\right.\right.$$

$$\left.\left. - \operatorname{ch}\left(\frac{1-i}{\sqrt{2}}\, Y^b\right) - \frac{1+i}{\sqrt{2}}\, \frac{\partial P^o}{\partial Y^b}\Big|_{Y^b=D^b} \frac{\operatorname{sh}\left(\frac{1-i}{\sqrt{2}}\, Y^b\right)}{\operatorname{ch}\left(\frac{1-i}{\sqrt{2}}\, D^b\right)}\right\} e^{-iT^b} \tag{3.4.5}$$

Written in dimensionless outer variables, (3.4.5) takes the form

$$p^b = \left\{\left[n_o\, P_w(x) - P^o\Big|_{Y=0}\right] \frac{\operatorname{ch}\left[\frac{1-i}{\sqrt{2}}\, \frac{D-Y}{\varepsilon}\right]}{\operatorname{ch}\left(\frac{1-i}{\sqrt{2}}\, \frac{D}{\varepsilon}\right)}\right.$$

$$\left. - \frac{1+i}{\sqrt{2}}\, \varepsilon\, \frac{\partial P^o}{\partial Y}\Big|_{Y=D} \frac{\operatorname{sh}\left(\frac{1-i}{\sqrt{2}}\, \frac{Y}{\varepsilon}\right)}{\operatorname{ch}\left(\frac{1-i}{\sqrt{2}}\, \frac{D}{\varepsilon}\right)}\right\} e^{-iT^b} \tag{3.4.6}$$

where

$$Y^b = \frac{Y}{\varepsilon} \tag{3.4.7}$$

The second term is in order of ε, if $\frac{\partial P^o}{\partial Y} \sim O(1)$. It is hence negligible compared to the first term. As a result, (3.4.6) is approximately given by

$$P^b = [n_o P_w(x) - P^o\Big|_{Y=0}] \frac{ch(\frac{1-i}{\sqrt{2}} \frac{D-Y}{\varepsilon})}{ch(\frac{1-i}{\sqrt{2}} \frac{D}{\varepsilon})} e^{-iT^b} \qquad (3.4.8)$$

The corrections of effective stress in the boundary layer are easily obtained from (2.2.52).

3.5 Summary of the Solution

The linear superposition of the solution components leads to the solution of the original problem.

The horizontal displacement,

$$U = {}^bU^o + {}^1U^o + {}^2U^o + {}^3U^o \qquad (3.5.1)$$

The vertical displacement,

$$V = {}^bV^o + {}^1V^o + {}^2V^o + {}^3V^o \qquad (3.5.2)$$

The shear stress,

$$T_{xy} = {}^bT^o_{xy} + {}^1T^o_{xy} + {}^2T^o_{xy} + {}^3T^o_{xy} \qquad (3.5.3)$$

The porewater pressure induced by the moving caisson,

$$P^o = -\frac{{}^bT^o_{xx} + {}^1T^o_{xx} + {}^2T^o_{xx} + {}^3T^o_{xx} + {}^bT^o_{yy} + {}^1T^o_{yy} + {}^2T^o_{yy} + {}^3T^o_{yy}}{2(1 + m_o)} \qquad (3.5.4)$$

The effective normal stresses induced by the outer problem,

$$T'^o_{xx} = {}^bT^o_{xx} + {}^1T^o_{xx} + {}^2T^o_{xx} + {}^3T^o_{xx} + P^o \qquad (3.5.5)$$

$$T'^o_{yy} = {}^bT^o_{yy} + {}^1T^o_{yy} + {}^2T^o_{yy} + {}^3T^o_{yy} + P^o \qquad (3.5.6)$$

The resultant effective normal stresses,

$$T'_{xx} = T'^{o}_{xx} + \frac{\nu}{1-\nu} P^b \qquad (3.5.7)$$

$$T'_{yy} = T'^{o}_{yy} + P^b \qquad (3.5.8)$$

The resultant porewater pressure,

$$P = P^o + P^b \qquad (3.5.9)$$

4. ANALYTICAL SOLUTION BEHAVIOR

The analytical model developed has been generalized for a caisson placed on a rubble bedding layer overlying a soil of finite depth. However, the response of the soil to waves and caisson motions is not readily apparent from the analytical solution. Therefore, in this chapter the general solution will be examined for different wave and soil conditions. In addition, the implications of the thin layer limitation will be discussed.

4.1 Wave Loadings and Soil Properties

4.1.1 Wave Loadings

An analytical model is being developed for the wave forces on the caisson in parallel with this study [Ward et al. (1986)]. The wave force model will include the modification of the wave field due to the rubble bedding layer. Forces are determined along the front face, bottom and back of the caisson. Unfortunately, the wave force model was not completed in time to be incorporated into the caisson-soil model. Therefore, an idealized wave condition is assumed. At a later date, the more realistic wave force model may be easily incorporated into the soil model.

The idealized wave condition is to assume that a partial standing wave is formed, in which the dynamic wave pressure underneath the caisson is linearly dissipated from the toe to the heel of the caisson. Thus, the pressure on the mudline is

$$P_w(x,t) = \begin{cases} \dfrac{(1+k_r)\gamma H}{2ch(kh)} \cos(kx)\, e^{-i\sigma t} \\ \dfrac{(1+k_r)\gamma H}{2ch(kh)} \dfrac{c'-x}{2c'} e^{-i\sigma t} \\ 0 \end{cases} \qquad (4.1.1)$$

in which γ is the unit weight of water; H is the incident wave height; k is the wave number; h is the water depth; and k_r is the reflection coefficient.

The horizontal force and moment induced by the wave acting on the front face of the caisson are obtained by integrating the pressure and pressure moment along the caisson face. The moment is taken around the midpoint of the caisson-soil interface. The force on the front face of the rubble bedding layer is assumed to be small and neglected. The vertical wave force on the bottom of the caisson is evaluated from a triangular wave pressure distribution. The moment induced by this pressure is also taken around the midpoint of the caisson-soil interface. For partial standing waves, the dynamic pressure on the vertical caisson face is

$$P_1 = \gamma \frac{ch[k(z+h)]}{ch(kh)} \eta \qquad (4.1.2)$$

in which η is the free surface fluctuation and given by

$$\eta = \frac{(1+k_r)H}{2} e^{-i\sigma t} \qquad (4.1.3)$$

and z is the vertical axis in a Cartesian coordinate system, conventionally, negative if below the still water level, and z=-y-h.

The horizontal wave force F_{w1} is given by

$$F_{w1} = \int_{-h+b}^{0} \gamma \frac{ch[k(z+h)]}{ch(kh)} \eta dz + \int_{0}^{\eta} \gamma(\eta - z)dz$$

$$= \frac{\gamma\eta}{k} \left[th(kh) - \frac{sh(kb)}{ch(kh)}\right] + \gamma \frac{\eta^2}{2} \qquad (4.1.4)$$

where the pressure above the still water level is assumed to be hydrostatic [Dean and Dalrymple (1984)].

The wave pressure at the caisson toe is

$$p_2 = \gamma \frac{ch(kb)}{ch(kh)} \eta \qquad (4.1.5)$$

from which the vertical wave force F_{w2} is readily obtained,

$$F_{w2} = \gamma c' \frac{ch(kb)}{ch(kh)} \eta \qquad (4.1.6)$$

Furthermore, the moment is

$$M_2 = \frac{c'}{3} F_2 \qquad (4.1.7)$$

The moment due to pressure on the front face of the caisson is

$$M_3 = \int_{-h+b}^{0} \gamma \frac{ch[k(z+h)]}{ch\ (kh)} \eta(z+h)dz + \int_{0}^{\eta} \gamma(\eta - z)(z+h)dz$$

$$= \frac{\gamma\eta}{k^2 ch(kh)} [(kh)sh(kh) - ch(kh) - (kb)sh(kb)$$

$$+ ch(kb)] + \gamma\eta\left(\frac{\eta^3}{6} + \frac{h\eta^2}{2}\right) \qquad (4.1.8)$$

Thus, the wave-induced total moment on the caisson is

$$F_{w3} = -(M_2 + M_3) \qquad (4.1.9)$$

where positive is counterclockwise.

Again, it should be noted that this idealized wave field was assumed so that the caisson-soil model could be exercised. The more accurate wave force model will only influence the boundary conditions in the caisson-soil model, i.e. the wave forces on the caisson and the pressure along the mudline.

4.1.2 Soil Properties

Typical values of Poisson's ratio, Young's modulus, shear modulus, and porosity of cohesionless soil are shown in Table 4.1.1 [Das (1983)]. Poisson's ratio, Young's modulus, and shear modulus are related by

$$G = \frac{E}{2(1+\nu)} \qquad (4.1.10)$$

Table 4.1.1 Typical soil properties [Das (1983)]

Soil Type	Poisson's Ratio	Modulus (psf)	Porosity 0.30	0.35	0.40
Coarse sand	0.15	E	943,200	820,800	676,800
		G	410,000	357,000	294,000
Medium coarse sand	0.20	E	943,200	820,000	676,800
		G	390,000	342,000	282,000
Fine-grained sand	0.25	E	763,200	576,000	489,600
		G	305,000	230,000	196,000
Sandy silt	0.30-0.35	E	288,000	244,800	208,800
		G	111,000	94,000	80,000

4.2 Examination of the Thin Layer Limitation

4.2.1 Examination of the Normal and Shear Stresses Along the Exposed Surface

As discussed in Chapter 2, the outer region solutions are developed under the assumption of a thin soil layer expecting negligible vertical normal stress and shear stress along the exposed mudline. The influence of the soil depth on the stresses along the exposed mudline is shown in Figs. 4.2.1 and 4.2.2 for eight soil depths and four points with dimensionless distances of 0.001, 0.005, 0.01, and 0.1 from the caisson toe. The following data are assumed for this calculation.

Wave period - 4 sec.

Wave height - 4 ft

Water depth - 8 ft

Rubblemound thickness - 1 ft

Caisson half-width - 4 ft

Mass of the caisson - 83 slugs

Mass moment of the inertia of the caisson - 3,660 slugs-ft^2

Poisson's ratio - 0.3

Shear modulus - 80,000 psf

Fig. 4.2.1 reveals that at a dimensionless distance of 0.1 from the toe, the normal stress is less than one percent of the peak stress at the caisson toe, even though the dimensionless soil depth is up to 6. At a distance of 0.001, the stress ratio is small (0.15%) only for dimensionless soil depths less than 0.25.

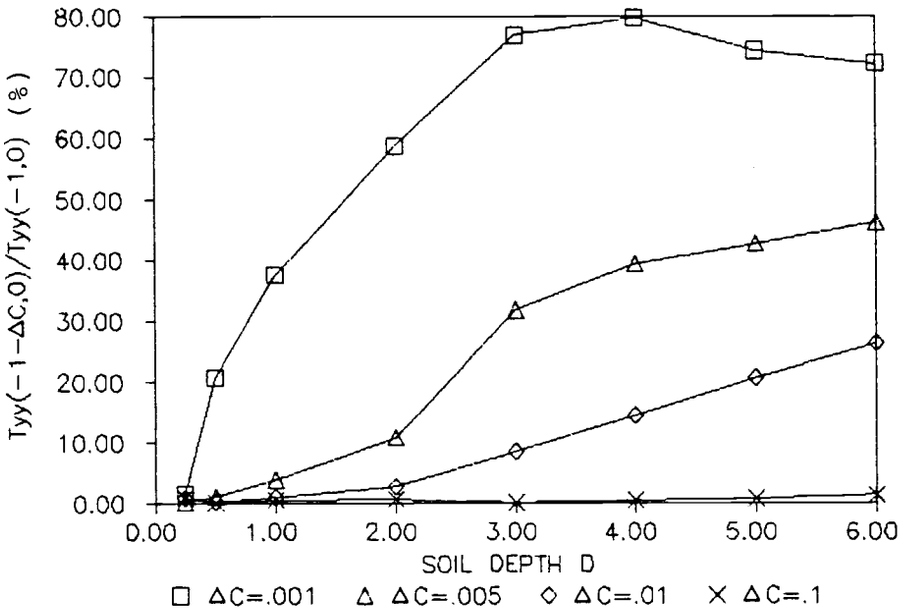

Figure 4.2.1. Outer vertical normal stress ratio along the exposed mudline as a function of soil depth for the radiation problem.

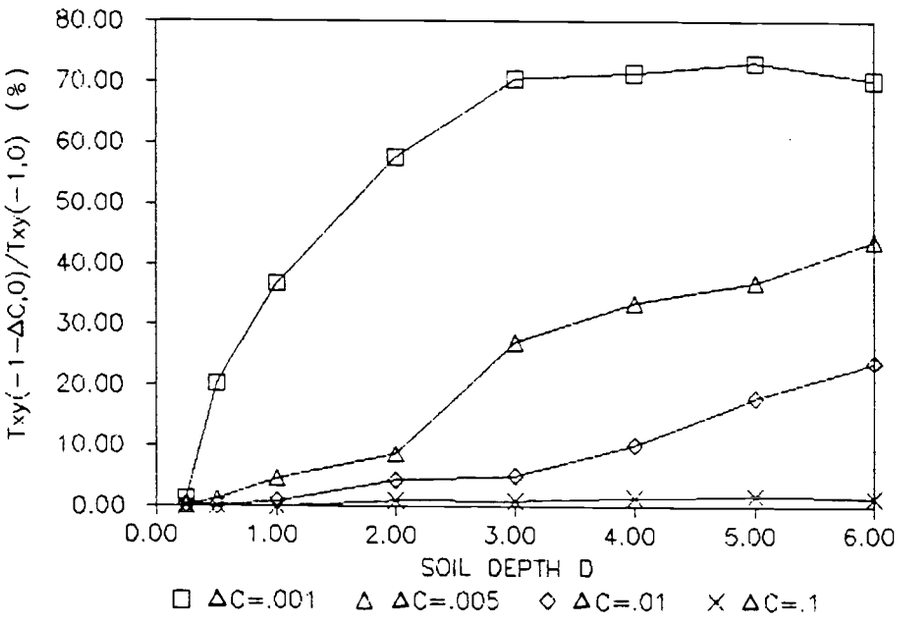

Figure 4.2.2. Outer shear stress ratio along the exposed mudline as a function of soil depth for the radiation problem.

Fig. 4.2.2 shows the shear stress ratio under the same conditions for the normal stress examination. At a dimensionless distance of 0.1 from the caisson toe, the shear stresses are less than 2% of the peak stress for all soil depths. At a distance of 0.001, only dimensionless depths less than 0.25 produce a small shear stress, (i.e. the stress ratio is about 1.3%).

Figs. 4.2.3 and 4.2.4 show the distribution of the normal stress and shear stress around the caisson toe for soil depths 0.25 and 6, respectively. The thinner the soil is, the higher and sharper the peak stress is. These results indicate that the assumption of negligible normal and shear stress are sensitive to the soil layer thickness. However, the error associated with this assumption appears to be small for dimensionless soil depths less than 0.25.

4.2.2 Comparison with the Finite Element Method for an Elastic Soil of Arbitrary Depth

A finite element solution for an elastic layer due to inclined and eccentric load over an infinitely long rigid strip was developed by Milovic et al. (1970). This numerical solution was for a static load on an impermeable elastic strip space. The present analytical solution is applicable to an elastic soil by defining the pore pressure to be zero. The definition sketch for the loading condition examined is shown in Fig. 4.2.5. The following conditions are assumed for this comparison.

Thickness of the elastic layer: 10 ft; 30 ft

(dimensionless D = 2.0; 6.0)

Eccentricity: e = 0.5; 1.0

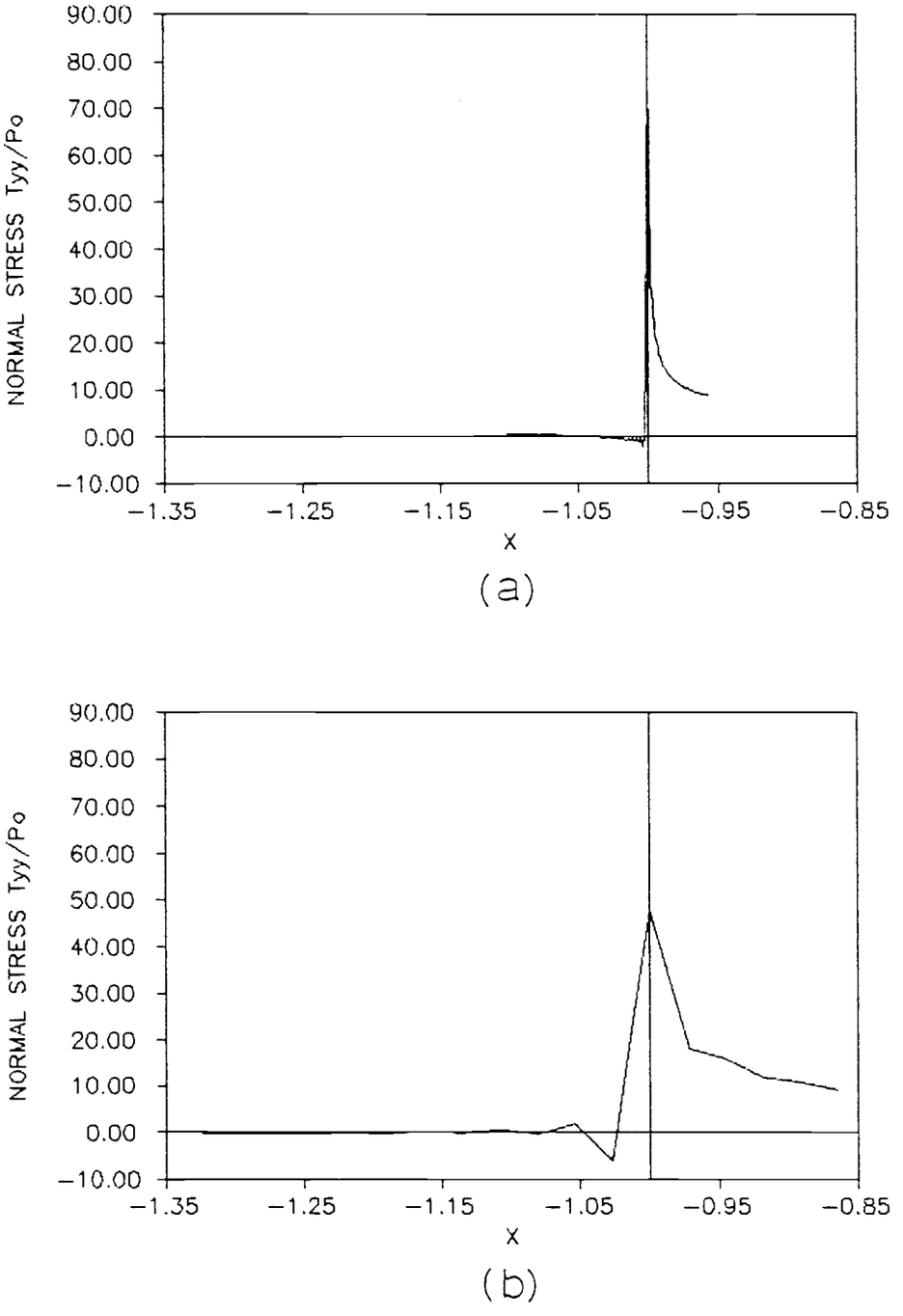

Figure 4.2.3. Outer vertical normal stress near the caisson toe in the radiation problem for two soil depths: (a) D=0.25 and (b) D=6.0.

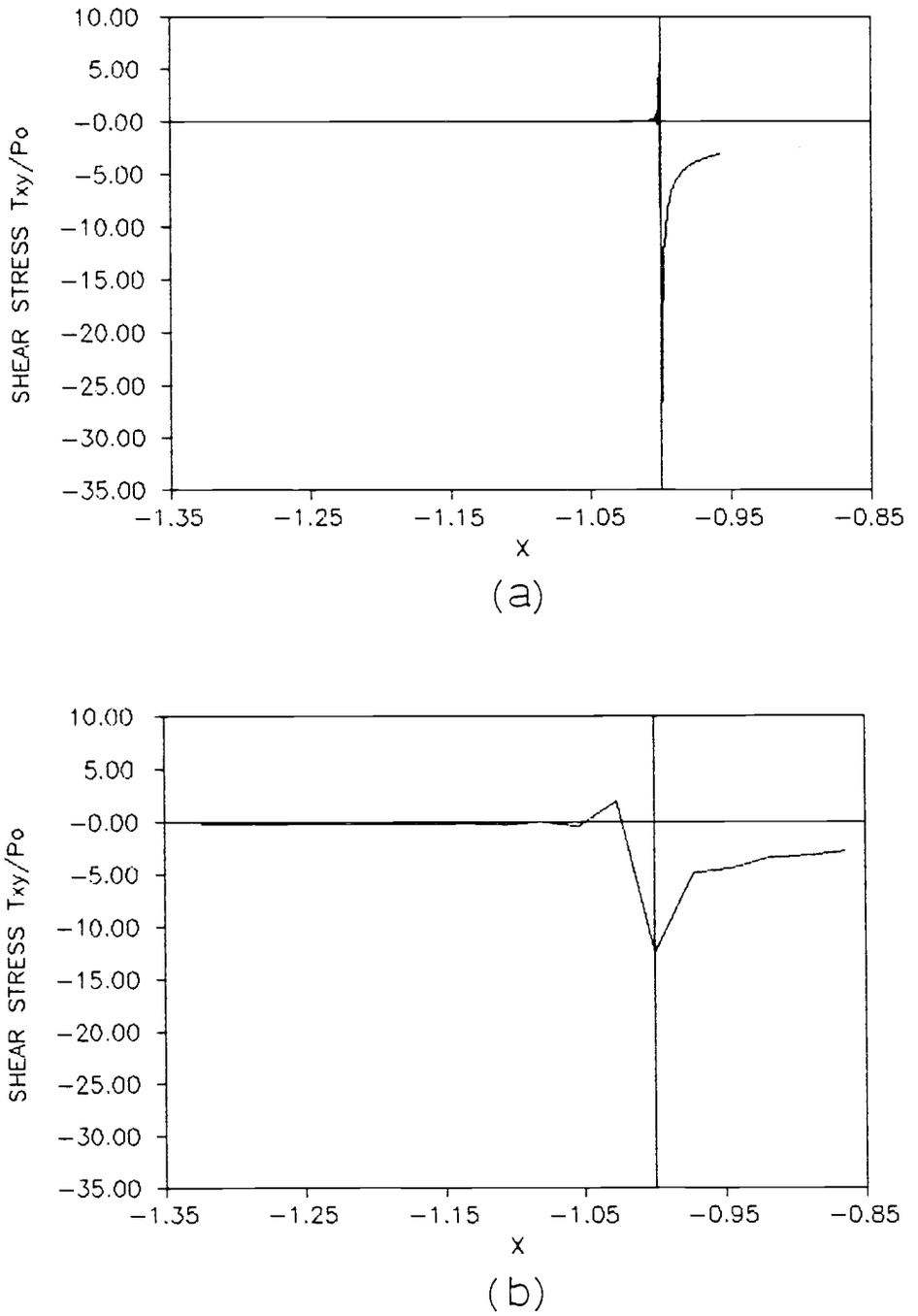

Figure 4.2.4. Outer shear stress near the caisson toe in the radiation problem for two soil depths: (a) D=0.25 and (b) D=6.0.

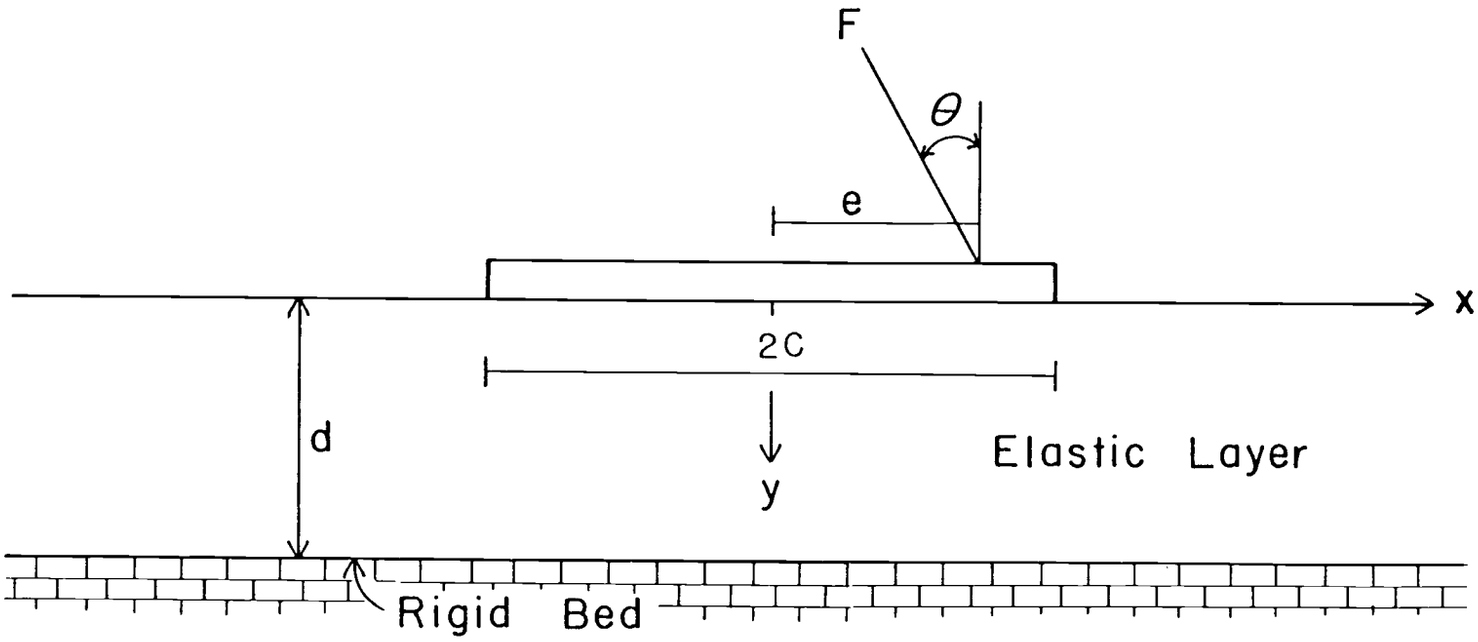

Figure 4.2.5. Definition sketch for a loaded infinite long rigid strip overlying an elastic layer.

Angle of the inclined load: 45.0°

Total load: F = 1000. lb

Averaged load per unit area: $P_{av} = F/2c$

Half-width of the strip: c = 5 ft

The comparison of contact stresses is shown in Figs. 4.2.6 through 4.2.9 The agreement between the two methods is reasonable for D = 2.0 and D = 6.0, particularly for the normal stresses. For larger eccentricity, the analytical solution has larger shear stress than the finite element solution. At the corners, the analytical solution also has bigger stresses; this may be due to the effect of the finite element size in the numerical model. The stresses change rapidly at the corners and a very fine element mesh must be used to get a more accurate solution.

The stress profiles at X = 0 are compared with the finite element method in Figs. 4.2.10 through 4.2.13. Generally, there is better agreement between these two solutions for D = 6 than for - D = 2. The normal stresses at X = 0 are independent of eccentricity in both methods. This property can be seen from Figs. 4.2.10 (b), 4.2.10 (c), 4.2.11 (b) and 4.2.11(c).

From the above comparison, the analytical solutions are in good agreement with the numerical solutions for both depths of elastic layer even though they are not thin. It is, therefore, concluded that the analytical model for predicting the stresses under the caisson is applicable to a much greater range of depths than suggested by the thin layer assumptions in the development of the solution.

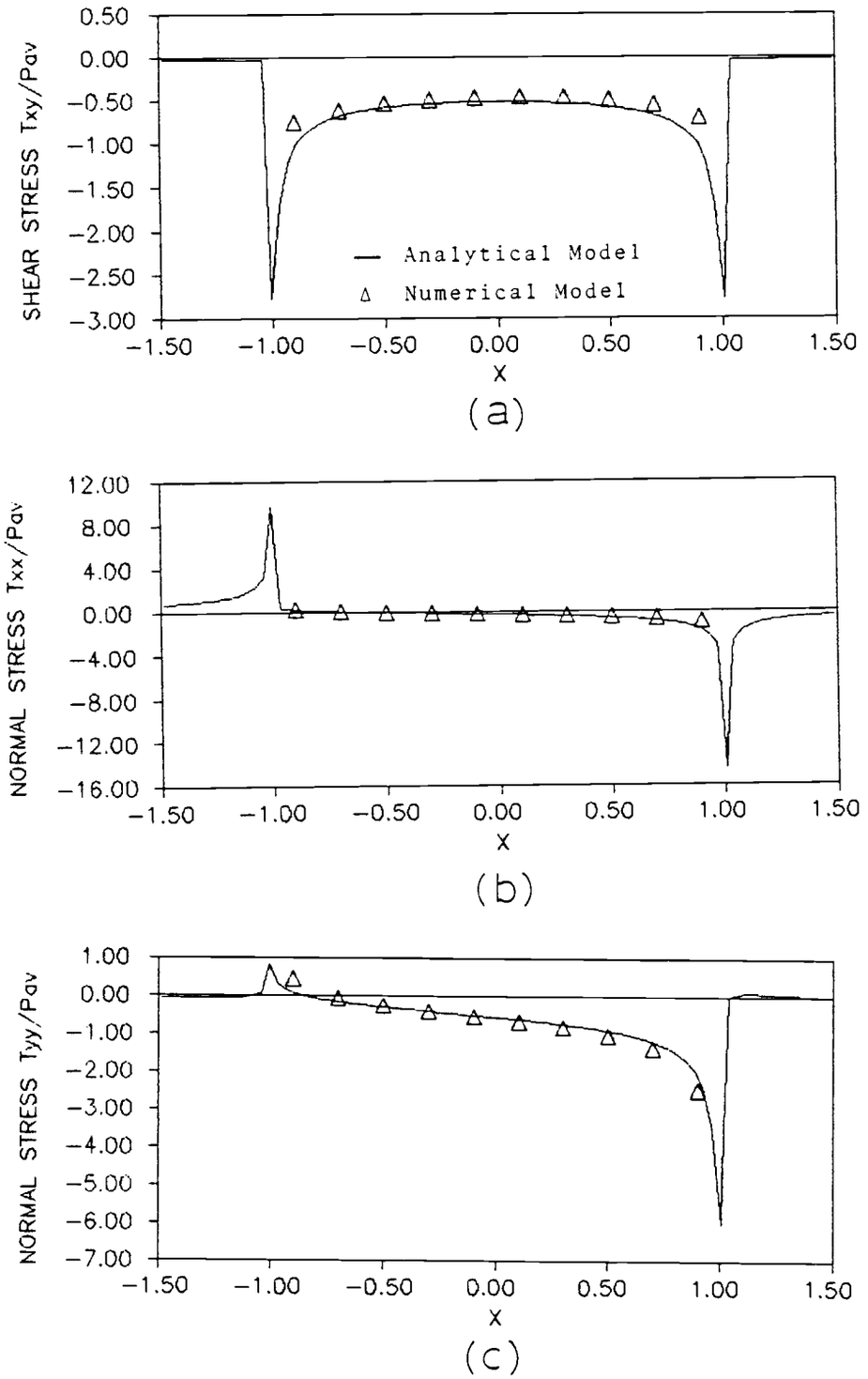

Figure 4.2.6. Comparison of the analytical model and numerical model for the contact stresses on an elastic layer: (a) shear stress, (b) horizontal normal stress, and (c) vertical normal stress (D=2.0, e=0.5).

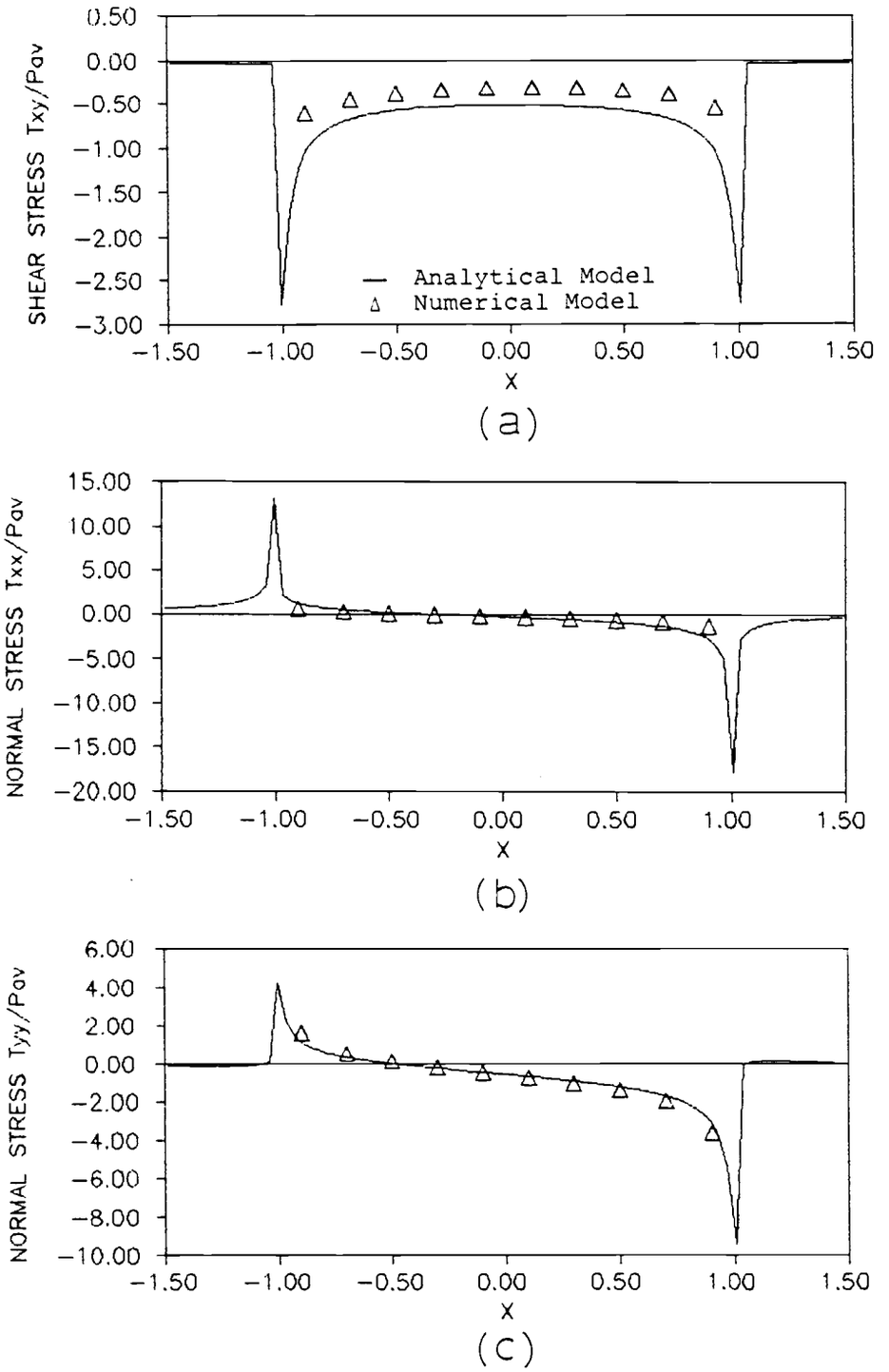

Figure 4.2.7. Comparison of the analytical model and numerical model for the contact stresses on an elastic layer: (a) shear stress, (b) horizontal normal stress, and (c) vertical normal stress (D=2.0, e=1.0).

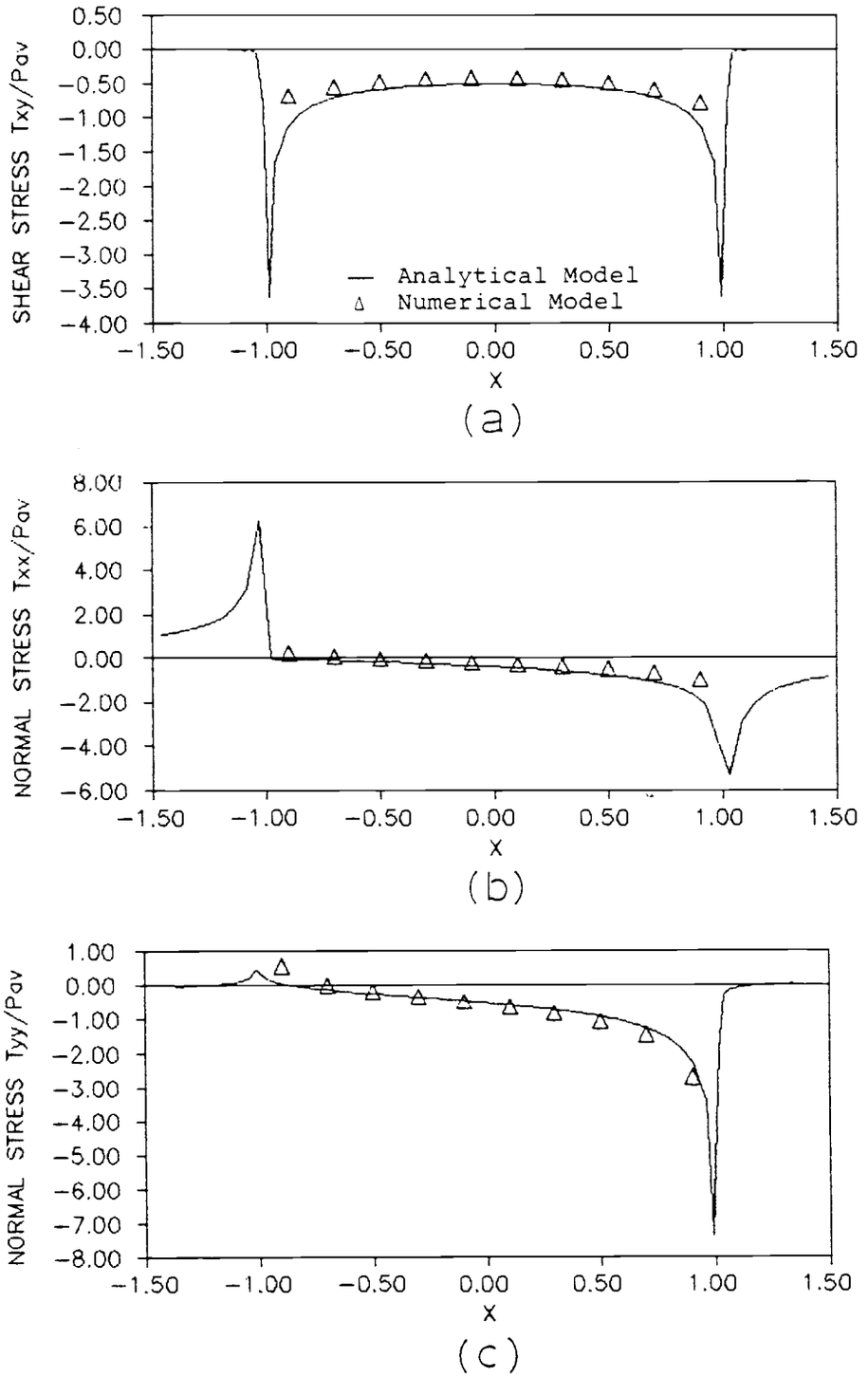

Figure 4.2.8. Comparison of the analytical model and numerical model for the contact stresses on an elastic layer: (a) shear stress, (b) horizontal normal stress, and (c) vertical normal stress (D=6.0, e=0.5)

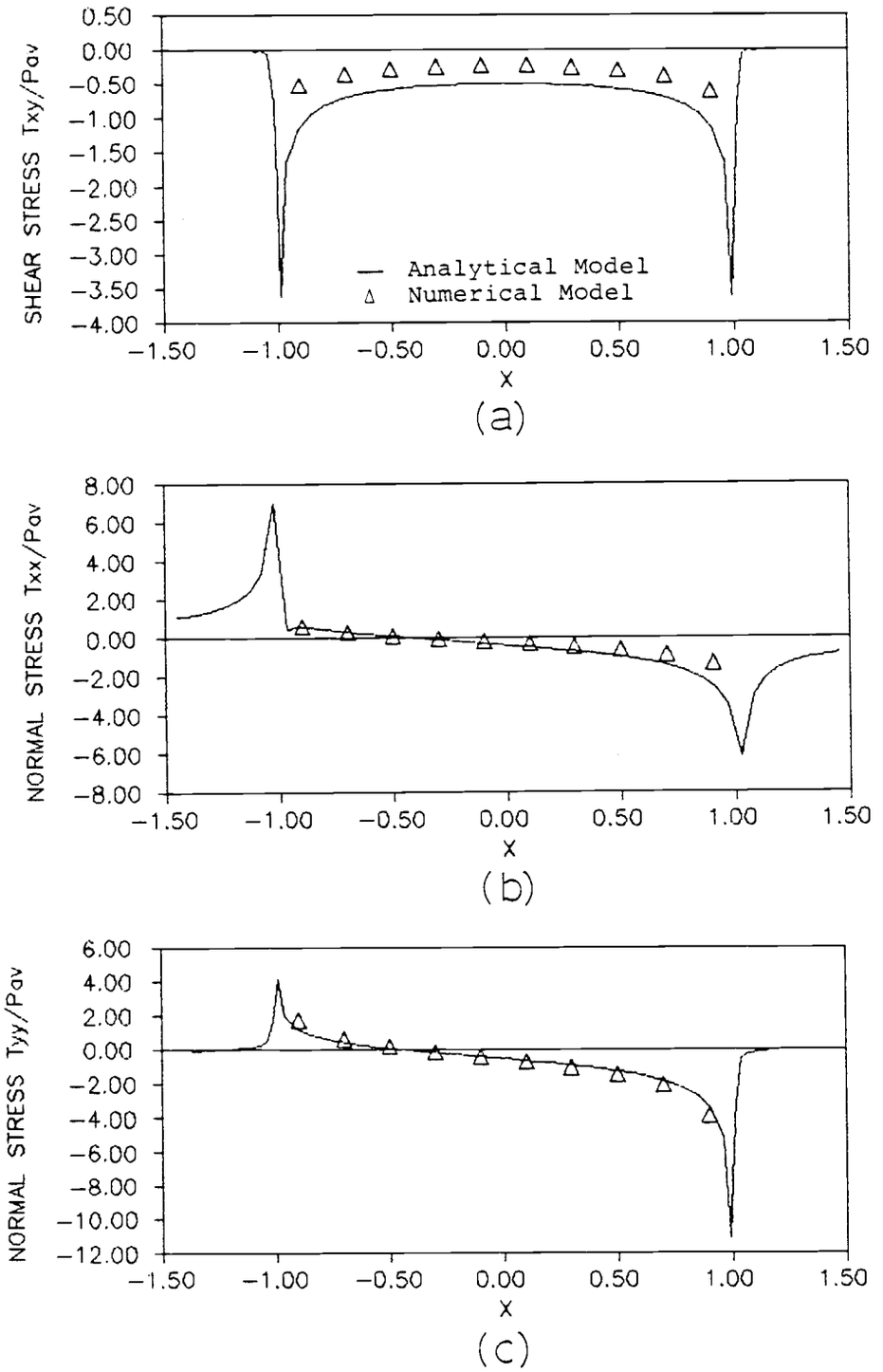

Figure 4.2.9. Comparison of the analytical model and numerical model for the contact stresses on an elastic layer: (a) shear stress, (b) horizontal normal stress, and (c) vertical normal stress (D=6.0, e=1.0).

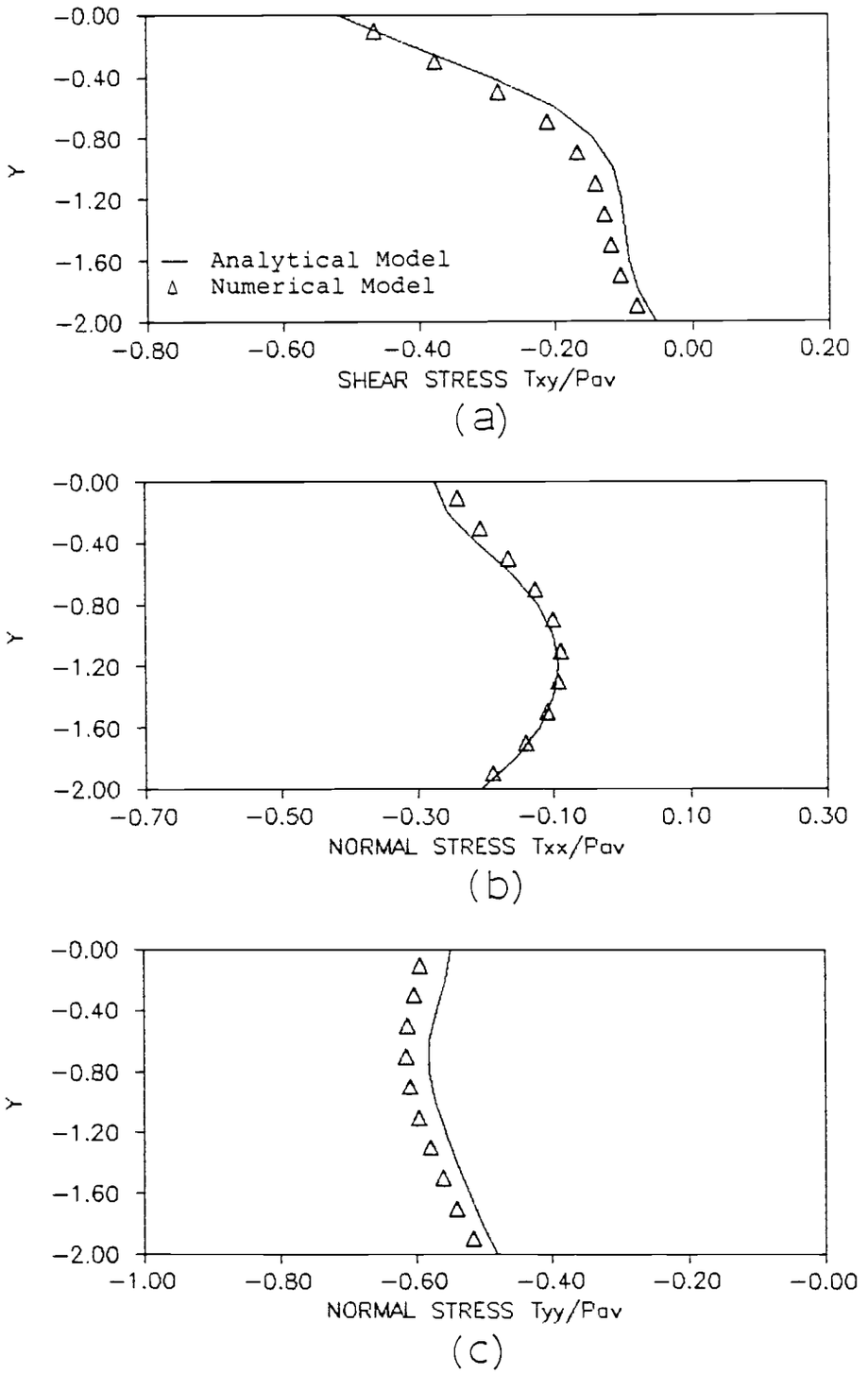

Figure 4.2.10. Comparison of the analytical model and numerical model for the stress profiles in an elastic layer: (a) shear stress, (b) horizontal normal stress, and (c) vertical normal stress at X=0 (D=2.0, e=0.5).

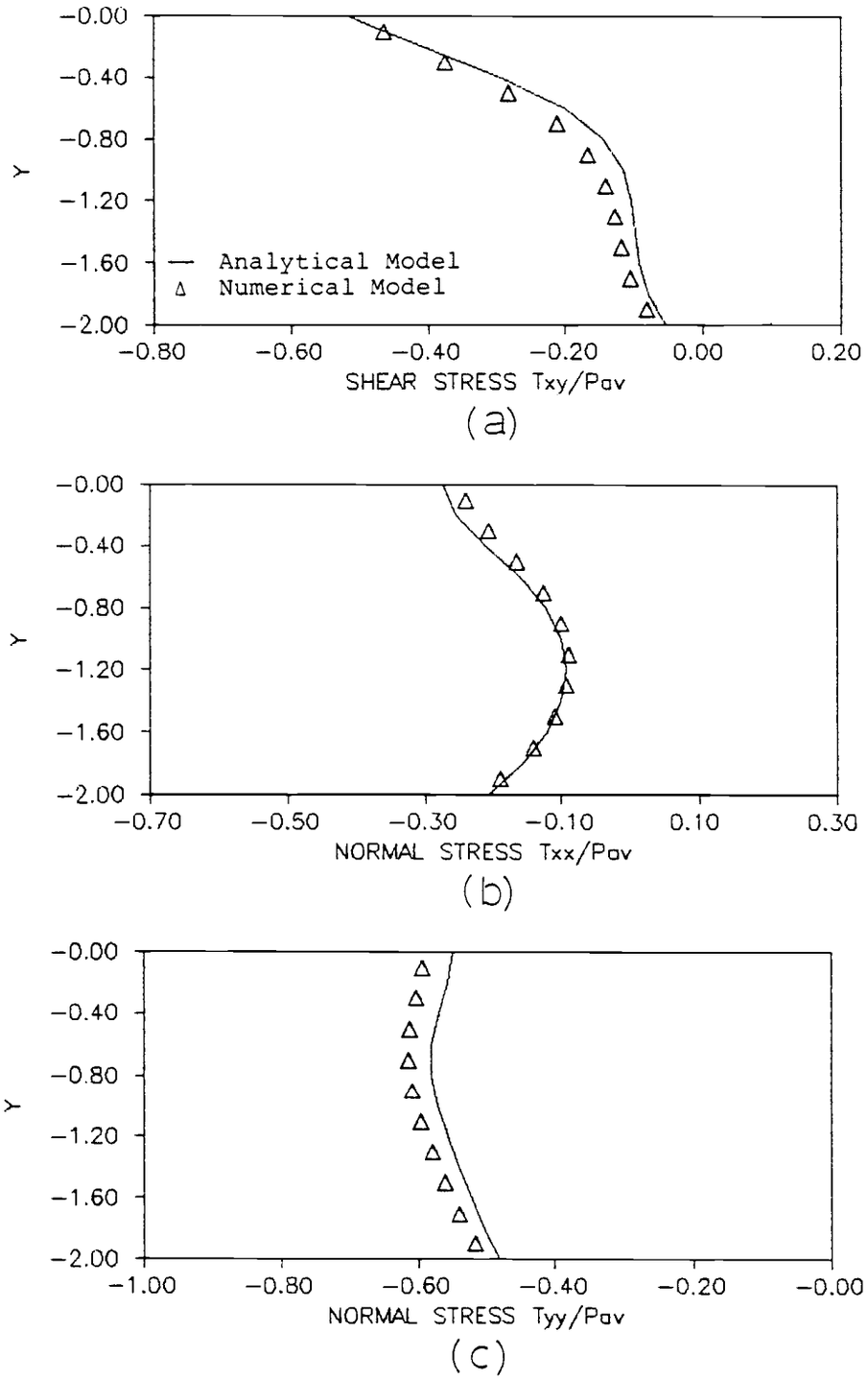

Figure 4.2.11. Comparison of the analytical model and numerical model for the stress profiles in an elastic layer: (a) shear stress, (b) horizontal normal stress, and (c) vertical normal stress at X=0 (D=2.0, e=1.0).

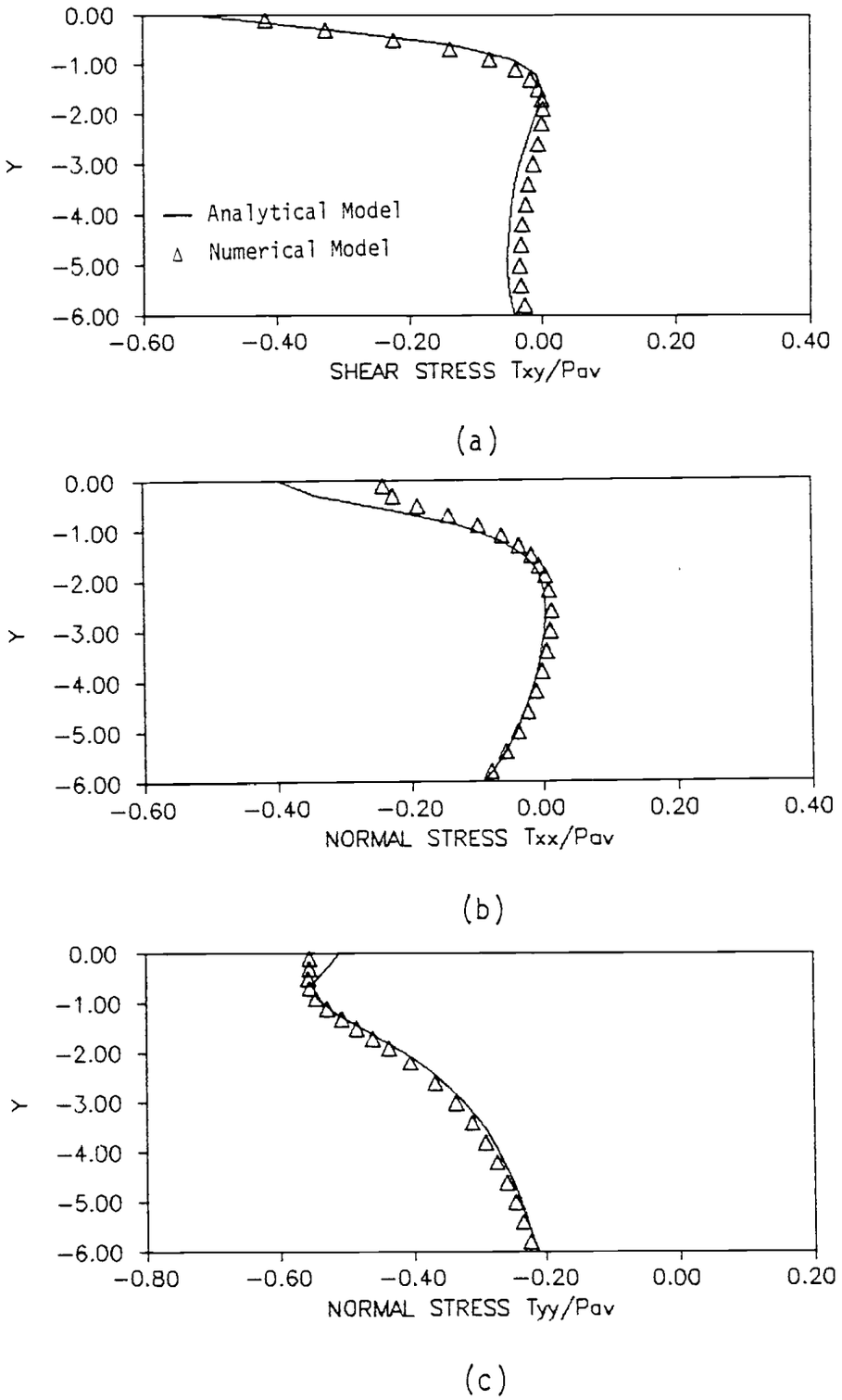

Figure 4.2.12. Comparison of the analytical model and numerical model for the stress profiles in an elastic layer: (a) shear stress, (b) horizontal normal stress, and (c) vertical normal stress at X=0 (D=6.0, e=0.5).

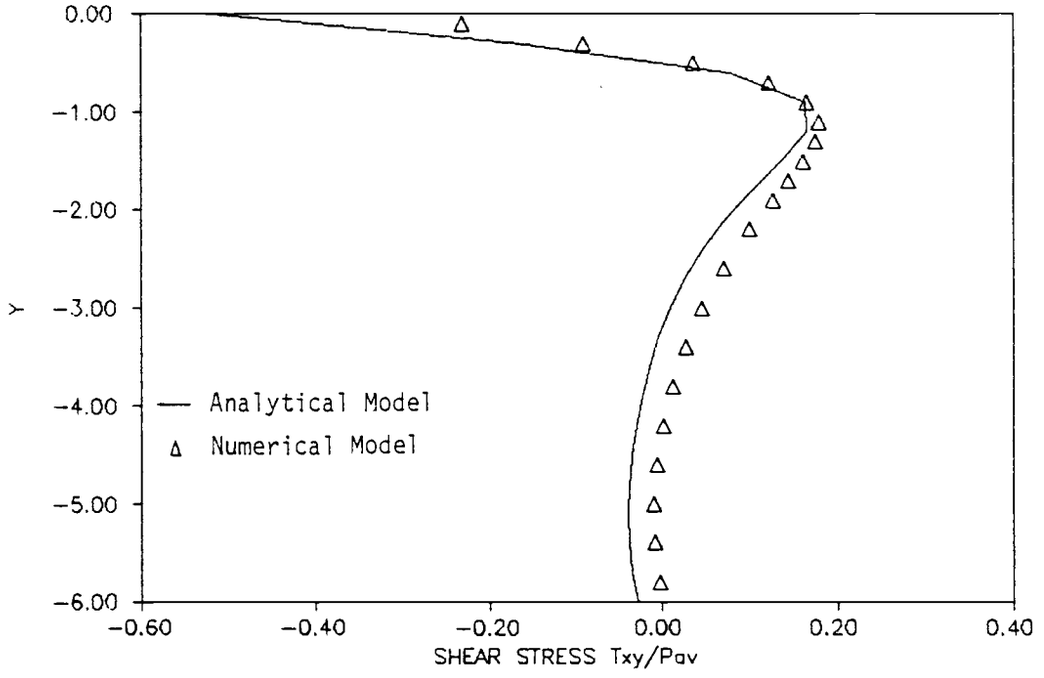

Figure 4.2.13. Comparison of the analytical model and numerical model for the shear stress profiles in an elastic layer at X=0 (D=6.0, e=1.0).

The analytical model is compared with the numerical model for displacements in the three degrees of freedom. These results are shown in Fig. 4.2.14. The analytical model predictions are little less than the numerical model values for all three modes of motion.

The distribution of the vertical contact stress is also compared with the base contact stress calculated by the finite element method for an offshore gravity structure subjected to waves. In the case of an elastic soil, the calculations show that the stress distribution is almost linear within the inner 80% of the diameter and that significant stress concentrations may occur towards the periphery - [Schjetne, et al. (1979)]. Figure 4.2.15 shows that the distribution of the caisson base contact stress follows the above statement. The distribution is linear in the inner 80% of the caisson width and concentrates at the caisson edges.

4.3 Examinations of the Behavior of Base Contact Stresses and Mudline Displacements

Base contact stresses are important for the design of a caisson base slab, and the mudline displacements are significant for the settlement prediction. In order to examine their behavior, the following conditions are assumed, unless otherwise defined.

Wave period - 10 sec.

Wave height - 20 ft

Water depth - 40 ft

Thickness of the rubblemound - 5 ft

Caisson half-width - 21 ft

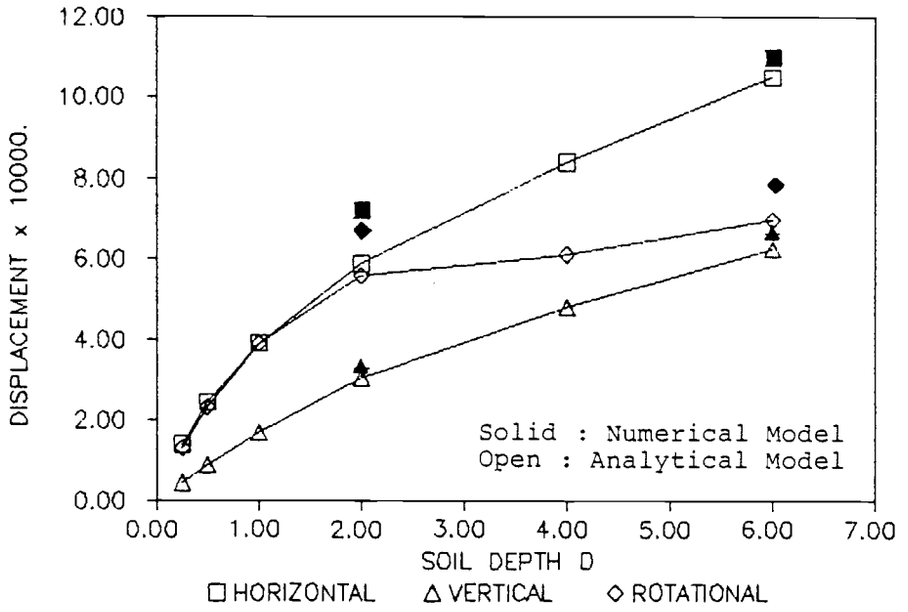

Figure 4.2.14. Comparison of the analytical model and numerical model for the surface displacements of an elastic layer.

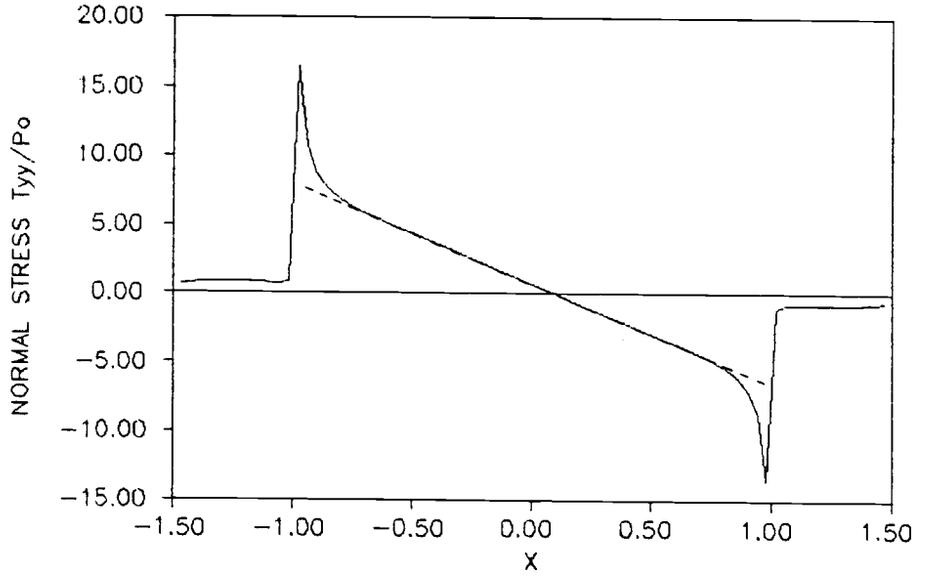

Figure 4.2.15. Distribution of the outer contact vertical normal stress on the caisson base for the radiation problem.

Mass of the caisson - 4400 slugs

Mass moment of inertia of the caisson - 4,716,800 slugs-ft^2

Dimensionless soil depth - 1.0

Poisson's ratio - 0.15

Shear modulus - 410,000 psf

Porosity - 0.4

Coefficient of permeability - 3.3×10^{-4} ft/sec

Figure 4.3.1 shows the dependency of contact shear stress, effective normal stresses, and displacements on wave period. For shorter waves, the shear stress is larger than for longer waves because the ratio of wave forces to P_o increases with the decrease of wave period. Dimensionless effective normal stresses are relatively insensitive to the wave period, except very long waves. However, displacements increase with the wave length.

Figure 4.3.2 shows the results for five different wave heights. Obviously, wave forces increase with an increase of wave height. Therefore, stresses and displacements are proportional to wave heights.

Figure 4.3.3 presents the results for four different Poisson's ratios with a constant shear modulus of 410,000 psf. The figures show that contact stresses depend slightly on Poisson's ratio, except the horizontal normal stress which is proportional to the Poisson's ratio. It is also interesting to note that the horizontal displacement at the exposed mudline is proportional to Poisson's ratio while underneath the caisson the displacement is inversely proportional to Poisson's ratio. Unlike the horizontal displacement, the vertical

displacement is inversely proportional to Poisson's ratio over the entire mudline.

Displacement amplitudes are obtained from the equation of motion of the caisson, Eq. (2.3.15), in which the soil scattering and restoring forces and the inertia forces of the caison are involved. Since the caisson motion has the same frequency as waves and this frequency is low, the inertia forces are much smaller than the soil resistance forces. The equation of motion is, therefore, essentially a static equilibrium equation. As a result, the displacement amplitude is inversely proportional to shear modulus, and stresses are independent of shear modulus. Conversely, displacements increase with a decrease in the shear modulus. Figure 4.3.4 shows the displacements for four different shear moduli with a constant Poisson's ratio 0.2.

The stresses and pore pressure for two soils with different porosity and permeability are shown in Fig. 4.3.5. The soil porosity has a significant influence on the pore pressure but not on the displacements or stresses except the vertical normal stress.

The effect of soil depth on the contact stresses and displacements is illustrated in Figs. 4.3.6. For deeper soil, the shear stress underneath the caisson becomes smaller, while the effective normal stresses and displacements become larger.

4.4 The Distribution of Displacements, Stresses, and Porewater Pressure in the Soil

Using the same data (unless otherwise defined) as in the previous section, the distribution of displacements, stresses and pore-

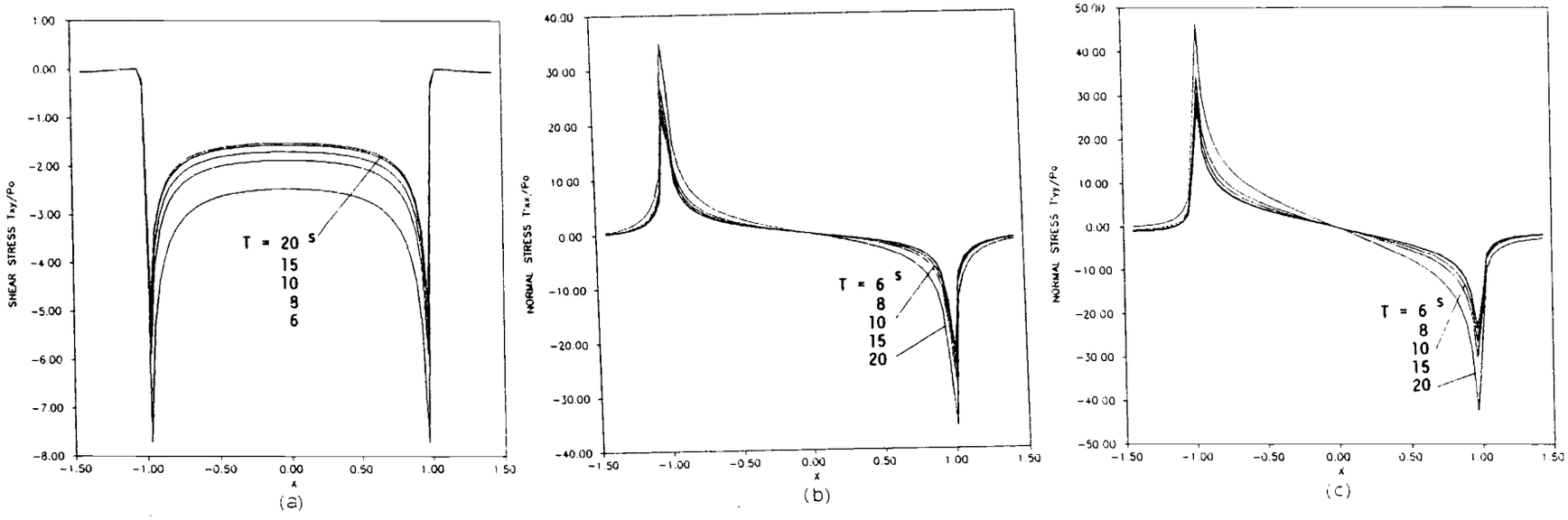

Figure 4.3.1. Wave period dependency of the soil responses along the mudline: (a) shear stress, (b) effective horizontal normal stress, (c) effective horizontal normal stress

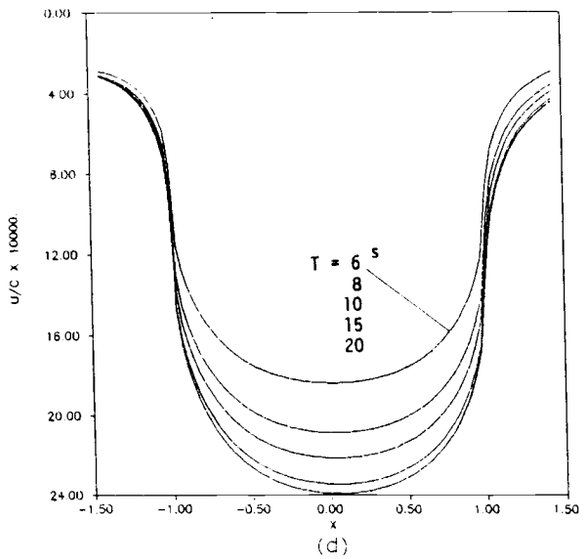

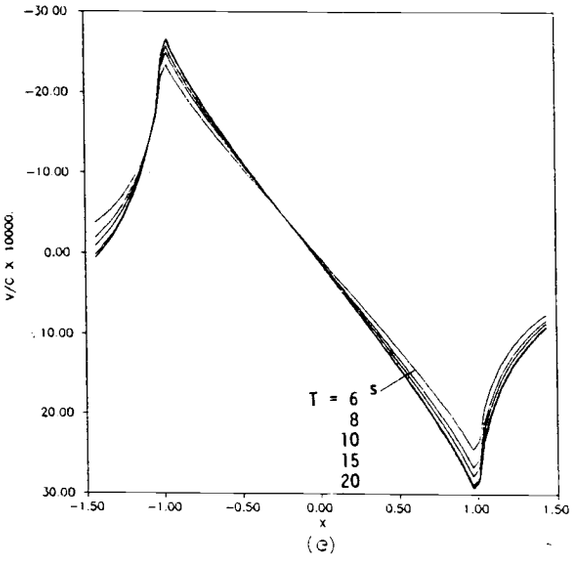

Figure 4.3.1. (contd.) Wave period dependency of the soil responses along the mudline: (d) horizontal displacement, and (e) vertical displacement

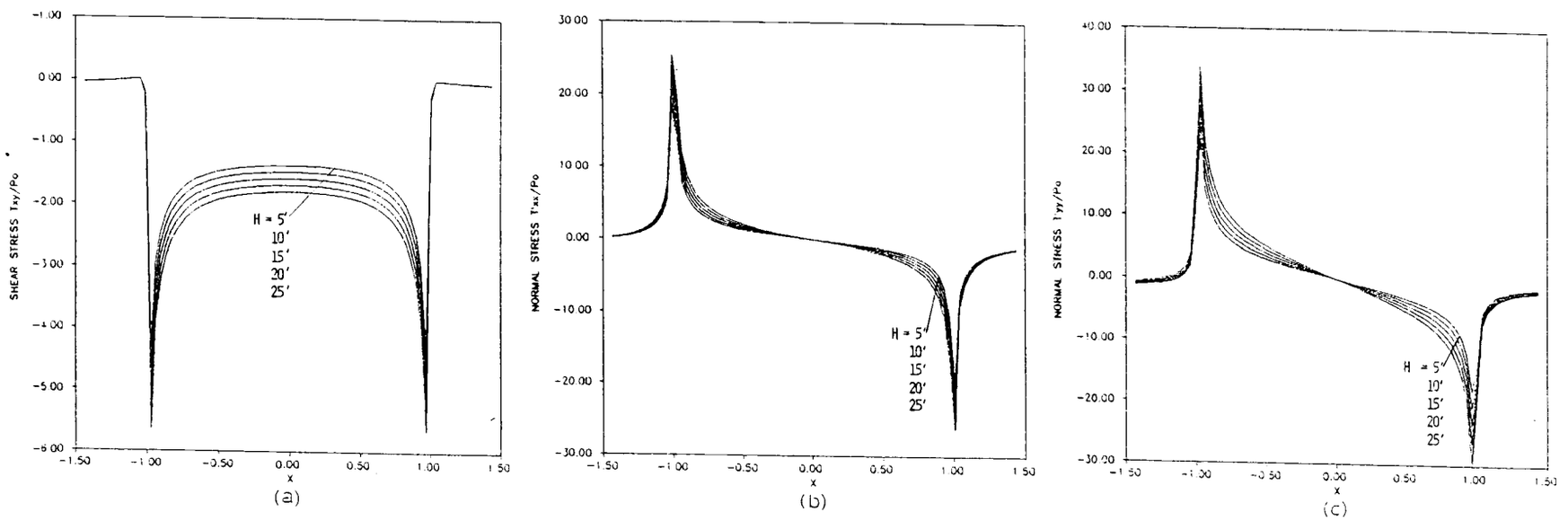

Figure 4.3.2. Wave height dependency of the soil responses along the mudline: (a) shear stress, (b) effective horizontal normal stress, (c) effective vertical normal stress

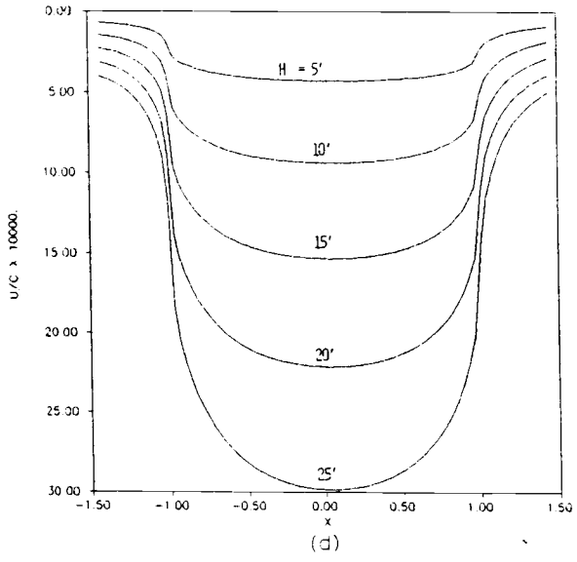

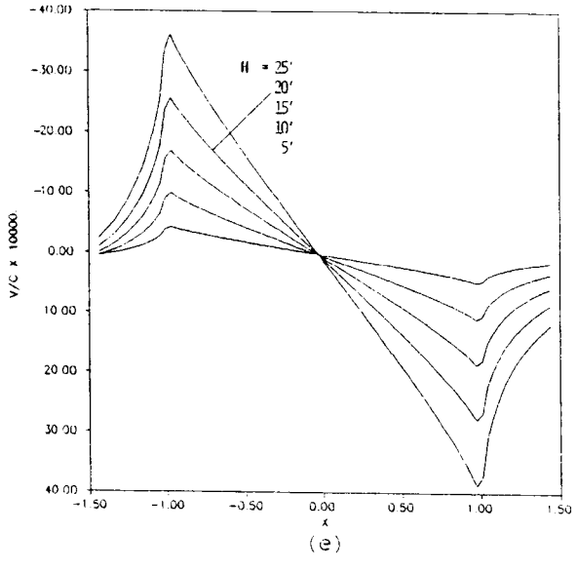

Figure 4.3.2. (contd.) Wave height dependency of the soil responses along the mudline: (d) hortizontal displacement, and (e) vertical displacement.

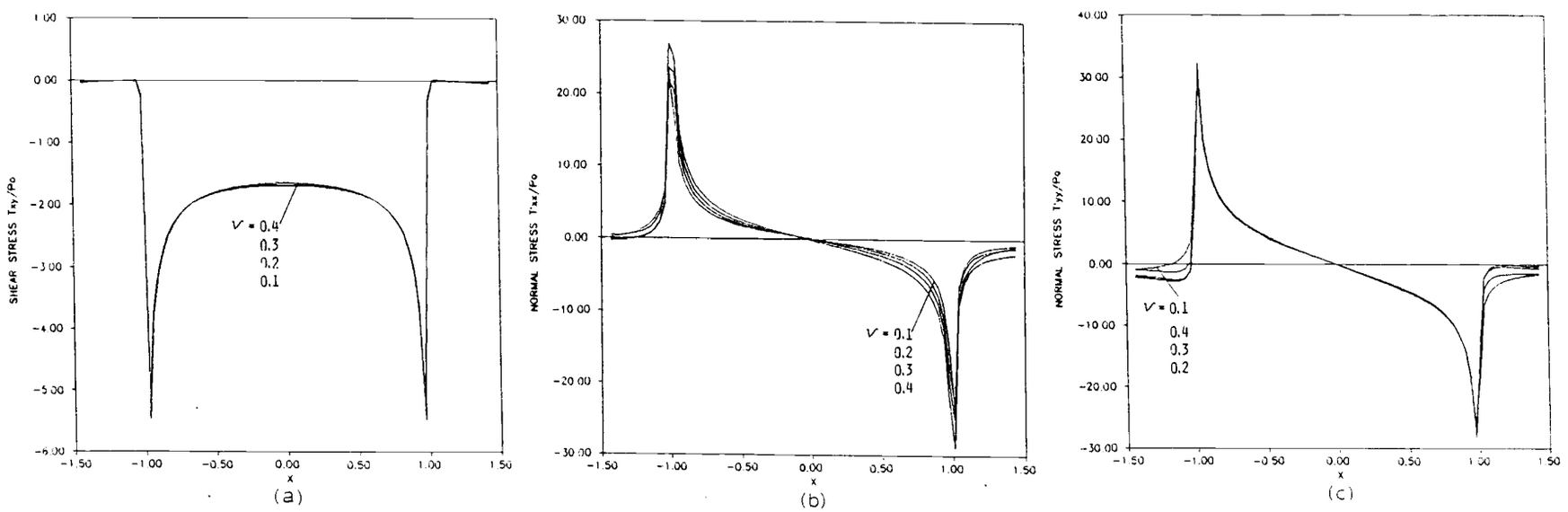

Figure 4.3.3. Poisson's ratio dependency of the soil responses along the mudline: (a) shear stress, (b) effective horizontal normal stress, (c) effective vertical normal stress

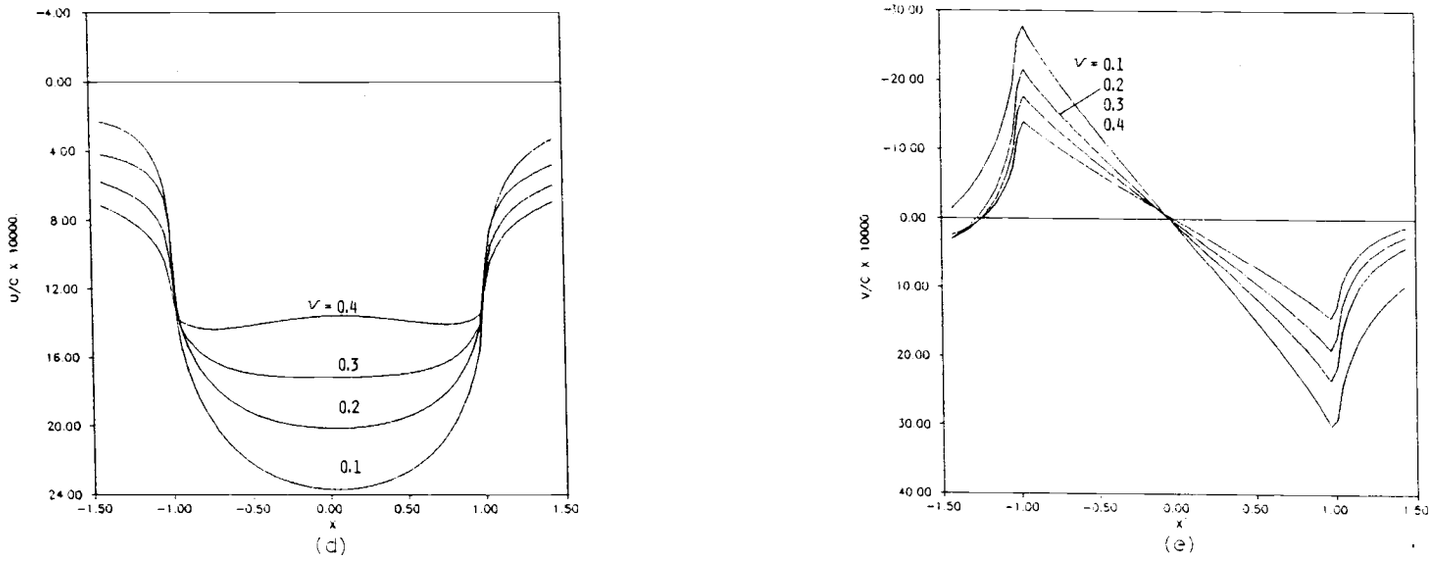

Figure 4.3.3. (contd.) Poisson's ratio dependency of the soil responses along the mudline: (d) horizontal displacement, and (e) vertical displacement

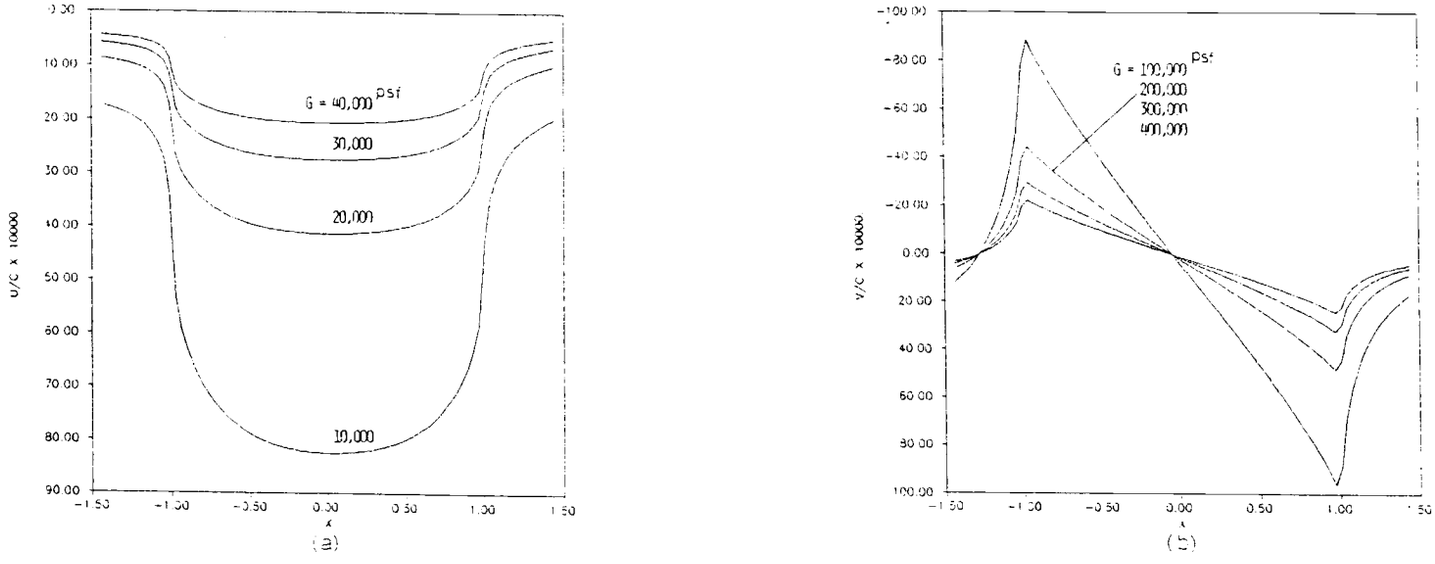

Figure 4.3.4. Shear modulus dependency of the soil displacements along the mudline: (a) hortizontal displacement and (b) vertical displacement.

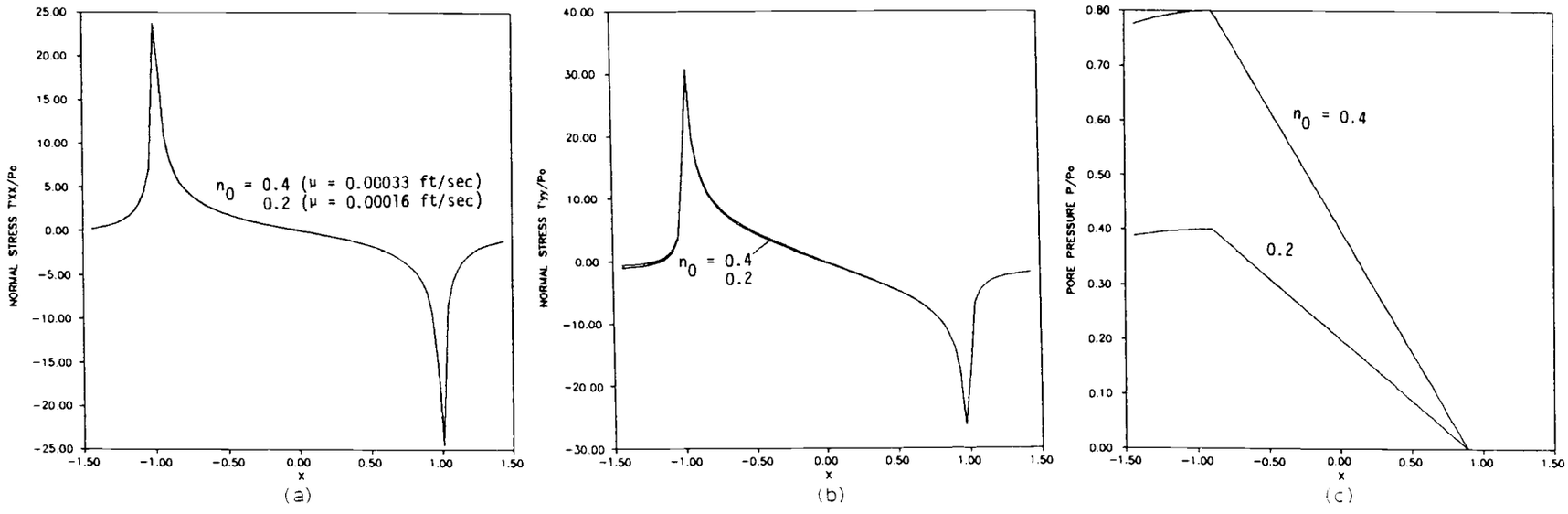

Figure 4.3.5. Porosity dependency of the soil responses along the mudline: (a) effective horizontal normal stress, (b) effective vertical normal stress, and (c) porewater pressure.

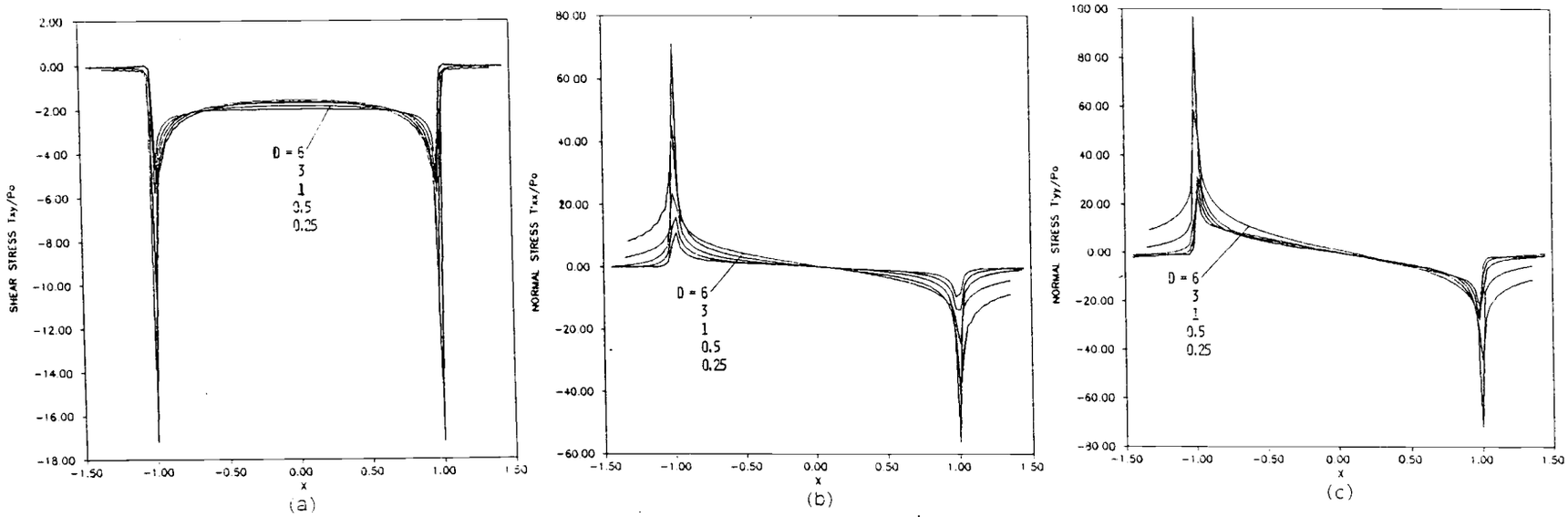

Figure 4.3.6. Soil depth dependency of the soil responses along the mudline: (a) shear stress, (b) effective horizontal normal stress, (c) effective vertical normal stress

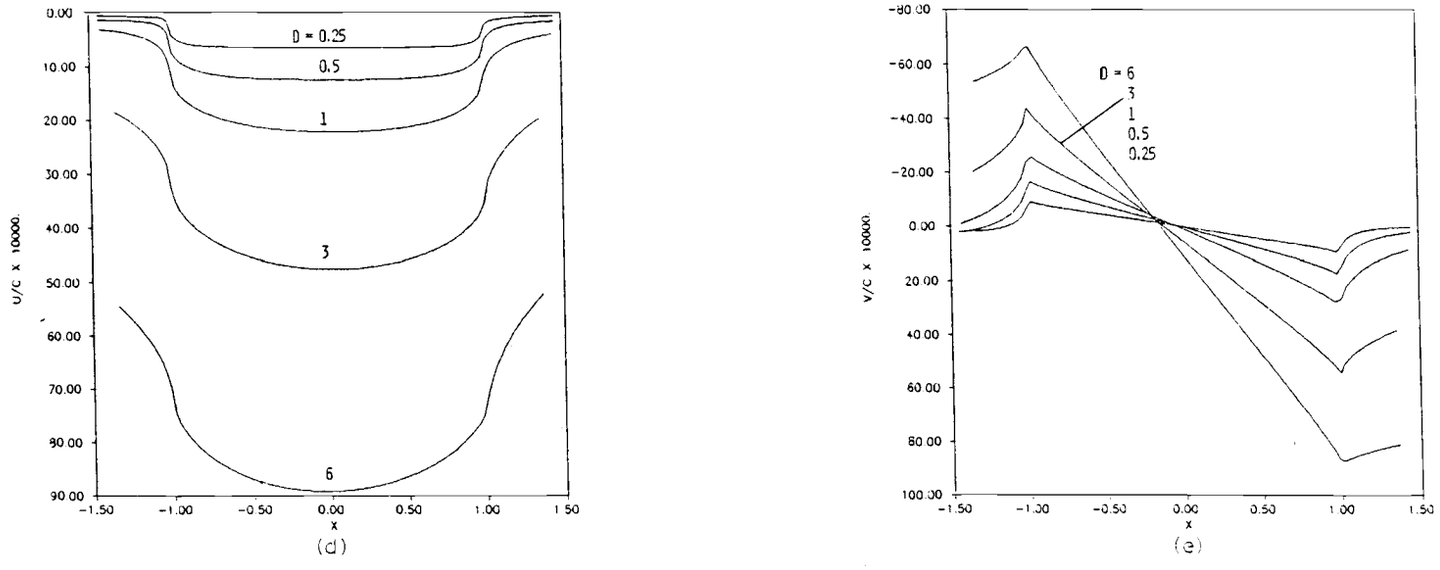

Figure 4.3.6. (contd.) Soil depth dependency of the soil responses along the mudline: (d) horizontal displacement, and (e) vertical displacement.

water pressure for the scattering problem and the radiation problem of outer region solution and the total solution including the boundary layer correction are shown in Figs. 4.4.1 through 4.4.5

4.4.1 The Scattering Problem

To more clearly reveal the behavior of the soil motion in problem (a) and problem (b), a soft soil is examined (i.e. Poisson's ratio $\nu = 0.35$, shear modulus $G = 111{,}000$ psf). Figure 4.4.1 shows the horizontal and vertical displacements in problem (a). Although wave pressure is restricted to the upstream portion of the mudline, this pressure causes soil motion beneath the caisson and behind the caisson. The maximum horizontal displacement occurs at the middle of the soil layer under the caisson toe. The horizontal displacement in the downstream portion in the soil layer is induced by the motion of the soil in the part which is under the caisson toe and adjacent to the hardbed. The vertical displacement spreads over from the maximum point at the caisson toe to some extent under the caisson. In problem (b), there are no displacements along the caisson-soil interface. The soil layer underneath the caisson is like a fixed-end column. The influence of the displacement on one side on the soil column is like a distributed load which induces deflection of the column. These phenomena are shown in Fig. 4.4.2. Therefore, the scattering problem does induce soil motion as well as stresses under the fixed caisson.

Figure 4.4.3 is the response of a stiff soil (i.e. $\nu = 0.15$, $G = 410{,}000$ psf) in the scattering problem. Comparison of Figs. 4.4.2 (a), (b) and 4.4.3 (a), (b) indicates that the stiffer soil has

less displacement. The high total stresses and porewater pressure are near the caisson toe and are due to larger displacements and displacement gradients of the soil.

4.4.2. The Radiation Problem

The horizontal displacement is rather symmetrical with respect to the caisson center line as shown in Fig. 4.4.4(a). The surge motion of the caisson tends to dominate this displacement. The vertical displacement, Fig. 4.4.4 (b), is antisymmetrical with respect to the caisson center line because the pitch motion is dominant in this displacement. Singularities result in high stress and pore pressure concentration at the caisson toe and heel. These phenomena are shown in Figs. 4.4.4 (c) through 4.4.4 (f). Interestingly, the total horizontal normal stress decays with the depth much faster than the vertical normal stress.

4.4.3 The Total Solution

The total horizontal displacement and shear stress are mainly due to caisson motion. The vertical displacement is influenced by both caisson motion and wave pressure, cf. Figs. 4.4.5 (a), (b) and (c). After including the boundary layer correction, the effective normal stresses and pore pressure have higher gradients under the caisson toe and heel, cf. Figs. 4.4.5 (d), (e) and (f). The pore pressure contours are similar to the numerical solution developed by deQuelerij et al. (1979).

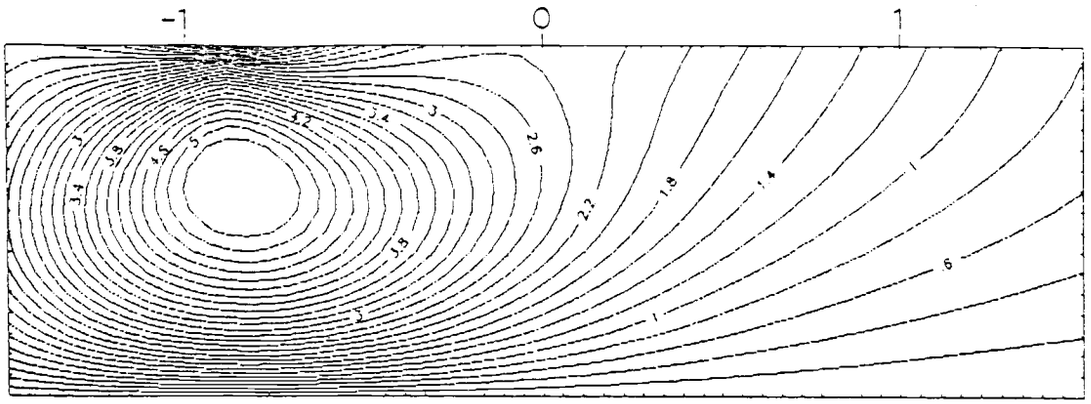

(a) HORIZONTAL DISPLACEMENT U/C X 10000.

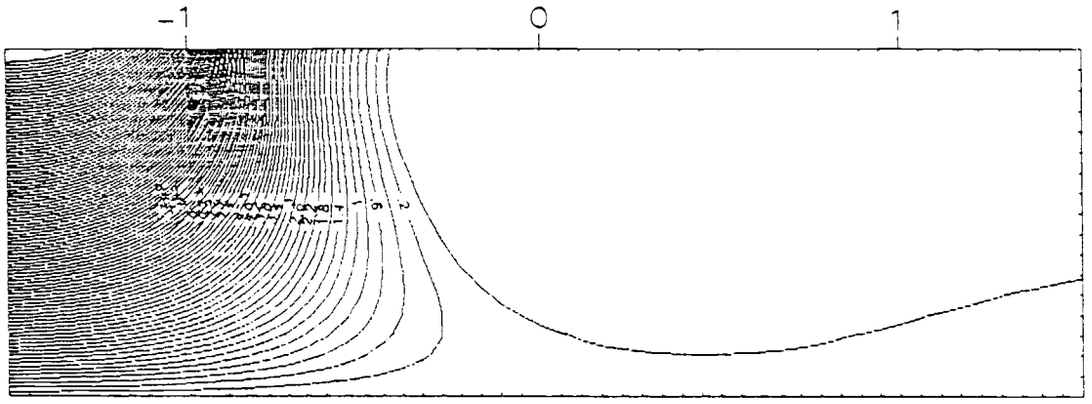

(b) VERTICAL DISPLACEMENT V/C X 10000.

Figure 4.4.1. Contours of the outer soil displacements for problem (a).

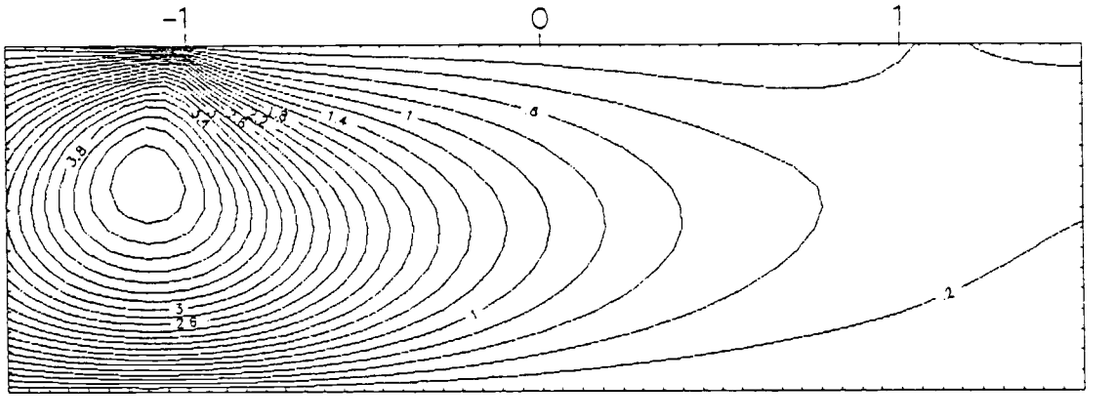

(a) HORIZONTAL DISPLACEMENT U/C X 10000.

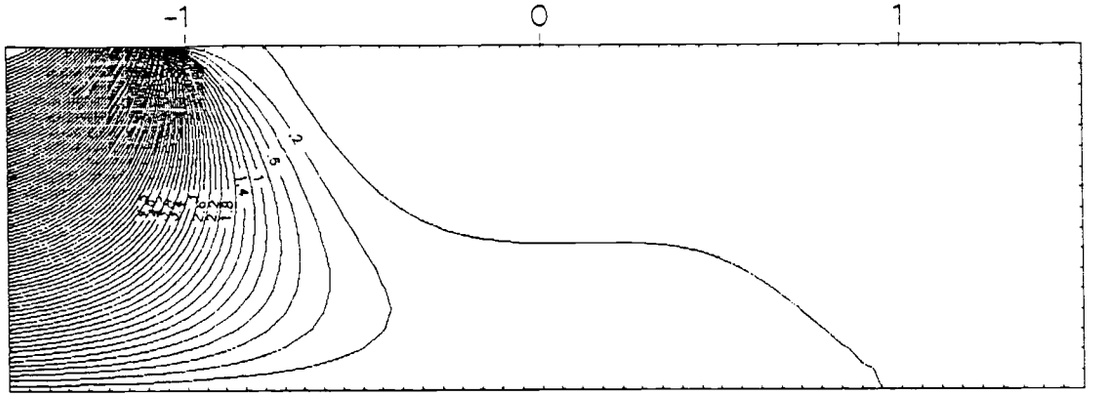

(b) VERTICAL DISPLACEMENT V/C X 10000.

Figure 4.4.2. Contours of the outer soil displacements for problem (b).

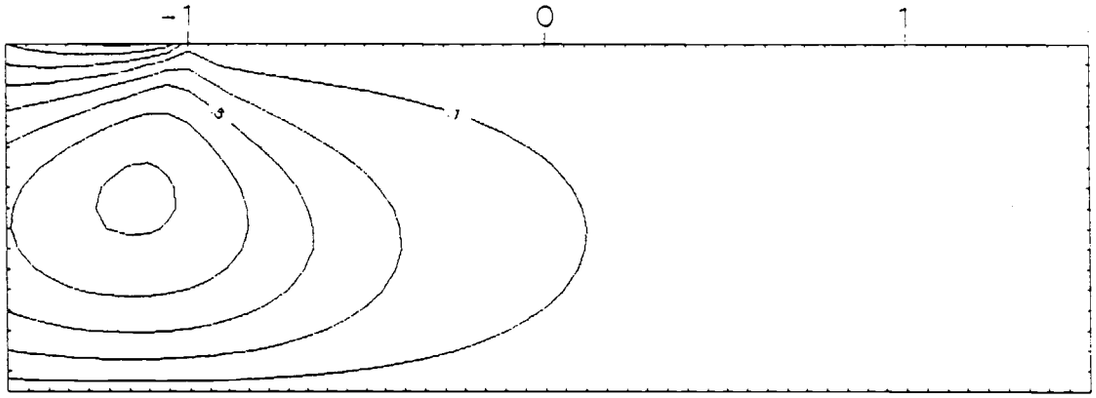

(a) HORIZONTAL DISPLACEMENT U/C X 10000.

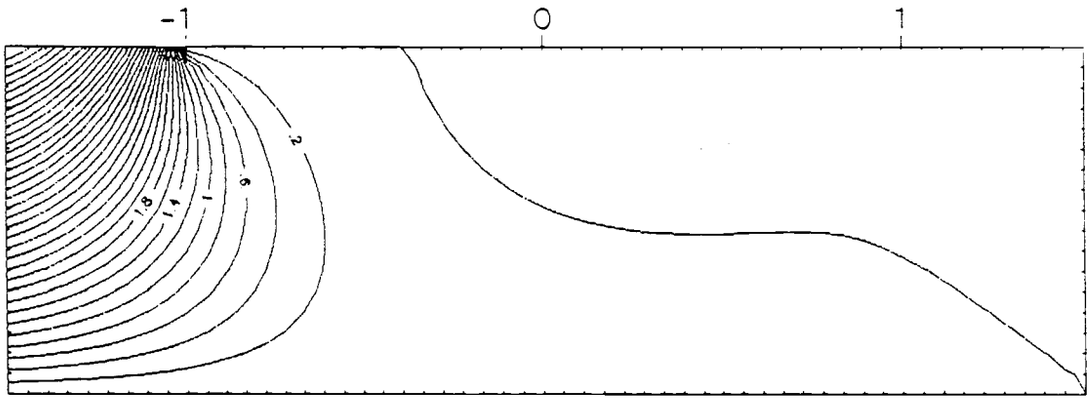

(b) VERTICAL DISPLACEMENT V/C X 10000.

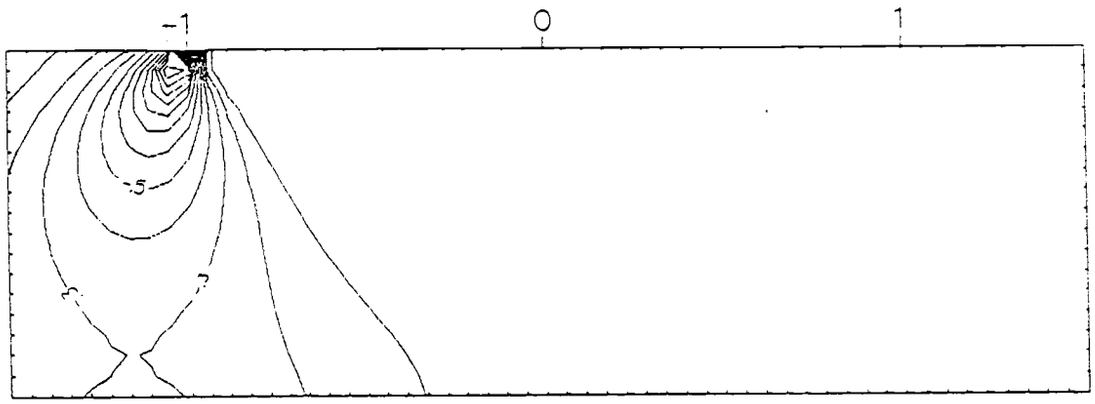

(C) SHEAR STRESS Txy/Po

Figure 4.4.3. Contours of the outer soil responses for the scattering problem

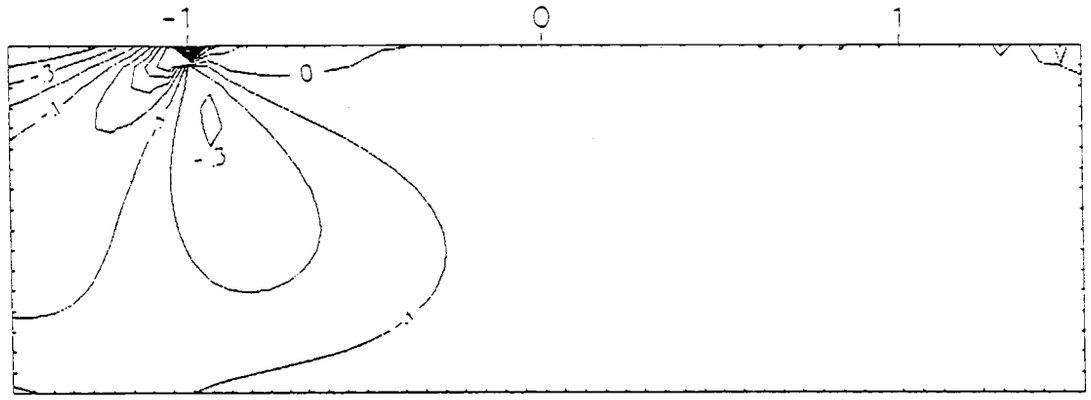

(d) HORIZONTAL NORMAL STRESS Txx/Po

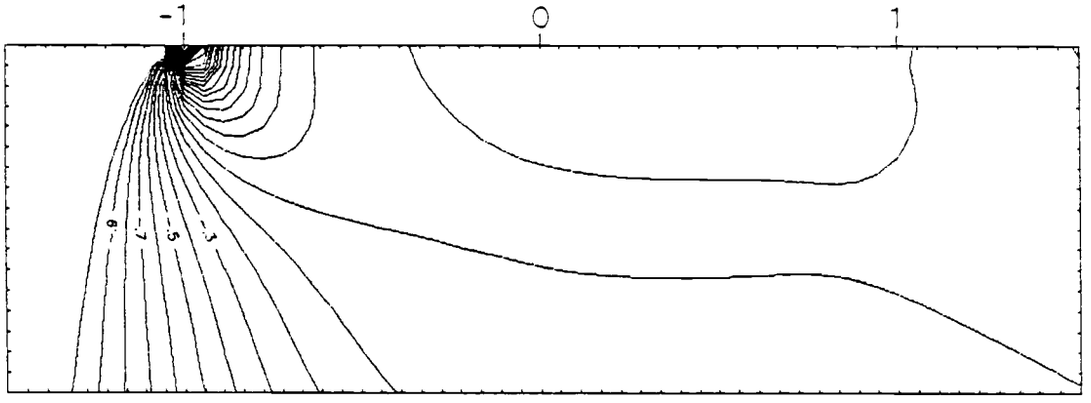

(e) VERTICAL NORMAL STRESS Tyy/Po

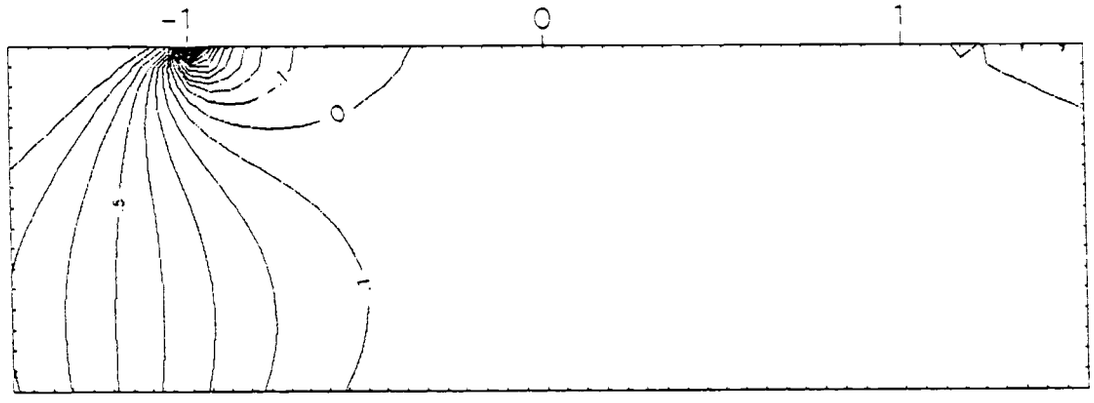

(f) POREWATER PRESSURE P/Po

Figure 4.4.3. (contd.) Contours of the outer soil responses for the scattering problem

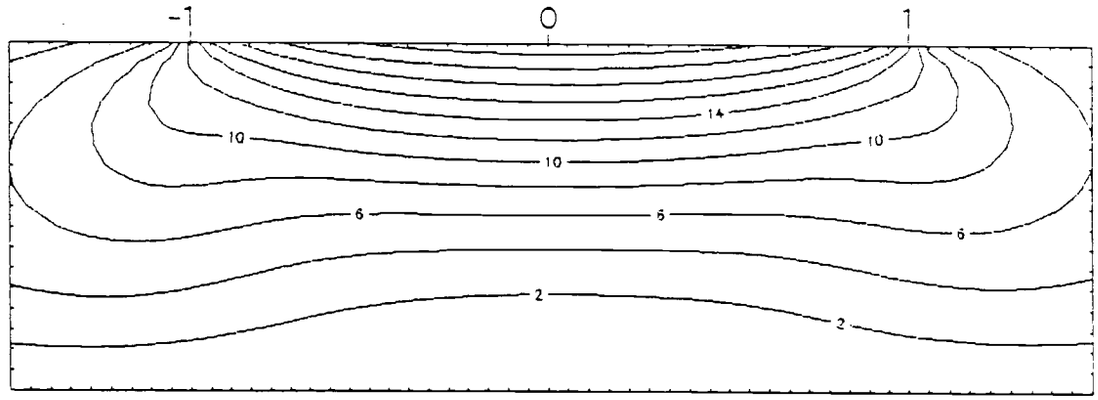

(a) HORIZONTAL DISPLACEMENT U/C X 10000.

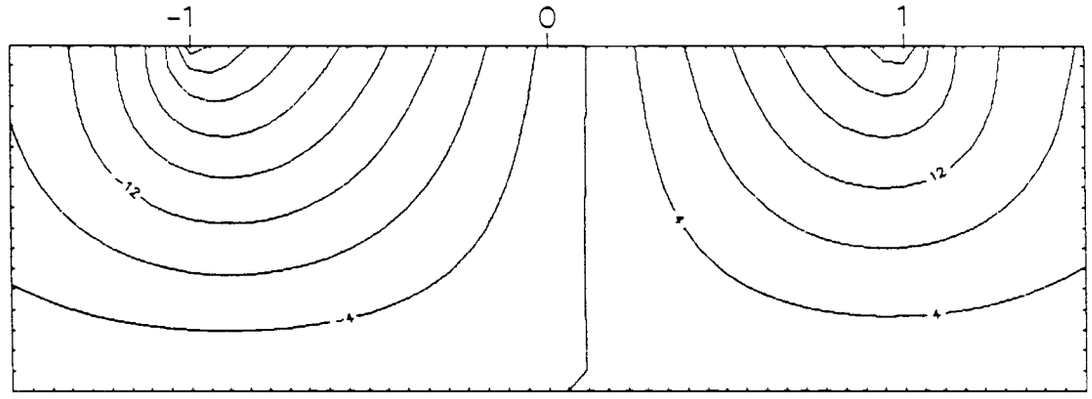

(b) VERTICAL DISPLACEMENT V/C X 10000.

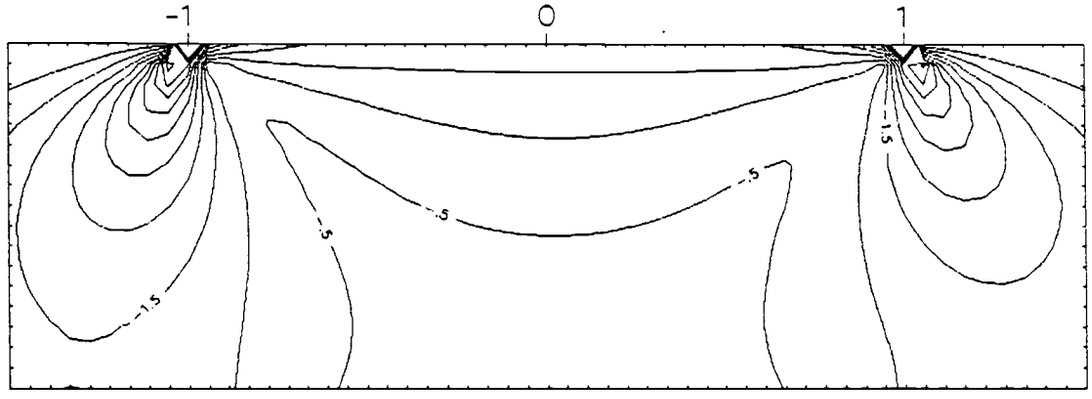

(c) SHEAR STRESS Txy/Po

Figure 4.4.4. Contours of the outer soil responses for the radiation problem

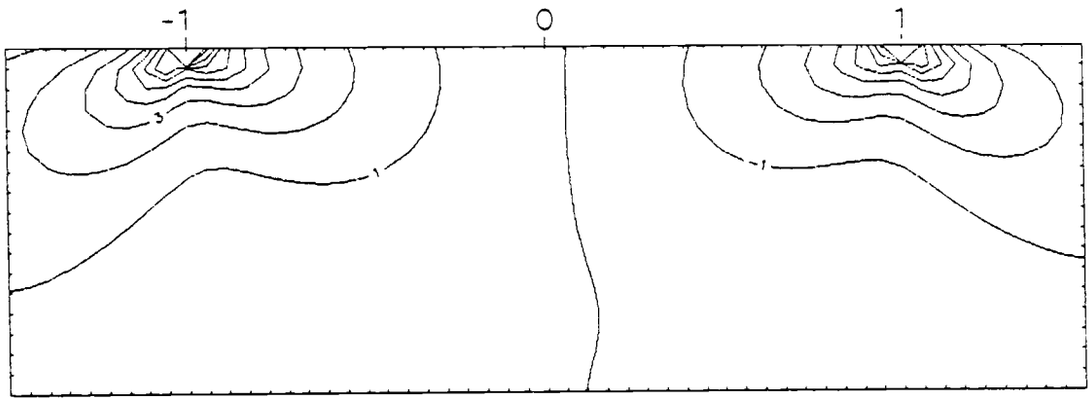

(d) HORIZONTAL NORMAL STRESS Txx/Po

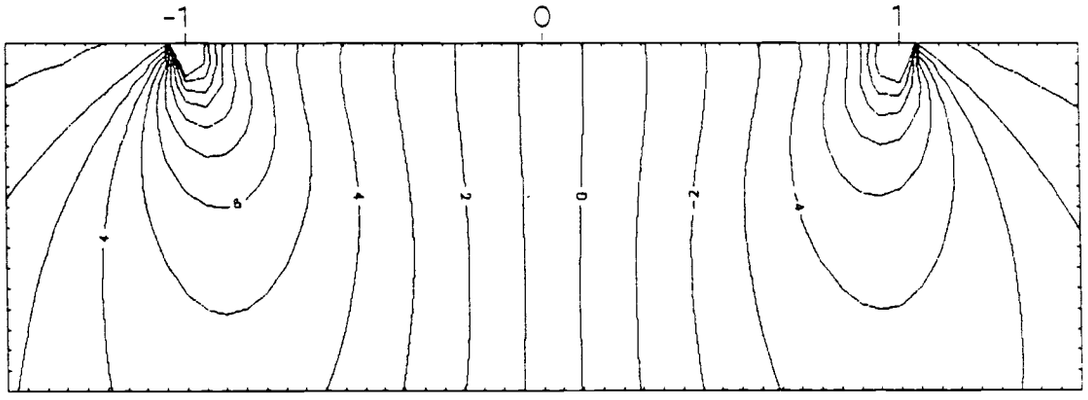

(e) VERTICAL NORMAL STRESS Tyy/Po

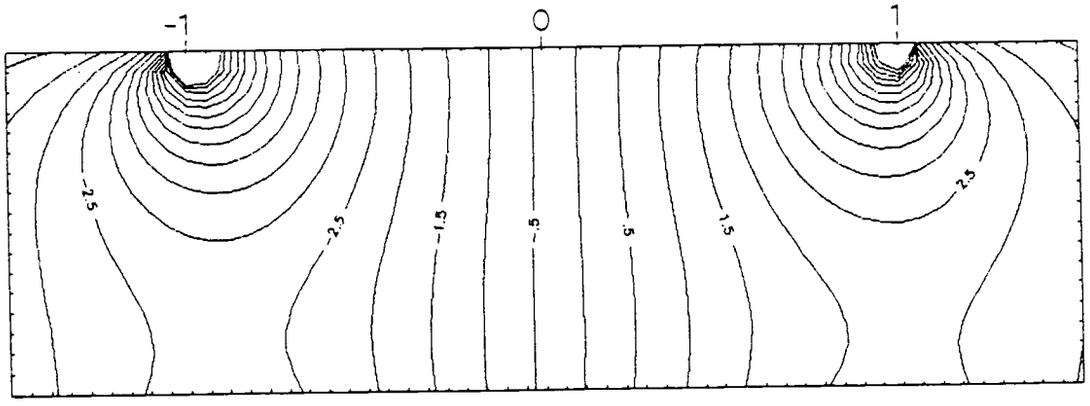

(f) POREWATER PRESSURE P/Po

Figure 4.4.4. (contd.) Contours of the outer soil responses for the radiation problem

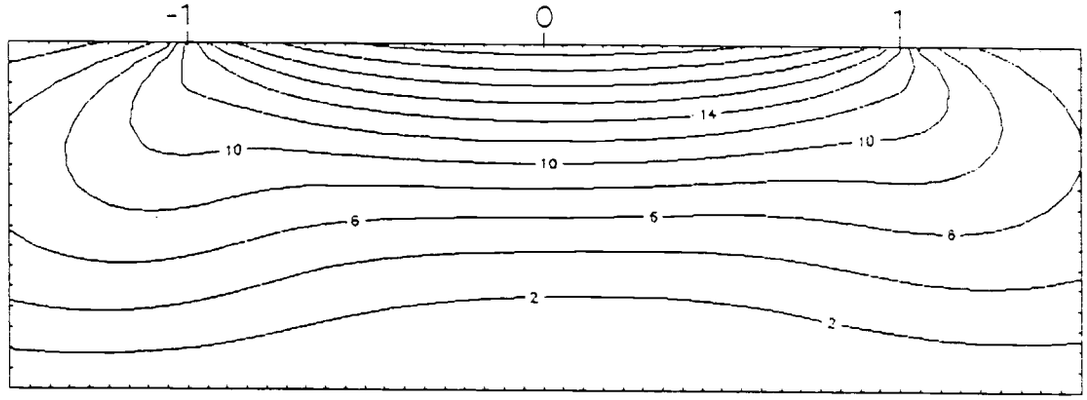

(a) HORIZONTAL DISPLACEMENT U/C X 10000.

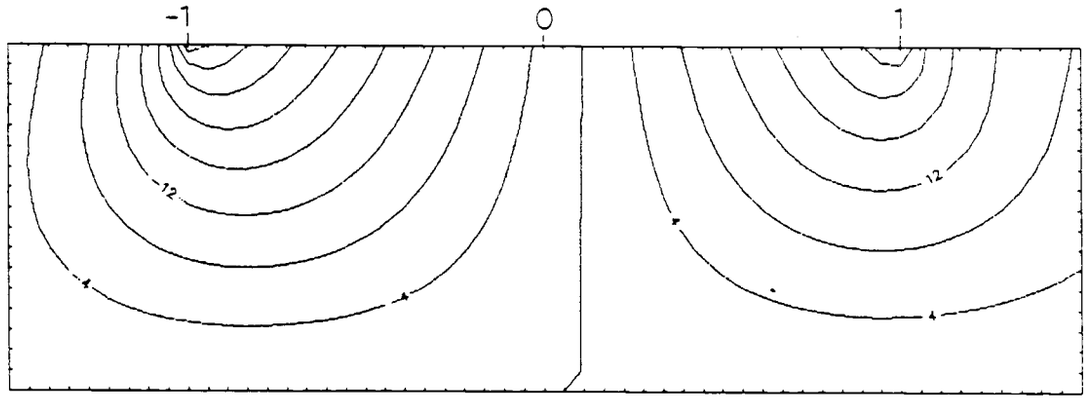

(b) VERTICAL DISPLACEMENT V/C X 10000.

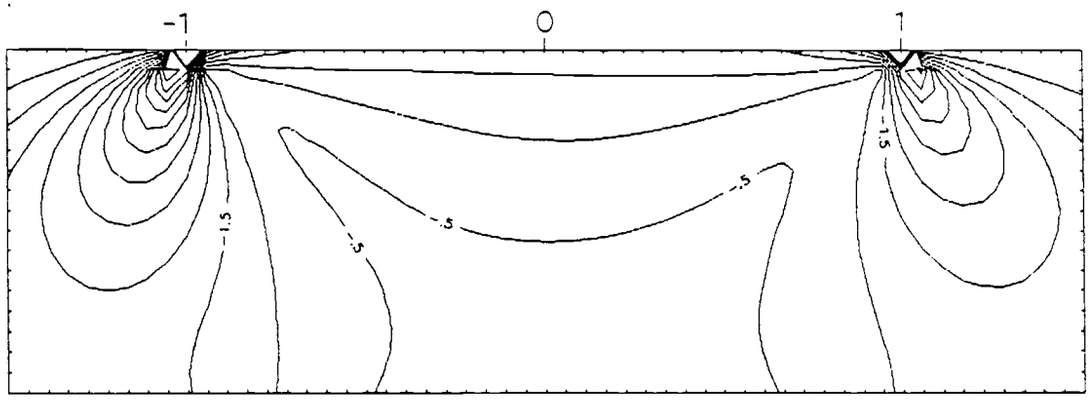

(c) SHEAR STRESS Txy/Po

Figure 4.4.5. Contours of the soil responses for the total solution

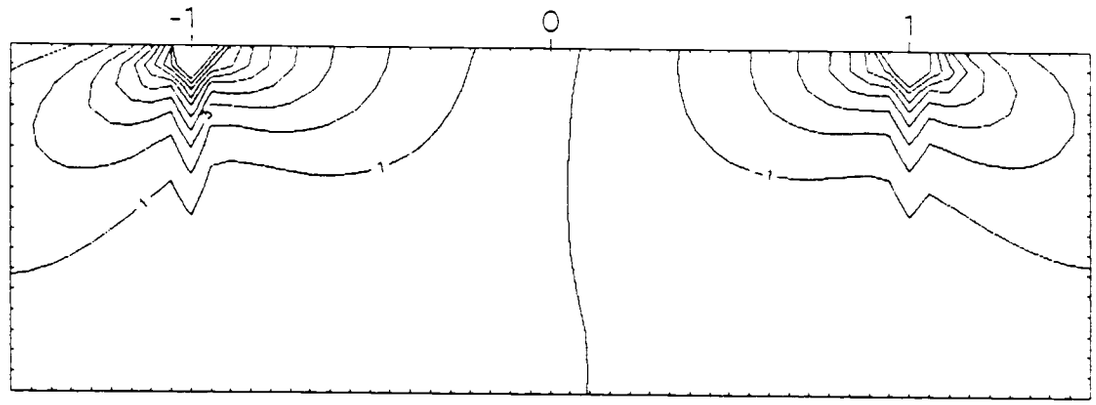

(d) EFFECTIVE NORMAL STRESS Txx'/Po

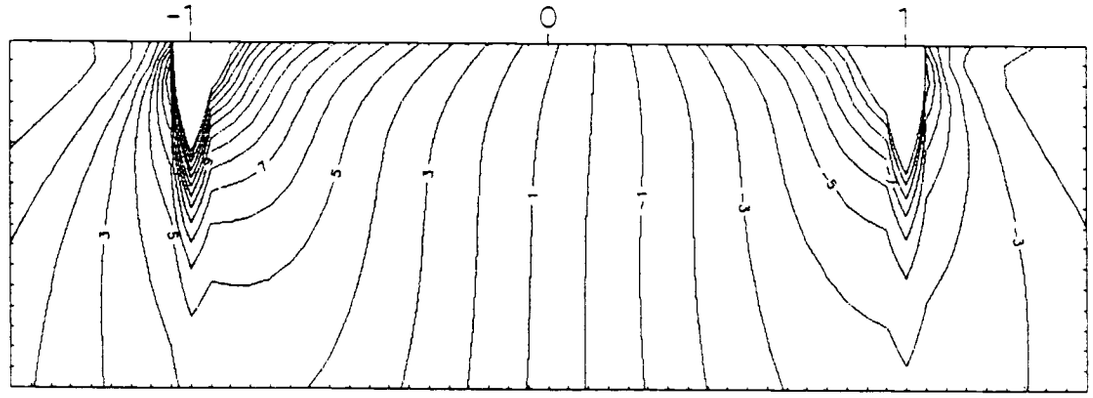

(e) EFFECTIVE NORMAL STRESS T'yy/Po

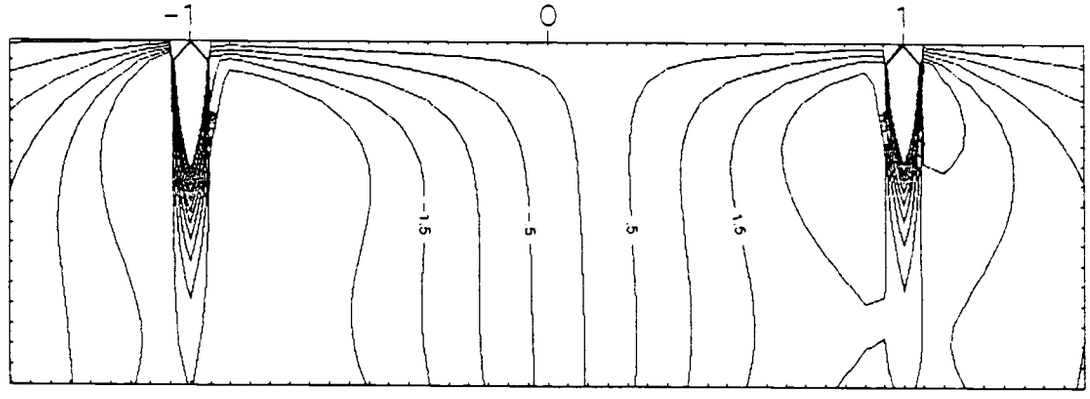

(f) POREWATER PRESSURE P/Po

Figure 4.4.5. (contd.) Contours of the soil responses for the total solution

5. LARGE-SCALE EXPERIMENTS

Two series of experiments of wave-soil-caisson interaction were conducted at the O. H. Hinsdale Wave Research Facility at Oregon State University during the springs of 1984 and 1985. A variety of wave conditions were examined. Incident waves, reflected waves and transmitted waves were measured. Wave pressures were measured along the front face and bottom of the caisson and along the upstream portion of the mudline. Porewater pressure was also monitored in the soil under the caisson. The three degrees of caisson motion, surge, heave, and pitch were measured with displacement transducers.

5.1 Experiment Apparatus and Conditions

5.1.1 Wave Tank

The OSU wave flume is 342 ft long, 12 ft wide and 15 ft deep. The hinged-flap-type wave generator is able to produce solitary, periodic, and random waves. Simple periodic waves up to 8 seconds in period and 5 ft in height can be generated. A polyeurathene seal around the edges of the wave board confines the water to one side of the board. Precast concrete panels are available to form a false bottom with the desired water depth and slope.

5.1.2 Test Section

A test section, 30 ft long, 5 ft wide and 4 ft deep, was constructed at the downstream end of the wave flume. A false channel bottom was installed to match the test section. The sides and ends of the test section were fabricated with reinforced plyboard. The entire test section was bolted to the channel bottom and side

walls. Figure 5.1.1 shows the test section. The side chambers of the test section were filled with highly permeable gravel to provide extra strength and prevent side wall deflection during the test. A perforated pipe was laid on the bottom of the channel to facilitate drainage during dewatering. In the middle chamber, a 3 ft layer of sand was used for the 1984 test. In the 1985 test, a 6 inch thick reinforced concrete slab was constructed as an impermeable hardbed 1.5 ft above the bottom to provide a 1 ft deep sand layer above the concrete slab. These sand beds were fluidized and then reconsolidated back to a homogeneous condition. The fluidization was accomplished by using an inverted T-shaped manifold to inject a high-pressure water jet into the sand [Nath et al. (1977)]. This procedure prepared a uniform soil layer to ensure the repeatability of the experiments. The reconsolidation was induced through an overburden of 6 to 12 inches of pea gravel separated from the sand by a geotextile. Rubble then was placed over the lift of the pea gravel to form a rubble bedding layer of approximately one foot thickness. The rubble had a mean diameter of 4 inches. The test caisson was then placed on the rubblemound foundation. Toe and heel protection were added. The cross section of the test structure is shown in Fig. 5.1.2.

To provide a continuous caisson face across the width of the flume, a fixed dummy side structure was constructed along each side of the caisson. These dummy sections were rigidly attached to the side walls of the wave flume. To allow caisson motion, a one-inch gap was left between the caisson and side structures. The front of

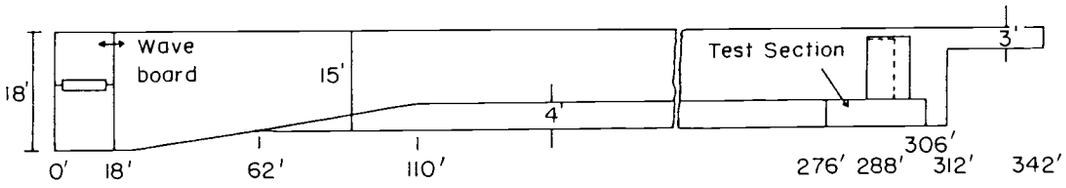

(a) Elevation

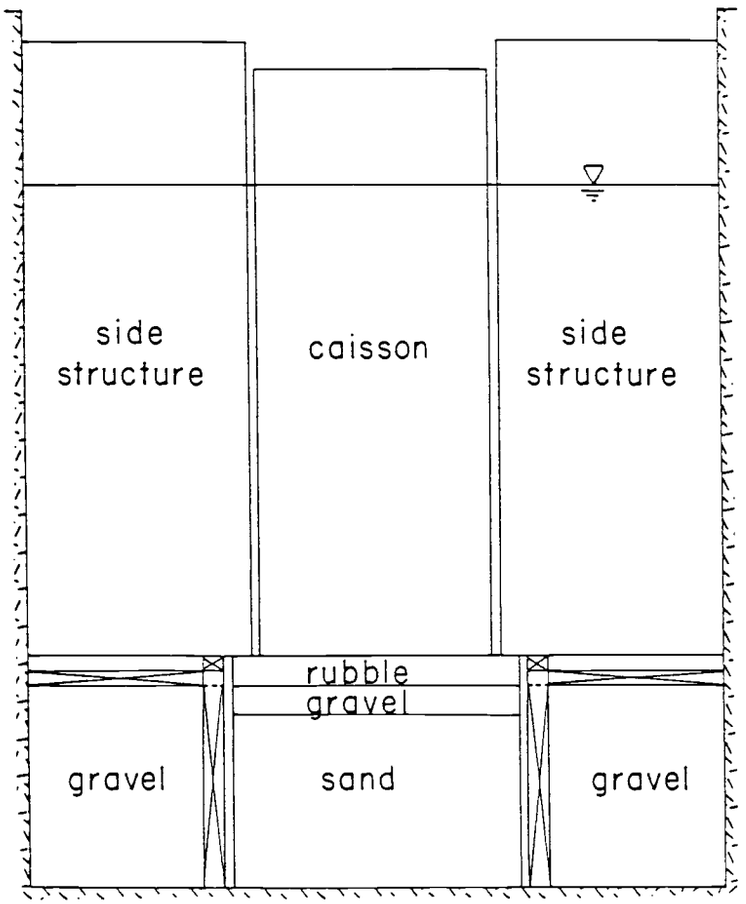

(b) Cross section

Figure 5.1.1. Test section: (a) elevation and (b) cross section.

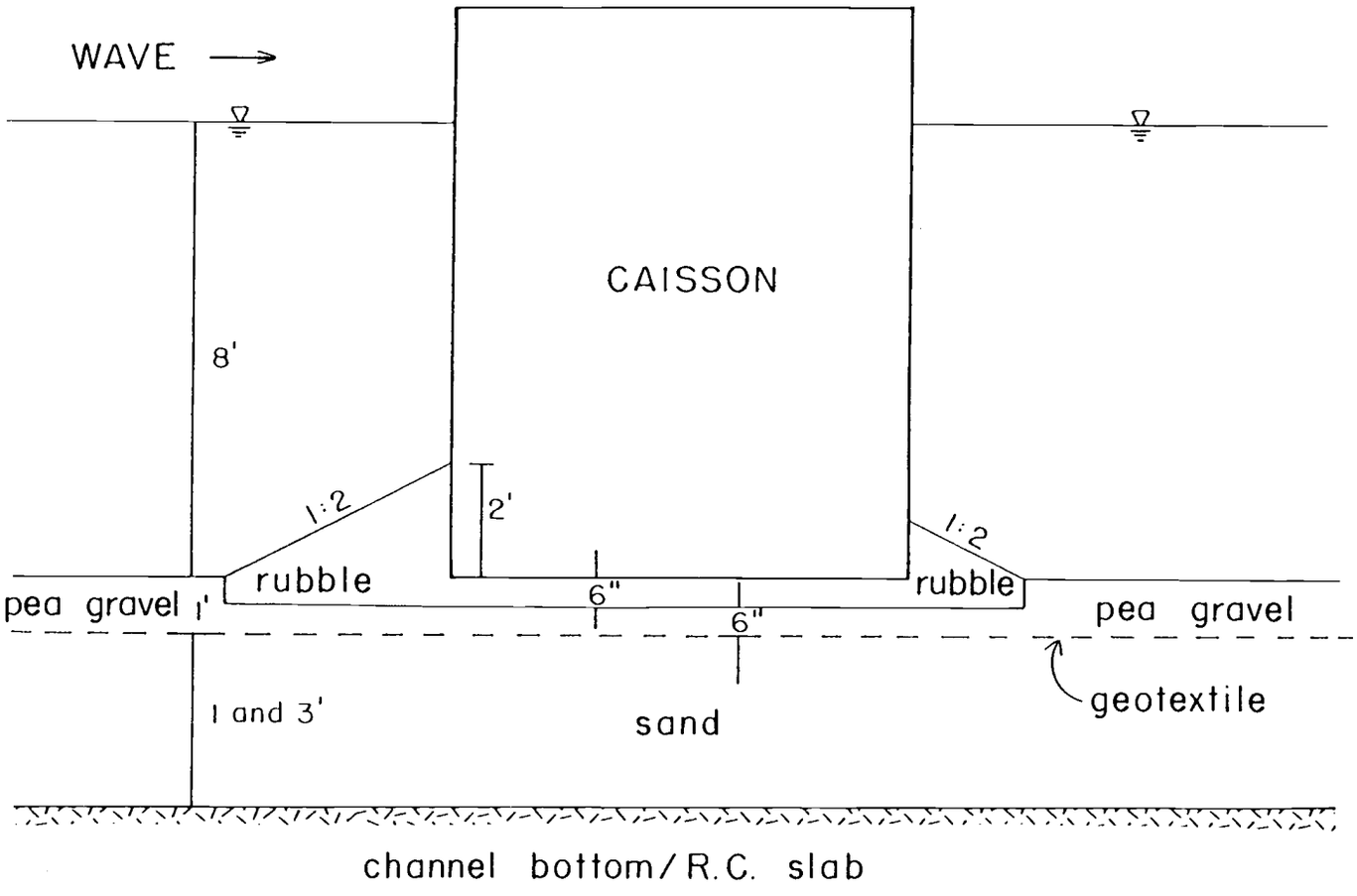

Figure 5.1.2. Cross section of the test structure.

the gap was covered with a rubber strip to provide a watertight seal. The side structures were 3 ft 10.5 inches wide, 12 ft 4 inches long, and 10.5 ft high. They were constructed of heavily reinforced plyboard and rigidly bolted to the bottom and sides of the wave flume.

5.1.3 The Test Caisson

The test caisson was 10 ft high, 8 ft long and 4 ft wide. It was also made of heavily reinforced plyboard. To obtain the desired mass, the caisson was filled with concrete cylinders and sand bags. For the 1984 test, only the weight of the cylinders and bags were measured. For the 1985 test, the locations of cylinders and bags were also measured. The weight of the empty caisson in air was 1470 pounds. The total weight of the caisson including the ballast was 5640 pounds in the 1984 test. For the 1985 test, three different weights of the caisson in water were tested, as shown in Table 5.1.1.

Table 5.1.1 Weight, mass, and mass moment of inertia of the caisson in water for the 1985 tests

Weight (pounds)	Mass (slugs)	Mass Moment of Inertia (slugs-ft^2)
5,280	164	2,765
7,150	222	5,630
10,690	332	14,631

5.1.4 Sand Bed Properties

The physical properties of the soils for the 1984 and 1985 experiments are summarized in Table 5.1.2.

Table 5.1.2 Soil properties for the tests

Year	1984	1985
Poisson's ratio	0.3	0.3
Porosity	0.5	0.5
Shear Modulus	140,000 psf	110,000 psf
Permeability Coefficient	0.00033 ft/sec	0.00033 ft/sec

5.1.5 Instruments and Their Locations

The wave profiles and caisson motions were measured with sonic transducers. The dynamic pressures were measured with pressure transducers (Druck model PDCR10). Carborundum filter stones covered the transducer housings to prevent soil from clogging the pressure transducers. A small amount of air in the stone may significantly affect the dynamic response of the transducers. Therefore, the stones were first boiled to remove air and then always kept underwater. The transducers were calibrated by raising and lowering the still water level in the channel before and after each sequence of runs.

The instrument locations for the 1984 and 1985 tests are shown in Figs. 5.1.3 and 5.1.4, respectively.

5.1.6 Wave Conditions

The tests were run at a water depth of 8 ft. The periods and heights of simple periodic waves were based on Dean's stream function wave theory [Dean (1974)]. The relationship between the wave case, wave steepness, and relative water depth is shown in Fig. 5.1.5. The wave case, height, and period employed in the tests are shown in

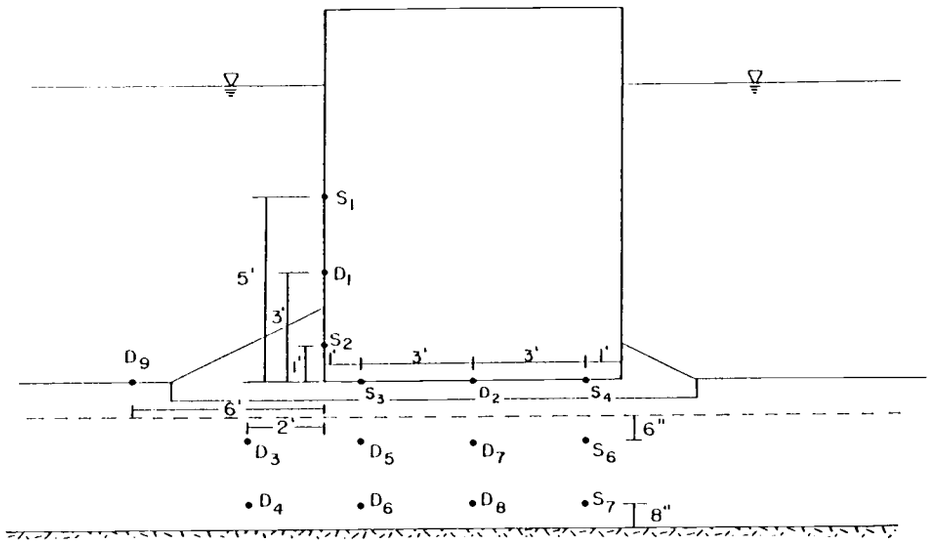

(a) pressure monitors

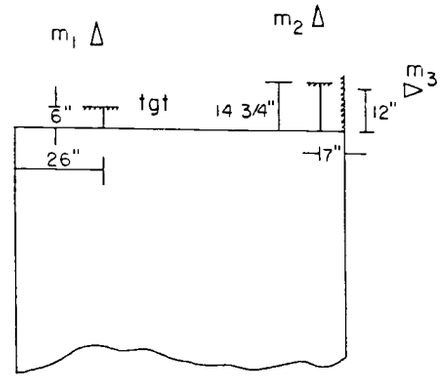

elevation

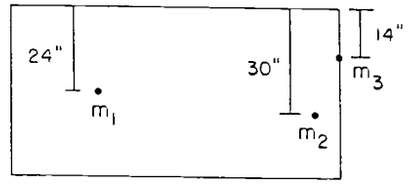

plan

(b) displacement monitors

Figure 5.1.3. Instrumentation for the 1984 test: (a) pressure monitors and (b) displacement monitors.

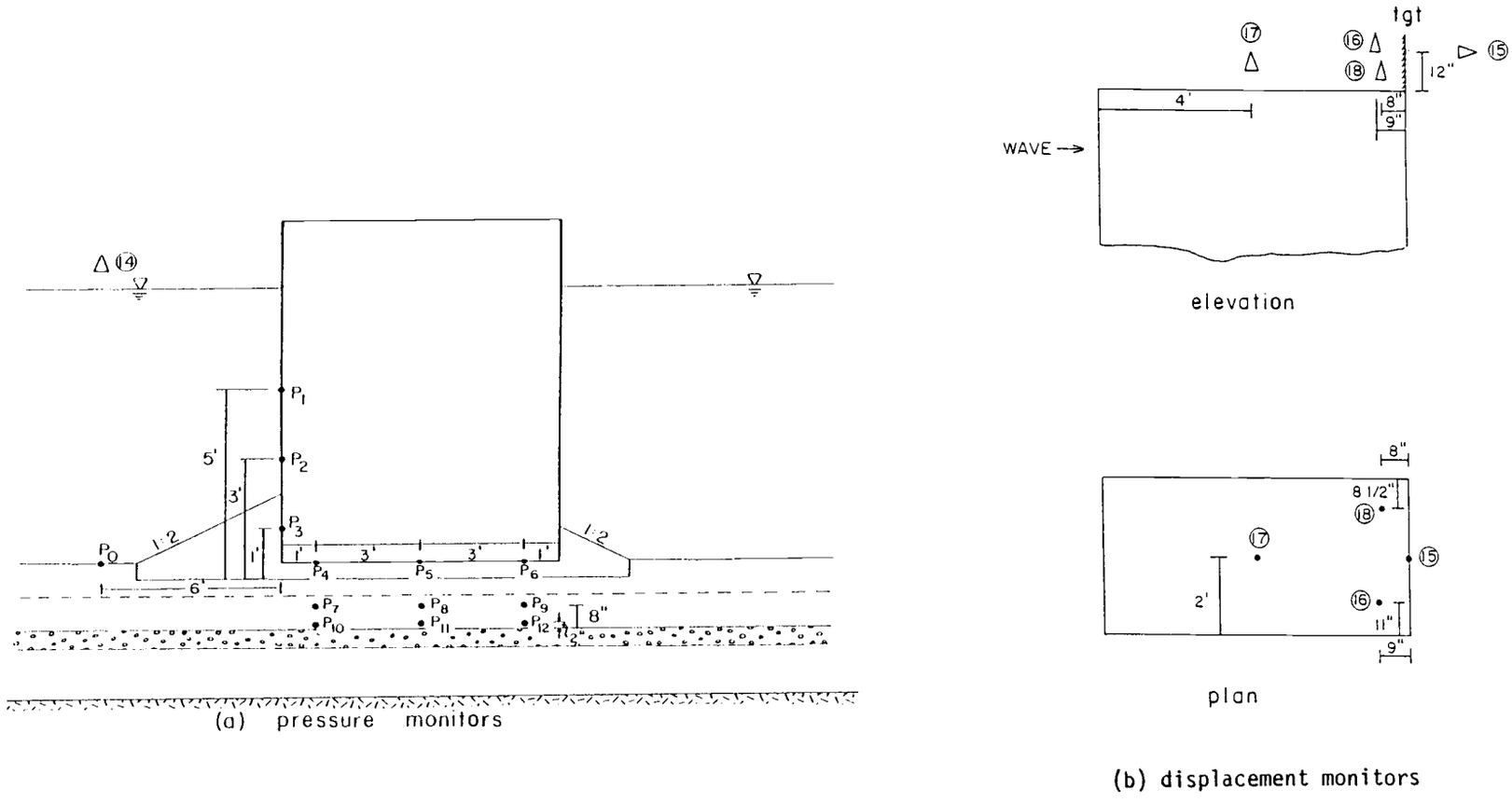

Figure 5.1.4. Instrumentation for the 1985 test: (a) pressure monitors and (b) displacement monitors.

Table 5.1.3. In the 1985 experiments, the wave periods were slightly adjusted to provide pure standing waves in the flume.

Table 5.1.3 Wave conditions for the tests

Wave Case	Wave Period (sec.)	Wave Height (ft)
8A	1.77	0.68
8B	1.77	1.36
8C	1.77	2.03
7A	2.80	1.28
7B	2.80	2.52
7C	2.80	3.76
6A	3.95	1.47
6B	3.95	2.92
6C	3.95	4.40
5A	5.59	1.55
5B	5.59	3.07
4A	8.84	1.56

5.2 Experimental Results

One of the sonic profilers used to measure the caisson motion malfunctioned in the 1984 experiment. Several of the pressure transducers in the 1985 experiment did not calibrate well. Therefore, only the pore pressure measurements of the 1984 tests and the caisson motion measurements of the 1985 tests were analyzed.

Typical records of pore pressure and displacement are shown in Figs. 5.2.1 (a) and 5.2.1 (b). Significant noise was observed in the displacement measurements. To remove this noise, a moving box car filter was used. Figs. 5.2.2 (a) and (b) show the mean and variance of the data with respect to different filter widths. An eleven-point

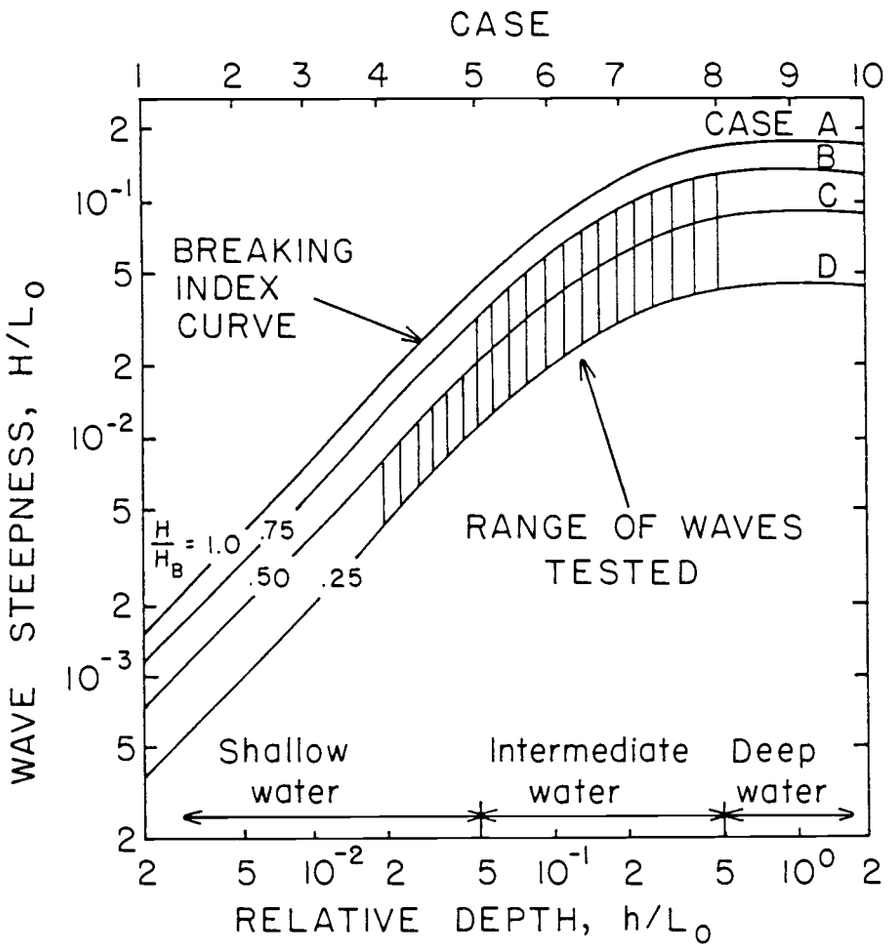

Figure 5.1.5. Definition diagram for Dean's stream function wave cases.

moving box car (i.e.Δt = 0.076~0.381 sec) was used. At this width, the mean and variance are expected to be nearly constant.

The dimensionless pore pressure amplitudes are shown as a function of the period in Fig. 5.2.3. The pressure amplitudes were scaled by S2; the pressure on the caisson front face measured one ft above the mudline. A line has been drawn through the means of each data set. The caisson motion had less influence on gages D3 and D4, and the pressure decayed with the soil depth. The two pairs D5, D6 and S6, S7 were obviously affected by the caisson motion because the pore pressure increased with the soil depth. This is predicted by the theory. For the gages D3, D4, D5, D6 and D7, the dimensionless pressure amplitudes are proportional to the wave period. For the gages S6 and S7, the pressure amplitudes are inversely proportional to the wave period.

The dimensionless mudline displacements are plotted against H/h (wave height to water depth) for various values of h/Lo (depth over deep water wave length) in Fig. 5.2.4. Generally, the displacements increase with increases in wave height or wave period. This result is anticipated because the wave force on the caisson is proportional to the wave height and wave period. However, the vertical and rotational displacements are somewhat scattered.

5.3 Comparison of Theory and Measurements

The measurements of D5, D6, D7, S6 and S7 (cf. Fig. 5.1.3) were compared with the analytical model. Figure 5.3.1 shows the calculated pressure versus the measured pore pressure. Although the trend is predicted, there is considerable scatter. This is clearly seen in

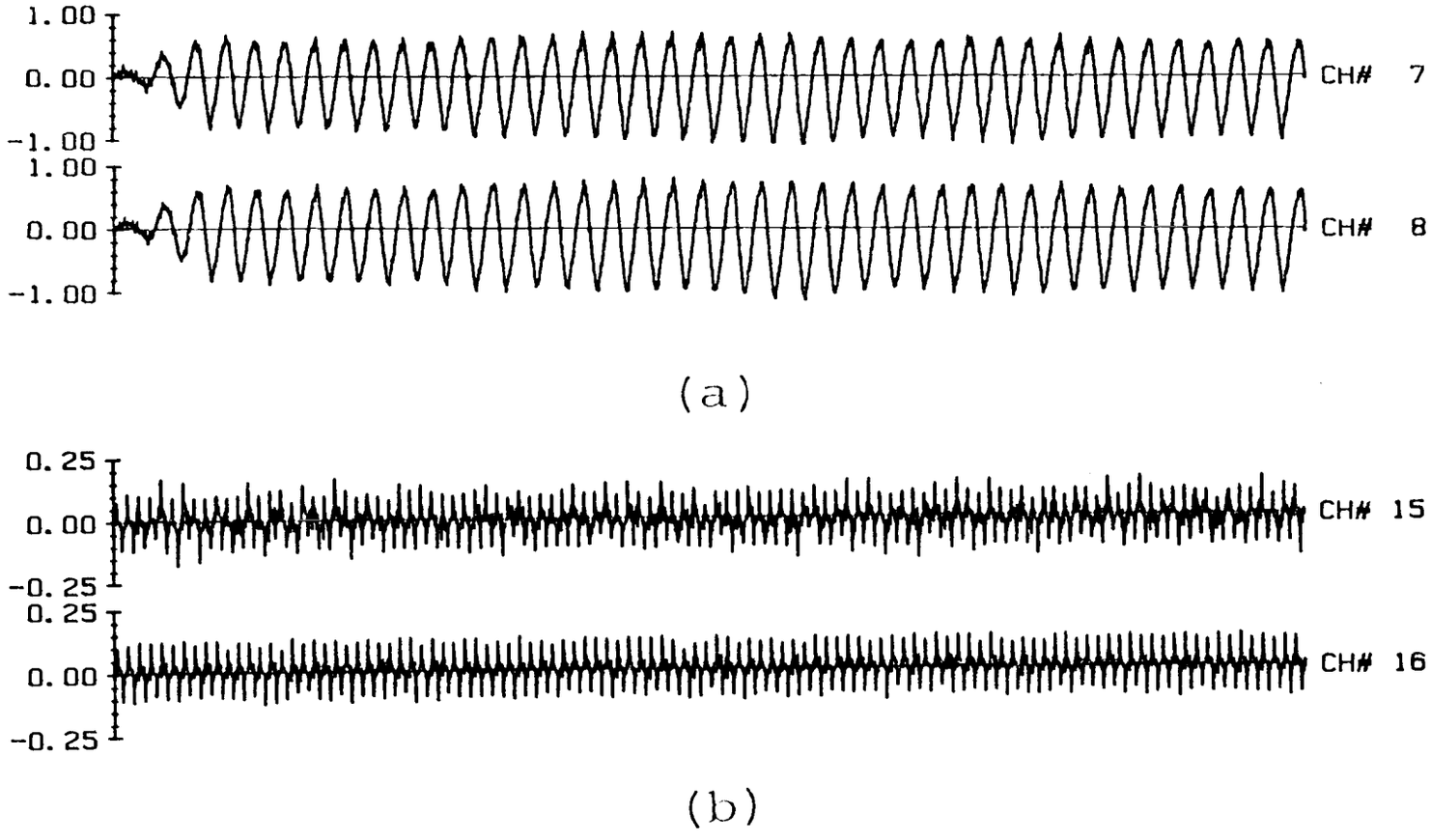

Figure 5.2.1. Measurement samples: (a) pore pressure and (b) caisson motion.

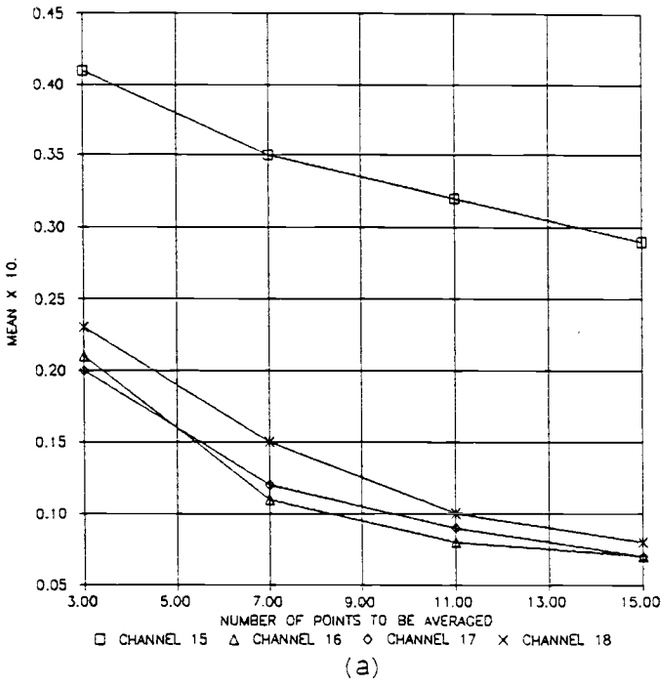

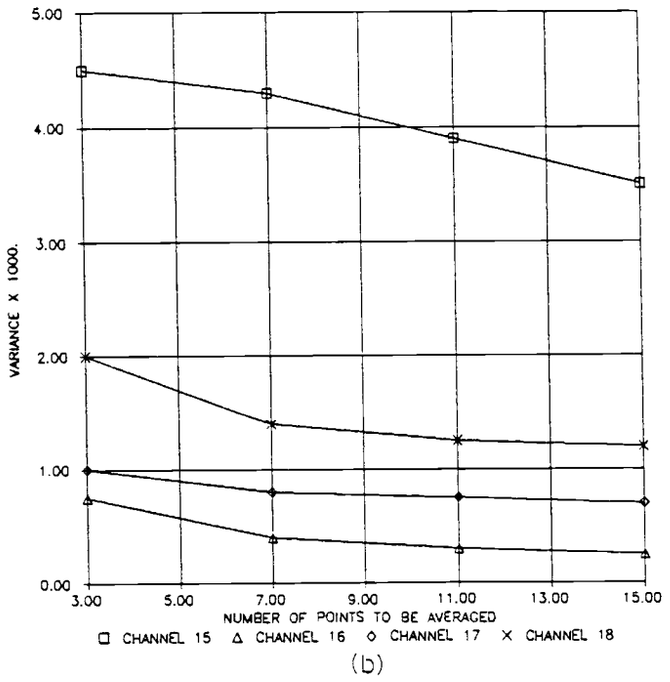

Figure 5.2.2. Typical (a) mean and (b) variance of the smoothed displacement measurements as a function of number of points to be averaged.

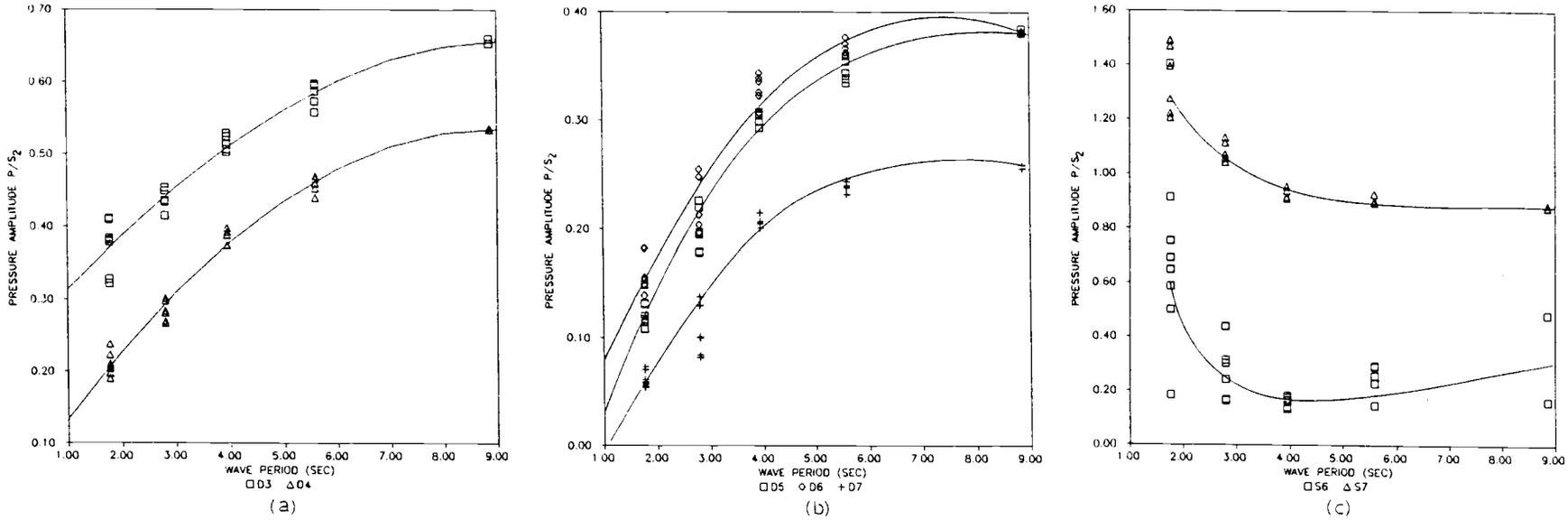

Figure 5.2.3. Pore pressure amplitude of laboratory measurements: (a) gages D3 and D4, (b) gages D5, D6, and D7, and (c) gages S6 and S7 as a function of wave period.

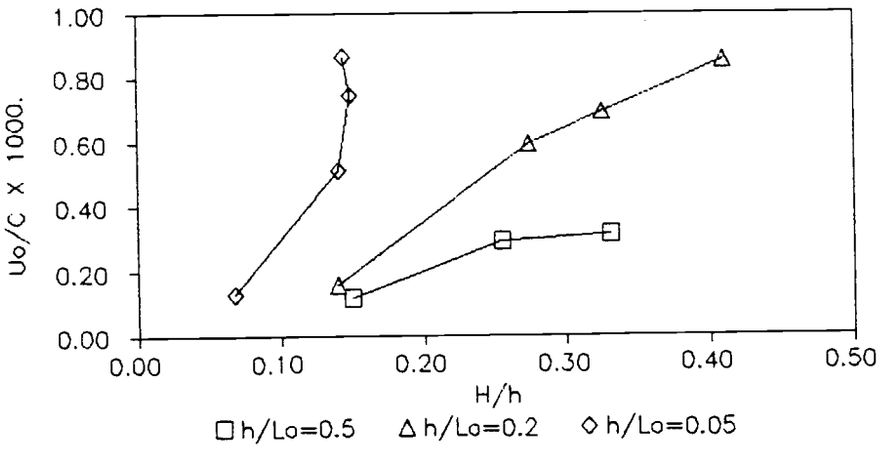

(a)

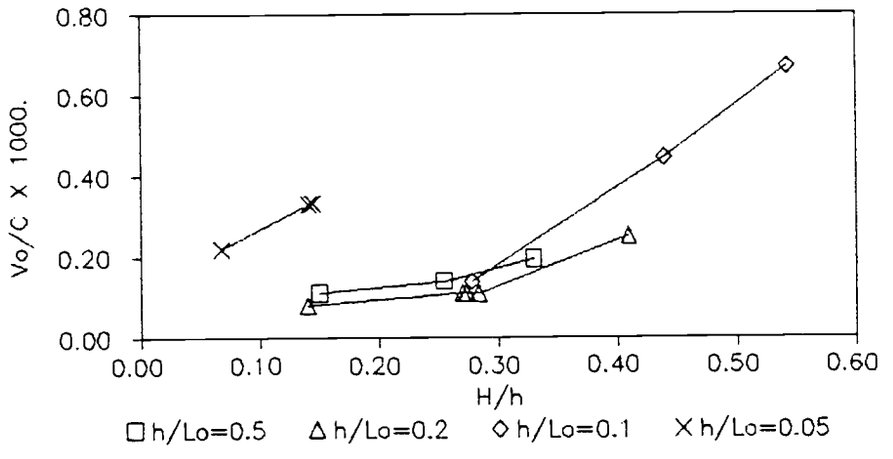

(b)

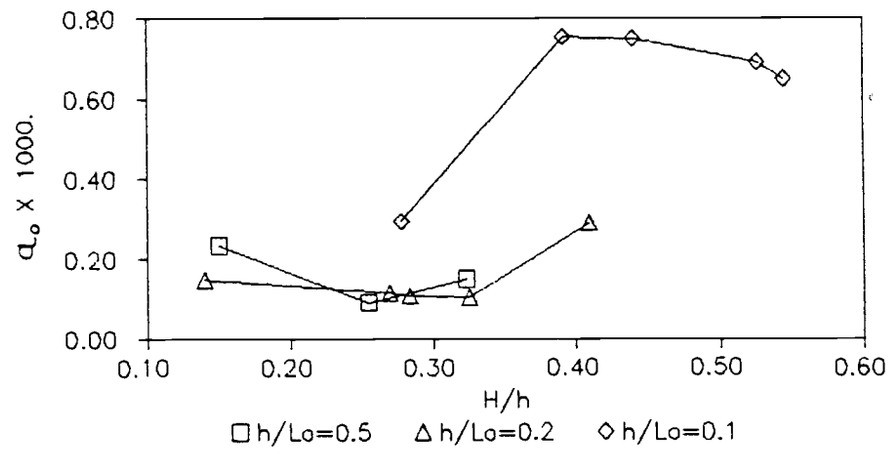

(c)

Figure 5.2.4. Dimensionless mudline displacements of laboratory measurements: (a) horizontal displacement, (b) vertical displacement, and (c) angular displacement as a function of dimensionless wave height for different dimensionless water depth.

Fig. 5.3.2 which shows the ratio of the measured to the predicted for each gage. Except D5 and S7, the ratios are all within one standard deviation from the mean. Figure 5.3.3 shows the computed contours of pore pressure and measurements. Again, the trend is in general agreement but there is considerable scatter. The deviation of the predicted porewater pressure from the measured may result from the assumption of a linear wave pressure distribution underneath the caisson. A more accurate pressure model being developed by Ward (1986) may be employed to obtain a more realistic pressure boundary condition. Unfortunately, this model was not completed in time to be used in present study.

The measured and the predicted displacements are shown in Fig. 5.3.4. The dimensionless displacements were plotted to the dimensionless calculated horizontal wave force on the caisson F_1/wh^2. The wave force F_1 was calculated by the method recommended in the Shore Protection Manual (1984). The measured displacements are rather scattered. The horizontal and the vertical displacement data are larger than the predicted. However, the measured rotational displacement data are in reasonably good agreement with the predicted. The predicted angular displacement is in better agreement with the laboratory results than both the horizontal and vertical displacements because the angular motion is the largest among the three degrees of the caisson motion. Thus, the noise effect on the measured angular displacement is less than on the horizontal and vertical displacement measurements.

The predicted horizontal displacements were also compared with the data obtained from large-scale caisson experiments conducted at the Delft Hydraulic Laboratory [Lindenberg et al. (1982)]. This comparison is shown in Fig. 5.3.5. For smaller wave forces, theory and observation agree very well. However, for the larger waves, the predicted horizontal displacement is somewhat above the measured. This result is surprising since the displacement was underpredicted for the OSU experiments. A similar observation was also made by Lindenberg et al. (1982). The horizontal displacement predicted by a finite element model was larger than the measured. One possible reason is that the calculated wave force is larger than the real force acting on the caisson model for the higher waves. Another possible reason is the difference of the soil properties used for the theory and the physical model. This would result from the soil bed not being uniformly placed or reconsolidated back to the expected density. In addition, the displacement data from the OSU experiments was very noisy and required significant filtering. This reduces the confidence in the data.

The noise reduces confidence in the displacement measurements. Thus, the following modifications to the experimental procedure are recommended:

a) Using an LVDT for displacement measurements.

b) Occupying entire wave channel width for caisson to avoid the effects on the measurements from both the side channels and dummy structures.

c) Making a stiffer caisson, e.g., concrete.

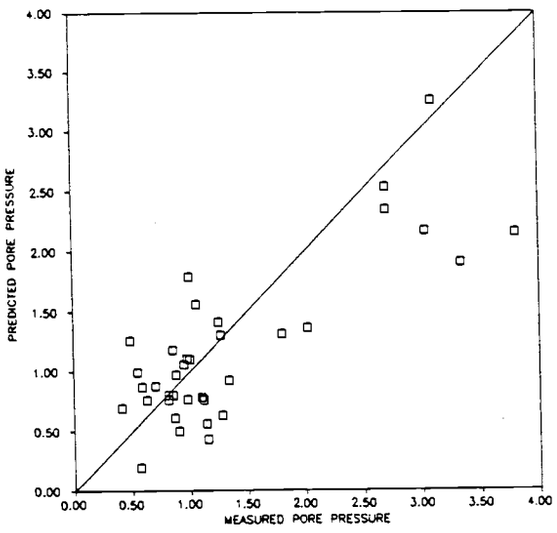

Figure 5.3.1.
Comparison of theory and measurements for pore pressure.

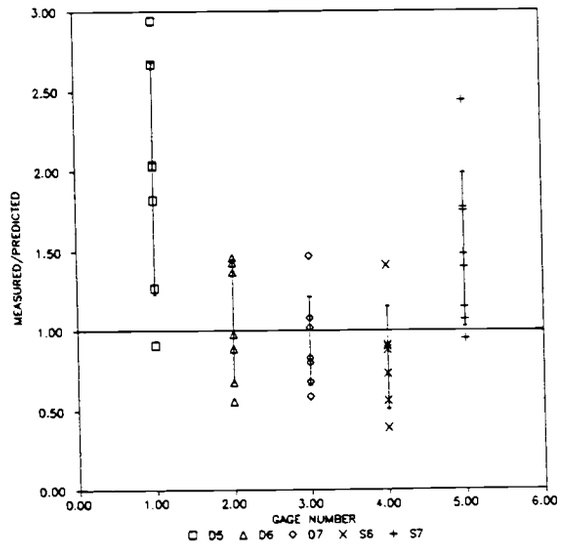

Figure 5.3.2.
Pressure ratio of the measured to the predicted for each gage.

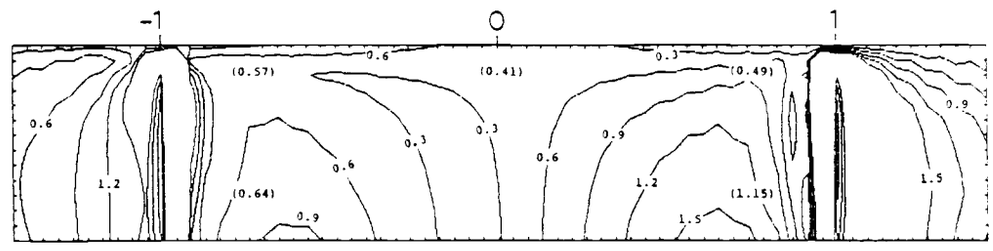

(.) Measured Data

Figure 5.3.3. Comparison of the predicted pressure contours and the measured data (T=5.6 sec and H=3.2 ft).

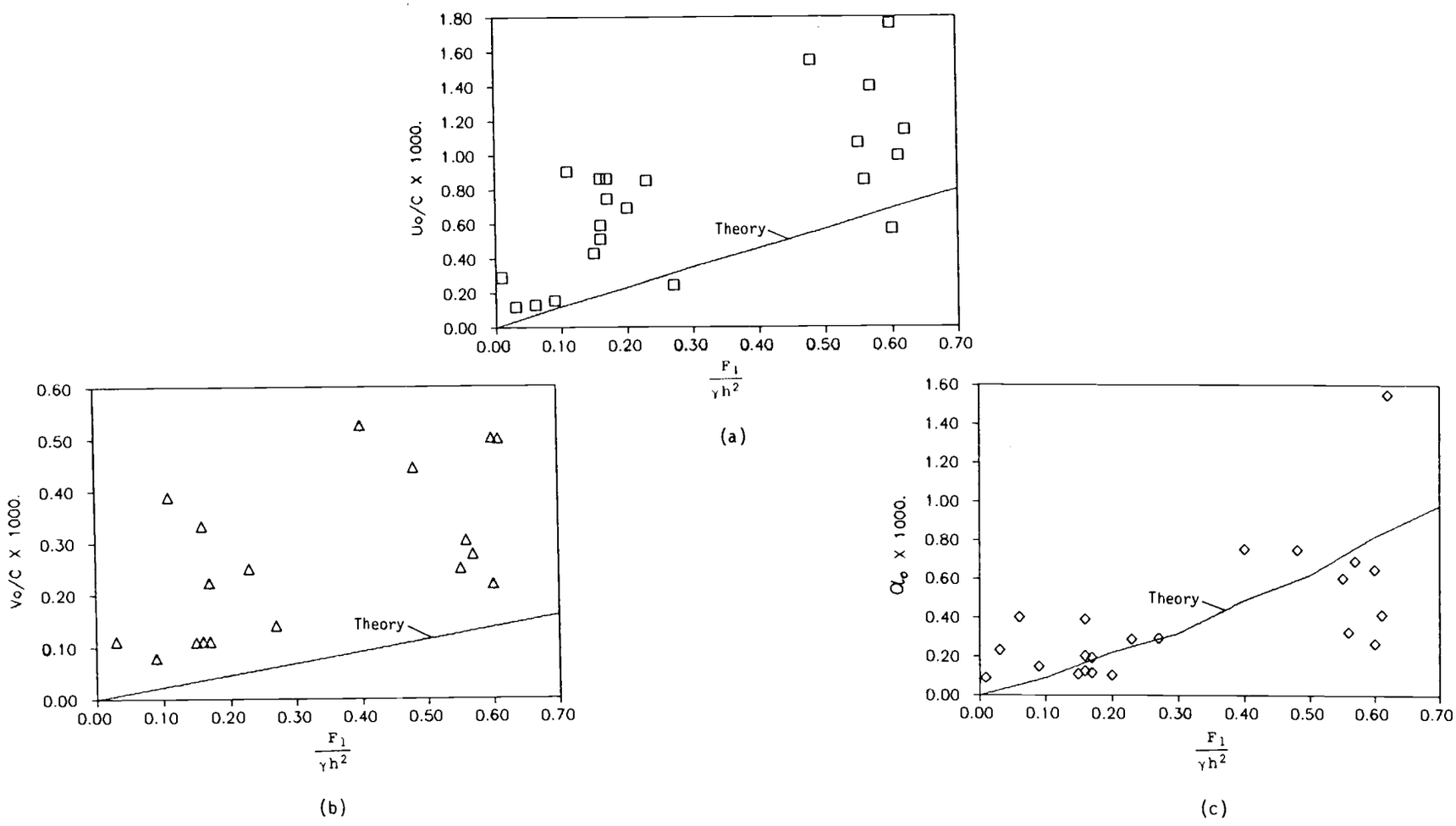

Figure 5.3.4. Comparison of the predicted and the measured displacements: (a) horizontal, (b) vertical, and (c) angular.

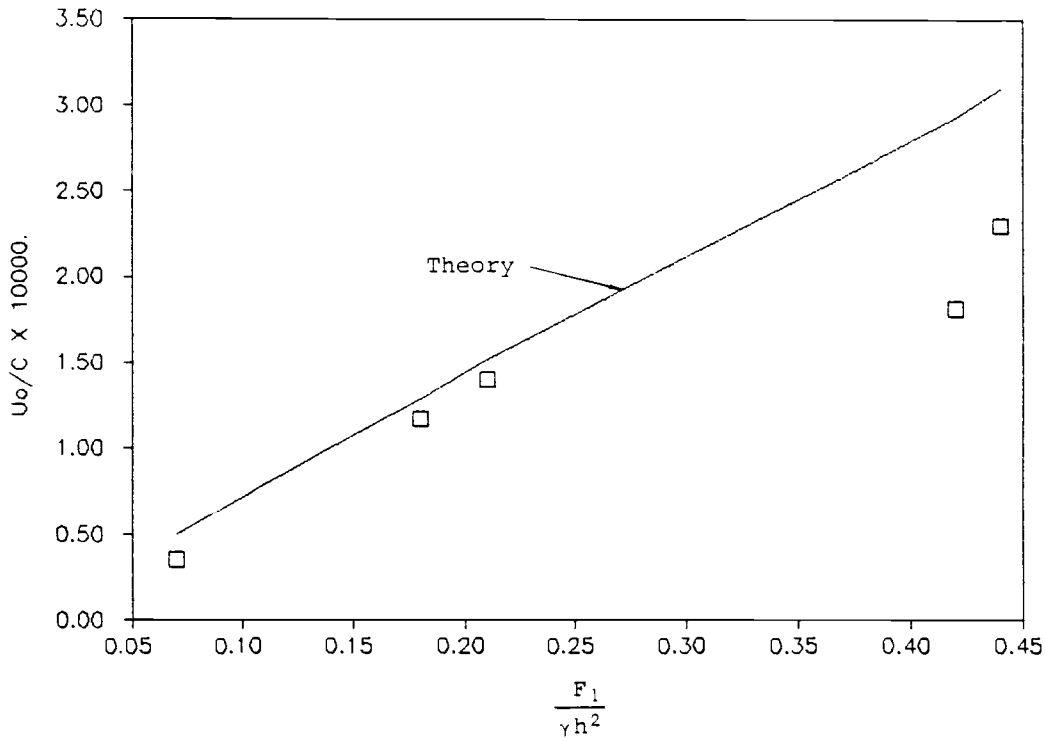

Figure 5.3.5. Comparison of theory and the Delft Hydraulic Laboratory measurements for the horizontal displacement.

6. CONCLUSIONS

6.1 Summary

The linear ocean wave-soil-caisson interaction system has been addressed analytically. Two approximations were applied: the boundary layer approximation and contact solution for a thin elastic layer.

Using the boundary layer approximation, the soil displacement and porewater pressure can be decoupled. Thus, solving the Biot equations is essentially solving the soil displacement and porewater pressure separately. Near the mudline, there exists a boundary layer in which drainage is relatively unimpeded and the relative motion between the fluid and solid is significant. Farther from the mudline, there is little drainage so the fluid and soil tend to move in phase. This is termed the outer region problem.

In the outer region problem, the soil displacement is solved from the quasi-static equation of motion by neglecting the inertia force in the case of sandy seabed. The porewater pressure is related to total normal stresses by combining the equations of mass and momentum.

In the boundary layer problem, the porewater pressure correction is solved from the one-dimensional Terzaghi consolidation equation. The stress corrections are related to the porewater pressure correction by taking the dominant terms in the equation of momentum. The displacement corrections are of the order of the ratio of the boundary layer thickness to the effective caisson half-width. Hence, they are negligible.

To solve the outer region problem, the original problem is decoupled into two problems. The scattering problem is for a fixed caisson. The exciting soil and wave forces from the scattering problem are applied to the radiation problem in which caisson motions are imposed on a still seabed.

Employing the contact solution for a thin elastic layer determines the unknown displacement boundaries along the exposed portion of the mudline. This yields a boundary condition along the mudline for the outer region problem is no longer of a mixed-type. The contact solution was modified by introducing the hyperbolic tanh function; hence, the approximate solution approaches the original solution near the caisson and approaches the undeformed mudline at a large distance.

From the numerical results and comparisons with a finite element numerical model solution, the influence of the thin soil layer assumption on the analytical model may be summarized as:

a) For the soil regions under the caisson and under the exposed mudline greater than 0.1c from the caisson, the analytical model is applicable for all soil depths.

b) For the response in the region (0~0.1)c from the caisson, the model is applicable only for soil depths $d/c < 0.25$.

An examination of the solution behavior indicates that Poisson's ratio and the shear modulus have a significant influence on the dis-

placements but not on stresses. The porosity is important for the pore pressure only. The soil depth affects the displacements and stresses significantly. The solution also reveals that the caisson motion induces much larger displacements, stresses, and porewater pressure in the soil skeleton than the wave alone. Pitch motion makes the most significant contribution, while heave is the least. At the caisson corners, high stresses and porewater pressure result from singularities. It is, therefore, strongly recommended that the dynamic caisson-soil interaction be considered in the foundation design of caissons.

A general agreement between the analytical model and physical model was obtained. However, more accurate methods to estimate the wave pressure on the mudline, forces on the caisson and measure caisson motions are recommended.

6.2. Applications

This analytical model only accounts for the dynamic response of the soil behavior. For practical applications, the static loads should also be considered. In addition to the design of caisson foundations, this analytical model could also be applied to the following cases:

1) The caisson-soil interaction solution can be applied to the design of machine foundations which are usually subjected to periodic loadings. The soil can be either elastic or poroelastic.
2) If the caisson is attached to the seabed directly, this solution is still applicable. The seepage pressure could

be separately estimated by using the methods developed by Liu (1985) or Dias and Monkeyer (1986).

3) The preliminary design of gravity offshore structure foundations in which a three dimensional model is required.

6.3. Future Research

This study provides the theoretical foundation for the examination of a number of other wave-soil-structure interaction problems, such as:

1) The wave-induced pore pressure, displacement, and stress around a pipeline laid on the poroelastic seabed of finite depth. This study of the caisson-soil interaction problem employed a solution for a rectangular stamp contact problem. An analogous contact solution has also been developed for a cylindrical stamp on a finite elastic layer.

2) The wave-soil-caisson interaction problem for an inhomogeneous poroelastic soil of finite depth. To solve this problem, the technique for a multi-layer system developed by Yamamoto (1981) or McDougal et al. (1982) may be applied.

3) The three-dimensional offshore structure-soil interaction problem. In this case the water depth is often very large. The stress induced directly by the wave becomes minor compared with the structure-soil interaction.

REFERENCES

Agerchou H. et al., (1983), Planning and Design of Ports and Marine Terminals, John Wiley and Sons, New York. 320 pp.

Alblas, J.B. and M. Kuipers, (1969), Contact problems of a rectangular block on an elastic layer of finite thickness, part I: the thin layer, Acta Mechanica, 8: 133-145.

Alblas, J.B. and M. Kuipers, (1970a), On the two dimensional problem of a cylindrical stamp pressed into a thin elastic layer, Acta Mechanica, 9: 293-311.

Alblas, J.B. and M. Kuipers, (1970b), Contact problems of a rectangular block on an elastic layer of finite thickness, part II: the thick layer, Acta Mechanica, 9: 1-12.

Biot, M.A., (1941), General theory of three-dimensional consolidation, J. Applied Physics, 12: 155-164.

Biot, M.A., (1956a), Theory of propagation of elastic waves in a fluid-saturated solid, part I, low-frequency range, J. Ascoust. Soc. Am., 28: 168-178.

Biot, M.A., (1956b), Theory of propagation of elastic waves in a fluid-saturated solid, part II, higher-frequency range, J. Ascoust. Soc. Am., 28: 179-191.

Booker, J.R., (1973), A numerical method for the solution of Biot's consolidation theory, Quart. J. Mech. Appl. Math., 26: 457-470

Bowles, J.E. (1982), Foundation Analysis and Design, McGraw-Hill Book Company, New York., 816 pp.

Broughton, P., (1975), Offshore gravity based oil production platform interaction with the seabed, OTC, 7: 387-398.

Christian, J.J. and J.W. Boehmer, (1970), Plane strain consolidation by finite elements, J. Soil Mech. Found. Div. ASCE, 96: 1435-1457.

Dalrymple, R.A., J.T. Kirby and P.A. Hwang (1984), Wave diffraction due to areas of energy dissipation, J. WPCOE Div., ASCE, 110: 67-79.

Dalrymple, R.A., J.T. Kirby and P.A. Hwang (1984), Wave diffraction due to areas of energy dissipation, J. WPCOE Div., ASCE, 110: 67-79.

Das, B.M., (1983), Advanced Soil Mechanics, McGraw-Hill Book Co., New York, 511 pp.

Dawson, T.H., (1978), Wave propagation over a deformable sea floor, Ocean Engr., 5: 227-234.

Dawson, T.H., J.N. Suhayad and J.M. Coleman, (1981), Correlation of field measurements with elastic theory of seafloor response to surface waves, Proc. OTC, 201-210.

Dean, R.G., (1974), Evaluation and Development of Water Wave Theory for Engineering Application, Vol. I, Special Report No. 1, U.S. Army Corps of Engineers, Coastal Engineering Research Center, 121 pp.

Dean, R.G. and R.A. Dalrymple, (1984), Water Wave Mechanics for Engineers and Scientists, Prentice-Hall, Inc., Englewood Cliffs, New Jersey. 353 pp.

Demars, K.R. and E.A. Vanover, (1985), Measurement of wave-induced pressures and stresses in a sandbed, Marine Geotech., 6: 29-59.

deQuelerij L., J.K. Nieuwenhuis and M.A. Koenders, (1979), Large model tests for the Oosterschelde storm surge barrier, Boss'79, 257-278.

Dias, F.C. and P.L. Monkmeyer, (1986), The effects of wave-induced seepage on a foundation plate resting on the seabed, Ocean Structural Dynamics Symposium '86, Corvallis, Oregon State University, 483-497.

Durand, T.J.P. and P.L. Monkmeyer, (1982), Wave-induced seepage effects on an impervious breakwater, Ocean Structural Dynamics Symposium '82, Corvallis, Oregon State University, pp. 196-210.

Foda, M.A., (1980), Dynamics of fluid filled porous media under wave action, PhD thesis, Dept. of Civil Engr. MIT.

Francavilla, A. and O.C. Zienkiewicz, (1975), A note on numerical computation of elastic contact problems, Int. J. Num. Meth. Engr., 9: 913-924.

Fung, Y.C., (1965), Foundation of Solid Mechanics, Prentice-Hall, Inc., New Jersey, 525 pp.

Hwang, C.T., N.R. Morgenstern and D.T. Murray, (1971), On solutions of plane strain consolidation problems by finite element methods, Can. Geotechnical J., 8: 109-118.

Ippen, A.T., (1966), Estuary and Coastline Hydrodynamics, McGraw-Hill, New York, 744 pp.

Jaber, W.Y., M.S. Rahman and C.C. Tung, (1986), Probabilistic analysis of wave-induced response and instability of oceanfloor soils, Ocean Structural Dynamics Symposium '86, Corvallis, Oregon State University, pp. 544-558.

Jonsson, I.G., (1966), Wave boundary layers and friction factors, Proc. 10th Conf. Coastal Engr., ASCE, 127-148.

Kamphuis, J.W., (1978), Attenuation of gravity waves by bottom friction, Coastal Engr., 2: 111-118.
Kraft, L.M. and S. C. Helfrich, (1983), Stresses due to wave-induced bottom pressures, J. Geotech. Div., ASCE, 109: 986-994.

Kreyszig E., (1983), Advanced Engineering Mathematics, John Wiley and Sons, New York., 988 pp.

Lindenberg, J., J.H. Swart, C.J. Kenter and K. den Boer, (1982), Wave induced pressures underneath a caisson: A comparison between theory and large scale tests, Boss'82, 1: 337-357.

Liu, P.F. and R.A. Dalrymple, (1984), The damping of gravity water-waves due to percolation, Coastal Engr., 8: 33-50.

Liu, P.F., (1985), Wave-induced pressure under gravity structures, J. WPCOE Div., ASCE, 111: 111-120.

Liu, P.F. and T.K. Tsay, (1985), Numerical prediction of wave transformation, J. WPCOE Div., ASCE, 111: 843-855.

Liu, P.F., (1986), Viscous effects on evalution of Stokes waves, J. WPCOE Div., ASCE, 112: 55-63.

Madsen, O.S., (1978), Wave-induced pore pressure and effective stress in a porous bed, Geotechnique, 28: 377-393.

Mallard, W.W. and R.A. Dalrymple, (1977), Water waves propagating over a deformable bottom, Proc. OTC, 141-146.

McDougal, W.G., C.K. Sollitt, T.S. Vinson and J.R. Bell, (1981), Ocean wave-soil-geotextile interaction, Sea Grant Report, Oregon State University, 143 pp.

McDougal, W.G. and P.F. Liu, (1986), Wave-induced pore water pressure accumulation in marine soils, Proc. 5th Int. OMAE, 1: 574-581.

Mei, C.C. and M.F. Foda, (1981a), Wave-induced responses in a fluid-filled poroelastic solid with a free surface--a boundary layer theory, Geophys. J. R. Astr. Soc., 66: 597-631.

Mei, C.C. and M.F. Foda, (1981b), Wave-induced stresses around a pipe laid on a poroelastic seabed, Geotechnique, 31: 509-517.

Mei, C.C. and M.F. Foda, (1982), Boundary layer theory of waves in a poroelastic seabed in Soil Mechanics-Transient and Cyclic Loads, G.N. Pande and O.C. Zienkiewicz eds., John Wiley, New York. 17-35.

Milovic, D.M., G. Touzot and J.P. Tournier, (1970), Stress and displacements in an elastic layer due to inclined and eccentric load over a rigid strip, Geotechnique, 20: 231-252.

Munro, J.G.A., C.J. Cudworth and A.A. Rodger, (1985), Soil-structure interaction in the dynamic response of an offshore structure, BOSS'85, 939-950.

Mynett, A.E. and C.C. Mei, (1982), Wave-induced stresses in a saturated poroelastic seabed beneath a rectangular caisson, Geotechnique, 32: 235-248.

Mynett, A.E. and C.C. Mei, (1983), Earthquake-induced stresses in a poroelastic foundation supporting a rigid structure, Geotechnique, 33: 293-305.

Nath, J.H., et al., (1977), Pressures in Sand from Waves and Caisson Motion, Oregon State University Wave Research Facility, Transportation Research Institute, 266 pp.

Nielsen, P., (1983), Analytical determination of nearshore wave height variation due to refraction, shoaling and friction, Coastal Engr., 7: 233-251.

Ozhan, E. and H. Shi-igai, (1977), On the development of solitary waves on a horizontal bed with friction, Coastal Engr., 1: 167-184.

Putnam, J.A., (1949), Loss of wave energy due to percolation in a permeable sea bottom, Trans. Am Geophys. Un., 30: 349-356.

Rahman, M.S., H.B. Seed and J.R. Booker, (1977), Pore pressure development under offshore gravity structures, J. Geotech. Div., ASCE, GT12: 1419-1436.

Rahman, M.S. and F.M. Layas, (1986), Wave-induced instability of oceanfloor soils, Proc. 5th Int. OMAE, 1: 547-554.

Schjetne, K., K.H. Andersen, R. Lauritzsen and O.E. Hansteen, (1979), Foundation engineering for offshore gravity structure, Marine Geotechnology, 3: 369-421.

Shore Protection Manual, (1984), U.S. Army Coastal Engineering Research Center, U.S. Government Printing Office, Washington, D.C.

Sleath, J.F.A. (1970), Wave induced pressure in beds of sand, J. Hyd. Div., ASCE, 96: 367-378.

Stematiu, D. and C. Stera, (1985), A FEM model of the breakwater-foundation dynamic interaction, unpublished.

Terzaghi, K., (1943), Theoretical Soil Mechanics, John Wiley and Sons, New York, 510 pp.

Tseng, J. and M.D. Olson, (1981), The mixed finite element method applied to two-dimensional elastic contact problems, Int. J. Num. Meth. Engr., 17: 991-1014.

Tsui Y. and S.C. Helfrich, (1983), Wave-induced pore pressures in submerged sand layer, J. of the Geotch. Div., ASCE, 109: 603-618.

Verruijt, A., (1969), Elastic storage of aquifers in Flow Through Porous Media, J.M. DeWiest, ed., Academic Press, New York. 331-376.

Ward, D.L., C.K. Sollitt, and W.G. McDougal, (1986), Wave interaction with a caisson style structure on a rubble foundation, Proc. 20th ICCE in press.

Wylie, C.R. and L.C. Barret, (1982), Advanced Engineering Mathematics, McGraw-Hill Book Co., New York. 1103 pp.

Yamamoto, T., (1977), Wave-induced instability in seabed, Proceedings, ASCE, Specialty Conference on Coastal Sediments, 898-913.

Yamamoto, T., H.L. Koning, H. Sellmeijer and E.V. Hijum, (1978), On the response of a poroelastic bed to water wave, J. Fluid Mech., 87: 193-206.

Yamamoto, T., (1981), Wave-induced pore pressures and effective stresses in inhomogeneous seabed foundations, Ocean Engineering, 8: 1-16.

Yamamoto, T., (1982), Nonlinear mechanics of water wave interactions with sediment bed, Applied Ocean Research, 4: 99-106.

Yamamoto, T., S. Takahashi and B. Schuckman, (1983a), Physical modeling of sea-seabed interactions, J. Eng. Mech. ASCE, 109: 54-72.

Yamamoto, T., (1983b), On the response of a Coulomb-damped poroelastic bed to water waves, Marine Geotech, 5: 93-105.

Yamamoto, T., and B. Schuckman, (1984), Experiments and Theory of wave-soil interactions, J. Eng. Mech. ASCE, 110: 95-112.

Zen, K., (1984), Study on the stability of subsoil under breakwaters subjected to cyclic wave loading (1st Report) - Analysis on wave-induced excess pore water pressure, Rep. Port and Harbor Res. Inst., Japan, 23: 182-206.

APPENDICES

APPENDIX A

LIST OF NOTATIONS

$^{j}a_1, ^{j}a_2, ^{j}a_3,$ $^{j}a_4; j=a,b,1,2,3$	solution constants of soil displacement in problem (a), problem (b), surge, heave, and pitch motion of caisson
b	thickness of rubble bedding layer
b_j; $j=1,2,3,4$	solution constants
c	caisson effective half-width
c'	caisson half-width
c_s	shear wave velocity
c_v	coefficient of consolidation
Δc	a distance from the caisson toe to a point on the exposed mudline
d	thickness of soil layer
e	base of natural logarithms (2.71828)/eccentricity
E	Young's modulus
f_{rj}; $j=1,2,3$	restoring forces on the caisson in surge, heave,and pitch of caisson motion
f_{sj}; $j=1,2,3$	scattering forces on the caisson in surge, heave, and pitch of caisson motion
f_{wj}; $j=1,2,3$	wave loads on the caisson in surge, heave, and pitch of caisson motion
F	total load on the rigid strip overlying an elastic layer

F_{rj}; j=1,2,3	restoring forces for the unit surge, heave, and pitch motion of the caisson
F_{sj}; j=1,2,3	amplitudes of horizontal, vertical, and moment scattering force
F_{wj}; j=1,2,3	amplitudes of horizontal, vertical, and moment of wave forces
g	gravitational acceleration
G	shear modulus of soil
h	water depth
H	incident wave height
i	$\sqrt{-1}$
I_m	inertial moment of mass of the caisson
k	wave number
k'	intrinsic permeability
k_r	reflection coefficient of waves
ℓ	shear wave length
Lo	deep water wave length
m	mass of the caisson
m_0	parameter indicating the relative stiffness between the solid matrix and the pore fluid
M_2	wave force moment on the caisson induced by the wave pressure on the caisson base
M_3	wave force moment on the caisson induced by the wave pressure on the caisson front face
n	soil porosity of dynamic perturbation
$\bar{n}$	soil porosity

n_0	soil porosity at static equilibrium
P	porewater pressure
P_a	absolute porewater pressure
P_{av}	average pressure on a rigid strip overlying an elastic layer
p_0	mudline pressure amplitude of the incident progressive wave
p_1	wave pressure on the caisson front face
P_2	wave pressure at the caisson toe
P_w	pressure distribution function along the mudline
s	Fourier transform parameter
s_r	degree of saturation of soil
t	time
T	wave period
u	displacement of soil in the x direction
u_i	displacement vectors of fluid
$\dot{u}_i$	velocity vectors of fluid
u_0	amplitude of horizontal displacement of caisson in surge
U_c, V_c, α_c	displacements of the caisson in surge, heave and pitch
$\ddot{U}_c$, $\ddot{V}_c$, $\ddot{\alpha}_c$	accelerations of the caisson in surge, heave and pitch

${}^{j}U^{o}$; j=a,b,1,2,3	horizontal displacements of soil in problem (a), problem (b), and surge, heave, and pitch of caisson motion
${}^{1}U_{f}^{o}$	mudline displacement along the exposed surface in the surge motion of the caisson
v	displacement of soil in the y direction
v_i, v_j, v_ℓ	displacement vectors of solid
$\dot{v}_i$	velocity vectors of solid
v_0	amplitude of vertical displacement of caisson in heave
${}^{j}V^{o}$; j=a,b,1,2,3	vertical displacements of the soil in problem (a), problem (b) and surge, heave, and pitch of the caisson motion
${}^{2}V_{f}^{o}$	mudline displacement along the exposed seabed in the heave motion of the caisson
${}^{3}V_{f}^{o}$	mudline displacement along the exposed surface in the pitch motion of the caisson
x	horizontal axis of Cartesian coordinates system
x_i, x_j, x_ℓ	axes of Cartesian coordinates system
y	vertical axis of Cartesian coordinates system, downward positive
z	vertical axis of Cartesian coordinates system, defined by z=-y-h
α_c	angular displacement of pitch motion of the caisson

$\ddot{\alpha}_c$	angular acceleration of pitch motion of the caisson
α_o	amplitude of angular displacement of pitch motion of the caisson
β	pure water compressibility
β'	combined air-water compressibility
γ	unit weight of water
δ	thickness of the boundary layer
δ_{ij}	Kronecker delta
ϵ	defined as δ/c
η	free surface fluctuation of the incident progressive wave
θ	the angle between the vertical and an inclined load
λ	variable of characteristic equation
μ	coefficient of permeability
ν	Poisson's ratio of soil
π	mathematical constant (3.14159)
ρ_s	soil density of dynamic perturbation
$\bar{\rho}_s$	soil density
ρ_{so}	soil density at static equilibrium
ρ_w	fluid density of dynamic perturbation
$\bar{\rho}_w$	fluid density
ρ_{wo}	fluid density at static equilibrium
σ	angular frequency of wave
τ_{ij}	total stress tensor

τ'_{ij}	effective stress tensor
τ_{xy}	shear stress
τ_{xx}, τ_{yy}	total normal stresses in the x and y directions
τ'_{xx}, τ'_{yy}	effective normal stresses in the x and y direction
$\nabla^2(\cdot)$	LaPlacian operator
(upper case letter)^b	dimensionless parameters in the boundary layer
(lower case letter)^b	parameters in the boundary layer
(upper case letter)^o	dimensionless parameters in the outer region
(lower case letter)^o	parameters in the outer region
$\hat{(\ )}$	Fourier transform of ( )

APPENDIX B

DISPLACEMENT BOUNDARIES ALONG THE EXPOSED MUDLINE

B.1 Contact Problem of a Rectangular Block on an Elastic Layer of Finite Depth by Alblas and Kuipers (1969)

B.1.1 Assumptions

The following assumptions are made for a rigid rectangular block on a thin elastic layer.

1. The thickness of the elastic layer is much smaller than the width of the block.
2. The deformation of the elastic layer is sufficiently small that linear elasticity theory is applicable.
3. The lower side of the layer is rigidly attached to an undeformable base.
4. The block has a smooth, rigid, and straight horizontal base.
5. The block is of infinite dimension in the longitudinal direction which allows the problem to be considered two-dimensional (plane strain).
6. An additional assumption is required for the surge. The friction between the mound foundation and the soil is sufficient to maintain a no-slip condition such that the caisson is welded to the soil.

B.1.2. A Rectangular Block with a Vertical Force Load

An elastic layer with a thickness d is loaded in plane strain by a rectangular block having width 2c (Fig. B.1). The block has pene-

trated into the layer a distance v_c in the y direction. The force to be exerted on the block of unit length is F_2.

The equations governing the behavior of the elastic layer are given by (2.2.8a) and (2.2.8b) which are classical elastostatic equations.

The boundary conditions along the upper boundary (y=0) are

$$f_2(x,0) = v(x) + g(x) \qquad ;0\leq|x|<\infty \qquad \text{(B.1.1a)}$$

$$\tau_{xy}(x,0) = 0 \qquad ;0\leq|x|<\infty \qquad \text{(B.1.1b)}$$

$$\tau_{yy}(x,0) = \begin{cases} 0 & ;|x|\geq 0 \\ -p(x) & ;|x|<0 \end{cases} \qquad \text{(B.1.1c)}$$

where $f_2(x,0)$ denotes the displacement in the y direction and p(x) is the normal pressure; and

$$v(x) = v_c \qquad g(x) = 0 \qquad ;|x|\leq c \qquad \text{(B.1.1d)}$$

$$v(x) = 0 \qquad g(x) \neq 0 \qquad ;|x|>c \qquad \text{(B.1.1e)}$$

Along the rigid base, the no-displacement conditions are imposed

$$u(x,d) = 0 \qquad ;0\leq|x|<\infty \qquad \text{(B.1.2a)}$$

$$v(x,d) = 0 \qquad ;0\leq|x|<\infty \qquad \text{(B.1.2b)}$$

The general solution to (2.2.8) has been given by (3.1.11) in the form of Fourier transform. From the Fourier transforms of the boundary conditions (B.1.1a), (B.1.1b), (B.1.2a), and (B.1.2b) the unknown coefficients in (3.1.11) are readily determined. Lengths are

denoted by upper case letters after they are non-dimensionlized by the block half-width c.

$$a_1 = \frac{-i\hat{f}_2(s)[(1-2\nu)(3-4\nu)sh^2(sD) - s^2D^2]}{2(1-\nu)[sD - (3-4\nu)ch(sD)sh(sD)]} \tag{B.1.3a}$$

$$a_2 = \frac{-i(1-2\nu)\hat{f}_2(s)}{2(1-\nu)} \tag{B.1.3b}$$

$$a_3 = \frac{-is\hat{f}_2(s)}{2(1-\nu)} \tag{B.1.3c}$$

$$a_4 = \frac{is\hat{f}_2(s)[(1-2\nu)-(3-4\nu)ch^2(sD)]}{2(1-\nu)[sD-(3-4\nu)ch(sD)sh(sD)]} \tag{B.1.3d}$$

The normal stress condition (B.1.1c) leads to

$$p(X,0) = -\frac{2E}{2(1+\nu)}\left[\frac{1-\nu}{1-2\nu}\frac{\partial V}{\partial Y} + \frac{\nu}{1-2\nu}\frac{\partial U}{\partial X}\right] \tag{B.1.4}$$

Scaling p(X,0) by $E/[2(1-\nu^2)]$ yields

$$P(X,0) = -2(1-\nu)\left[\frac{1-\nu}{1-2\nu}\frac{\partial V}{\partial Y} + \frac{\nu}{1-2\nu}\frac{\partial U}{\partial X}\right] \tag{B.1.5}$$

The Fourier transform of (B.1.5) takes the form

$$\hat{P}(s,0) = -2(1-\nu)\left[\frac{1-\nu}{1-2\nu}\frac{\partial \hat{V}}{\partial Y} + \frac{is\nu}{1-2\nu}\hat{U}\right] \tag{B.1.6}$$

Substituting $\hat{U}$ and $\hat{V}$ given by (3.1.11) associated with the solution coefficients a_1, a_2, a_3, and a_4, into (B.1.6) yields

$$\hat{P}(s,0) = \frac{1}{\hat{S}(s)}\hat{f}_2(s) \tag{B.1.7}$$

in which

$$\hat{S}(s) = \frac{(3-4\nu)\sinh(2sD)-2sD}{sD[(3-4\nu)\cosh(2sD)+5-12\nu+8\nu^2+2s^2D^2]} \qquad (B.1.8)$$

Since the solution is expected to have an accuracy of $O(e^{-c/d})$ (i.e. a thin elastic layer and negligible normal stress on the exposed upper surface), equation (B.1.7) is replaced by the Wiener-Hopf equation.

$$D\hat{P}_-(s) = \frac{1}{\hat{S}(s)}\left[\frac{-iV_c}{\sqrt{2\pi}\, s} + \hat{G}_+(s)\right] \qquad (B.1.9)$$

In which

$$\hat{P}_-(s) = \frac{1}{\sqrt{2\pi}} \int_{-\infty}^{0} P(X+1)e^{-isX} ds \qquad (B.1.10a)$$

and is regular in the lower-half plane.

$$\hat{G}_+(s) = \frac{1}{\sqrt{2\pi}} \int_{0}^{\infty} G(X+1)\, e^{-isX} ds \qquad (B.1.10b)$$

is regular in the upper-half plane.

By means of the decomposition [Alblas and Kuipers (1970a)],

$$\frac{1}{\hat{S}(s)} = \frac{\hat{S}_+(s)}{\hat{S}_-(s)} \qquad (B.1.11)$$

in which

$$\hat{S}_+(s) = \frac{\left(1+\frac{sD}{s_o^*}\right)e^{-\frac{sD}{s_o^*}} \prod_{k=1}^{\infty}\left(1+\frac{sD}{s_k^*}\right)e^{-\frac{sD}{s_k^*}} \prod_{k=1}^{\infty}\left(1-\frac{sD}{\bar{s}_k^*}\right)e^{-\frac{sD}{\bar{s}_k^*}} e^{-\chi(s)}}{\hat{S}(0)\left(1+\frac{sD}{s_o}\right)e^{-\frac{sD}{s_o}} \prod_{k=1}^{\infty}\left(1+\frac{sD}{s_k}\right)e^{-\frac{sD}{s_k}} \prod_{k=1}^{\infty}\left(1-\frac{sD}{\bar{s}_k}\right)e^{\frac{sD}{\bar{s}_k}}} \qquad (B.1.12a)$$

$$\hat{S}_-(s) = \frac{(1 - \frac{sD}{s_o})e^{\frac{sD}{s_o}} \prod_{k=1}^{\infty} (1 - \frac{sD}{s_k})e^{\frac{sD}{s_k}} \prod_{k=1}^{\infty} (1 + \frac{sD}{\bar{s}_k})e^{-\frac{sD}{\bar{s}_k}} e^{-\chi(s)}}{(1 - \frac{sD}{s_o^*})e^{\frac{sD}{s_o^*}} \prod_{k=1}^{\infty} (1 - \frac{sD}{s_k^*})e^{\frac{sD}{s_k^*}} \prod_{k=1}^{\infty} (1 + \frac{sD}{\bar{s}_k^*})e^{-\frac{sD}{\bar{s}_k^*}}} \qquad \text{(B.1.12b)}$$

where

$$\left.\begin{aligned} s_k &= \tfrac{1}{2}\log\frac{(4k+1)\pi}{3-4\nu} + i(k + \tfrac{1}{4}) + O(\frac{\log k}{k}) \\ s_k^* &= \tfrac{1}{2}\log(\frac{4k^2\pi^2}{3-4\nu}) + ik\pi + O(\frac{\log k}{k^2}) \end{aligned}\right\} \quad k >> 1 \qquad \text{(B.1.13a)}$$

$$\chi(x) = isD \sum_{k=1}^{\infty} \{\frac{i(\bar{s}_k^* - s_k^*)}{s_k^* \bar{s}_k^*} - \frac{i(\bar{s}_k - s_k)}{s_k \bar{s}_k}\} - sD(\frac{1}{s_o^*} - \frac{1}{s_o}) \qquad \text{(B.1.13b)}$$

Equation (B.1.9) is found to be

$$sD\, \hat{P}_-(s)\, \hat{S}_-(s) = \hat{S}_+(s) [\frac{-iV_o}{\sqrt{2\pi}} + s\, \hat{G}_+(s)] \qquad \text{(B.1.14)}$$

Since an integrable singularity of the pressure at X=1 is allowed, the entire function (B.1.14) must be constant, indicated as c_o. Because $\hat{G}_+(s)$ has to be regular at the origin, thus

$$c_o = -\frac{iV_c \hat{S}_+(0)}{\sqrt{2\pi}} \qquad \text{(B.1.15)}$$

It follows that

$$\hat{G}_+(s) = \frac{-iV_c}{\sqrt{2\pi}\, s} [\frac{\hat{S}_+(0)}{\hat{S}_+(s)} - 1] \qquad \text{(B.1.16)}$$

in which [Alblas and Kuipers (1970a)]

$$\hat{S}_+(0) = A = \frac{2(1-\nu)^2}{1-2\nu} = \frac{1}{\hat{S}(0)} \qquad \text{(B.1.17)}$$

Using (B.1.10b) and (B.1.16), the displacement of the upper boundary just outside the block appears to be

$$G(X) \sim V_o\left[1-2\sqrt{\frac{A(X-1)}{\pi D}}\right] \qquad ; \; 0 < X-1 << 1 \qquad \text{(B.1.18)}$$

B.1.2 A Rectangular Block with a Moment Load

Due to the antisymmetry of the problem the displacement of the origin is zero (Fig. B.2). The angle of rotation is denoted by α_c.

Equation (B.1.1d) is replaced by

$$v(x) = -\alpha_c x \qquad ; \; |x| < c \qquad \text{(B.1.19)}$$

while the remainder of (B.1.1a) through (B.1.2b) continues to apply. Analogous to the vertical load problem, the Wiener-Hopf equation of this problem is expressed by

$$\hat{DP}_-(s) = \frac{1}{\hat{S}(s)}\left[-\frac{\alpha_c}{\sqrt{2\pi}}\left(-\frac{i}{s}-\frac{1}{s^2}\right) + \hat{G}_+(s)\right] \qquad \text{(B.1.20)}$$

Applying (B.1.11) to (B.1.20) yields

$$s^2\hat{DP}_-(s)\hat{S}_-(s) = \hat{S}_+(s)\left[-\frac{\alpha_c}{\sqrt{2\pi}}(-is+1) + s^2\hat{G}_+(s)\right] \qquad \text{(B.1.21)}$$

Again, an integrable singularity of the pressure at X=1 is allowed. On that account, the entire function defined by (B.1.21) is a polynomial of the first degree $d_o + d_1 s$. The regularity of $\hat{G}_+(s)$ at s=0 implies

$$d_o = -\frac{\alpha_c \hat{s}_+(0)}{\sqrt{2\pi}} \qquad \text{(B.1.22a)}$$

and

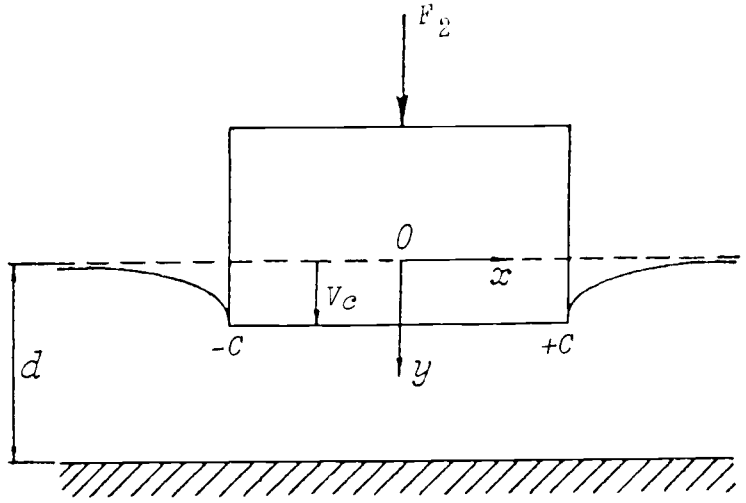

Figure B.1. The rectangular block with a vertical load.

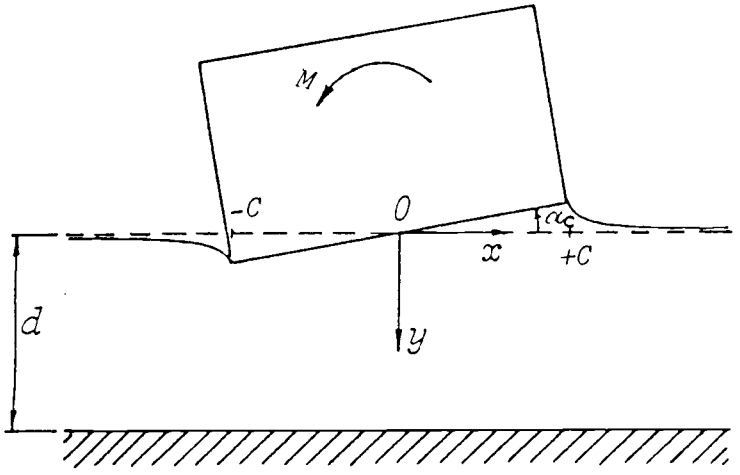

Figure B.2. The rectangular block with a moment load.

$$d_1 = \frac{\alpha_c}{\sqrt{2\pi}} [i \hat{S}_+(0) - \hat{S}'_+(0)] \qquad \text{(B.1.22b)}$$

in which $S'_+(0) = A \hat{S}'_-(0)$ and $\hat{S}'_-(0)$ is a function dependent on Poisson's ratio and the thickness of the elastic layer and is given in Table B.1 [Alblas and Kuipers (1970a)]. In this way $\hat{G}_+(s)$ is given by

$$\hat{G}_+(s) = \frac{\alpha_c}{\sqrt{2\pi}} \left\{ \frac{-\hat{S}_+(0) + s[i\hat{S}_+(0) - \hat{S}'_+(0)]}{s^2 \hat{S}_+(s)} - \frac{i}{s} + \frac{1}{s^2} \right\} \qquad \text{(B.1.23)}$$

Substitution of (B.1.23) into (B.1.10b) yields

$$G(x) \sim \alpha_c \left\{ 1 - 2\sqrt{\frac{A(X-1)}{\pi D}} [1 + i \hat{S}'_-(0)] \right\} \quad ; 0<X-1<<1 \qquad \text{(B.1.24)}$$

Table B.1. Dependency of $\hat{S}'_-(0)$ on Poisson's ratio [Alblas and Kuipers (1970a)].

ν	0.0	0.2	0.3	0.4
$\hat{S}'_-(0)$	-.176iD	-.173iD	-.115iD	0.118iD

B.2 Approximation of the Displacement Adjacent to the Block

Equations (B.1.18) and (B.1.24) are only valid in the region just outside the corner of the block as shown in Figs. B.3 and B.4. To formulate more realistic boundary conditions along the mudline, no-displacement conditions at large X are imposed. Equations (B.1.18) and (B.1.24) and the no-displacement condition at large X are fitted by the following equations.

Heave

$$V_2 = V_c \left\{ 1 - \text{th} \left[2\sqrt{\frac{A(X-1)}{\pi D}} \right] \right\} \quad ; 1<X<\infty \qquad \text{(B.2.1)}$$

Pitch

$$V_3 = \alpha_c\left[1 - \text{th}\left\{2\sqrt{\frac{A(X-1)}{\pi D}}\left[1+i\hat{S}'_{-}(0)\right]\right\}\right] \quad ;1<X<\infty \tag{B.2.2}$$

The hyperbolic function provides equations which are asymptotic to the original equations when X-1 is small and to the undeformed mud-line when X is large. The comparisons of (B.1.18) and (B.2.1), and (B.1.24) and (B.2.2) are shown in Figs. B.3 and B.4.

B.3 The Displacement of the Upper Boundary for Surge

Alblas and Kuipers (1969) did not develop a solution for the displacement of the upper boundary of a finite elastic layer to a surge motion of a rectangular block when the block is subjected to a horizontal load (Fig. B.5). Therefore, an approximate solution will be developed from the solution for the heave.

Equation (B.1.18) for the heave is rewritten to provide guidance for the surge.

$$G(X) = V_o\left[1 - 2\sqrt{\frac{X-1}{\hat{S}(0)\pi D}}\right] \tag{B.3.1}$$

In an attempt to seek a similar form for surge, it will be assumed

$$U'_1(X) = U_c\left[1 - 2\sqrt{\frac{X-1}{\hat{R}(0)\pi D}}\right] \tag{B.3.2}$$

where $\hat{R}(s)$, when s=0, is a transform function relating the shear stress and the displacement function on the upper boundary, and is similar to $\hat{S}(s)$ in (B.1.7).

If the horizontal stress on the block base is designated h(x,0), then

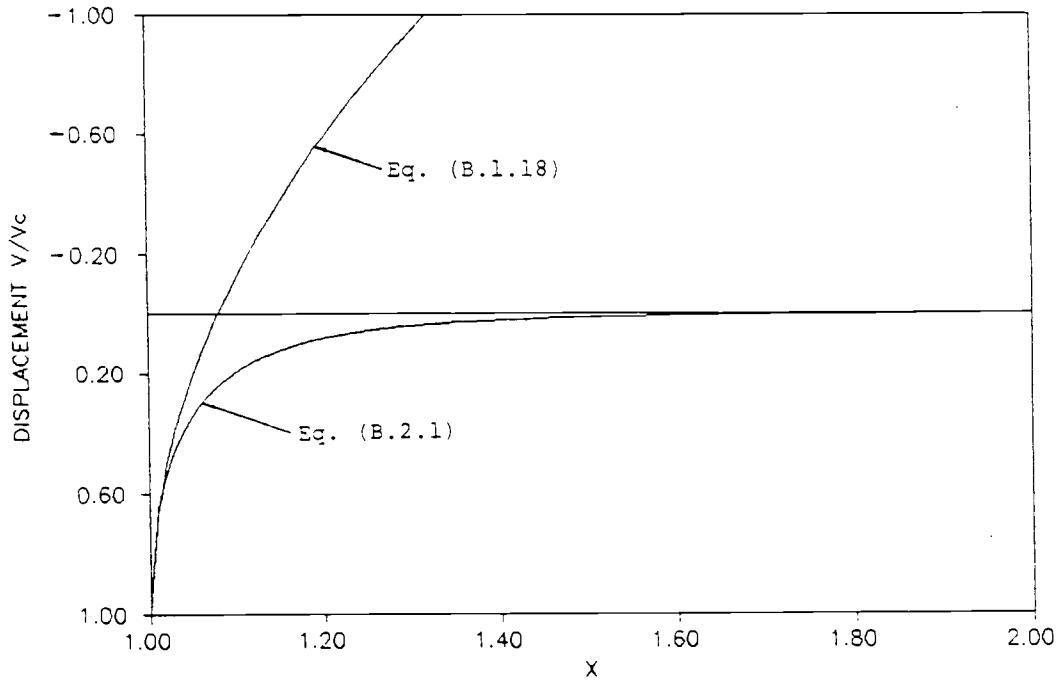

Figure B.3. Comparison of equations (B.1.18) and (B.2.1) for heave motion.

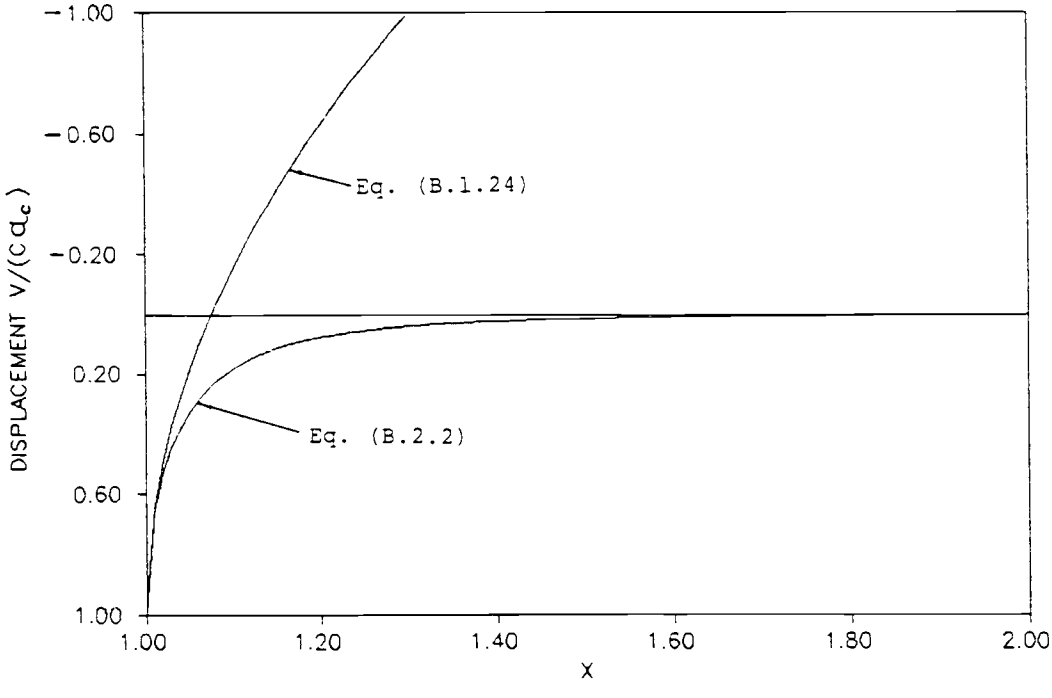

Figure B.4. Comparison of equations (B.1.24) and (B.2.2) for pitch motion.

$$h(x,0) = -\tau_{xy}\Big|_{y=0} \tag{B.3.3}$$

$$h(x,0) = -\frac{E}{2(1+\nu)}\left(\frac{\partial u}{\partial y} + \frac{\partial v}{\partial x}\right)\Big|_{y=0} \tag{B.3.4}$$

Scaling $h(x,0)$ by $E/[2(1-\nu^2)]$ and length by c yields

$$H(X,0) = -(1-\nu)\left(\frac{\partial U}{\partial Y} + \frac{\partial V}{\partial X}\right)\Big|_{Y=0} \tag{B.3.5}$$

Taking the Fourier transform of (B.3.5) yields

$$\hat{H}(s) = -(1-\nu)\left(\frac{\partial \hat{U}}{\partial Y} + is\hat{V}\right)\Big|_{Y=0} \tag{B.3.6}$$

Substituting $\hat{U}$ and $\hat{V}$ from (3.1.11) and using the coefficients given by (3.3.6), in which (3.3.6a) is replaced by ${}^{1}a_1 = \hat{f}_1(s)$ for Y=0, into (B.3.6) yields

$$D\hat{H}(s) = \frac{1}{\hat{R}(s)}\,\hat{f}_1(s) \tag{B.3.7}$$

This equation has the same form as (B.1.7) and

$$\hat{f}_1(s) = \hat{u}(s) + \hat{u}_1'(s) \tag{B.3.8}$$

$$\hat{R}(s) = \frac{(3-4\nu)\mathrm{sh}(2sD)+2sD}{sD[(3-4\nu)\mathrm{ch}(2sD)+5-12\nu+8\nu^2+2s^2D^2]} \tag{B.3.9}$$

from which

$$\frac{1}{\hat{R}(0)} = 1-\nu \tag{B.3.10}$$

Accordingly, by analogy (B.3.2) may be written

$$U_1'(X) = U_c\left[1-2\sqrt{\frac{(1-\nu)(X-1)}{\pi D}}\right] \qquad ; 0 < X-1 << 1 \tag{B.3.11}$$

An approximation which matches (B.3.11) near the corners and is asymptotic to the undeformed mudline at large X is

$$U_1(X) = U_c\left[1 - \text{th}\left(2\sqrt{\frac{(1-\nu)(X-1)}{\pi D}}\right)\right] \qquad ;1\leq X<\infty \tag{B.3.12}$$

Thus, the upper displacement boundary is defined. The comparison of (B.3.11) and (B.3.12) is shown in Fig. B.6.

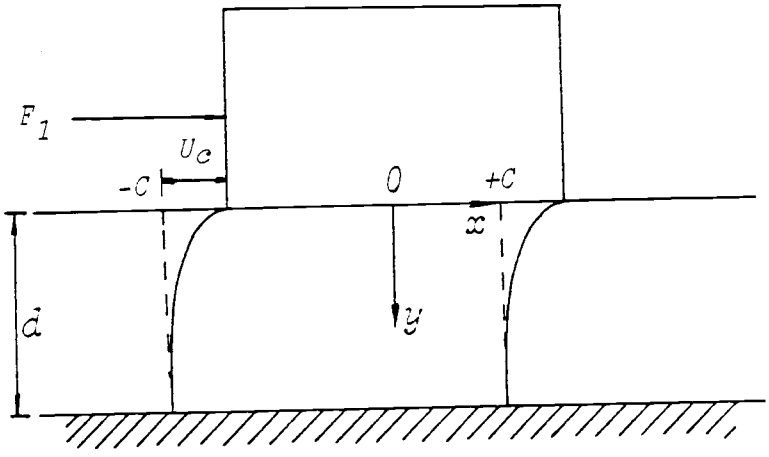

Figure B.5. The rectangular block with a horizontal load.

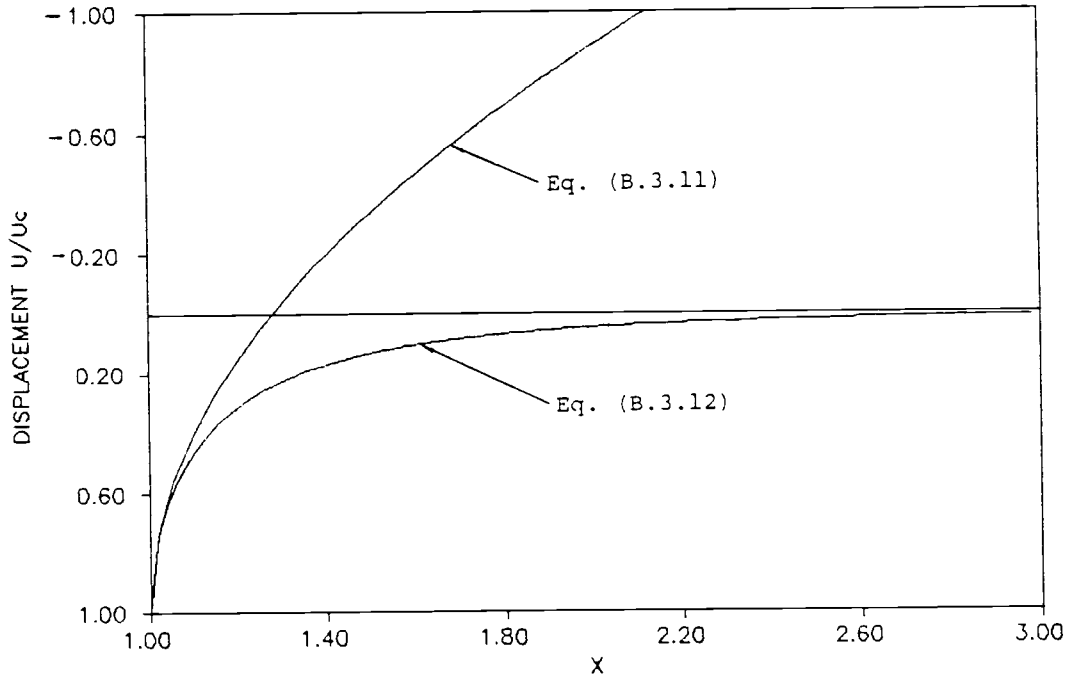

Figure B.6. Comparison of equations (B.3.11) and (B.3.12) for surge motion.